

THE UNIVERSITY OF CALGARY

**QUANTITATIVE ANALYSIS OF UNDERWATER STEREO VIDEO IMAGES**

by

HAIHAO LI

A THESIS

SUBMITTED TO THE FACULTY OF GRADUATE STUDIES  
IN PARTIAL FULFILLMENT OF THE REQUIREMENTS FOR THE  
DEGREE OF MASTER OF SCIENCE

DEPARTMENT OF GEOMATICS ENGINEERING

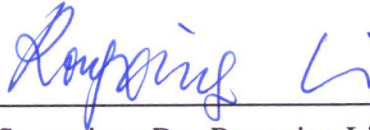
CALGARY, ALBERTA

JANUARY, 1995

© Haihao Li 1995

THE UNIVERSITY OF CALGARY  
FACULTY OF GRADUATE STUDIES

The undersigned certify that they have read, and recommend to the Faculty of Graduate Studies for acceptance, a thesis entitled "Quantitative Analysis of Underwater Stereo Video Images" submitted by Haihao Li in partial fulfillment of the requirements for the degree of Master of Science.



---

Supervisor, Dr. Rongxing Li  
Department of Geomatics Engineering



---

Dr. Mike A. Chapman  
Department of Geomatics Engineering



---

Dr. Tongwen Chen  
Department of Electrical and Computer Engineering

Date: January 26, 1995

## ABSTRACT

CCD-cameras mounted on Autonomous Underwater Vehicles (AUV) provide an efficient way for monitoring objects with high resolution and visual capability in an underwater environment. With digital underwater photogrammetry, quantitative analysis of underwater imagery can be conducted, such as measuring 3D object coordinates and others. In this research, a PC-based system for photogrammetric processing of underwater video images which includes modules of Graphical User Interface (GUI), image processing, imaging system calibration, measurement, and graphic display is presented. Some geometrical, optical and electrical properties of CCD-cameras and images in the underwater environment, for instance, lens distortion, multi-lens function, noise elimination/reduction, ray bending, etc. are investigated. Based on these, a photogrammetric model can be established for determining object space coordinates from measured image coordinates. This allows users to calculate positions and shapes in a 3D object space as long as the objects to be measured can be seen in stereo images. The GUI makes the modules involved transparent to users and provides a convenient, efficient and user-friendly environment for object-oriented measuring procedures.

Results of a water tank test for the camera calibration and object measurement are presented. Application of this technology can be found in precise seafloor mapping, underwater target tracing, object monitoring and identifying.

## ACKNOWLEDGMENTS

I wish to express my deep gratitude to my supervisor, Dr. R. Li, for his guidance, support, and encouragement throughout my graduate studies. I am grateful to Dr. M.A. Chapman for the encouraging and valuable discussion during my thesis research work. Dr. T.W. Chen is acknowledged for his critiques for this thesis. Appreciation should also go to my fellow graduate students, Mr. Liming Qian and Mr. Yubin Xin, for their great help during my graduate studies and thesis research. This research is supported by The University of Calgary and the Canadian Hydrographic Service. Mr. G.R. Smith and Mr. T.A. Curran did a lot of work for the field data collection and testing. Their support is gratefully acknowledged.

## TABLE OF CONTENTS

APPROVAL PAGE.....	ii
ABSTRACT .....	iii
ACKNOWLEDGMENTS.....	iv
TABLE OF CONTENTS.....	v
LIST OF TABLES .....	viii
LIST OF FIGURES .....	ix

<b>CHAPTER</b>	<b>Page</b>
<b>1 INTRODUCTION.....</b>	<b>1</b>
1.1 Underwater photogrammetry .....	1
1.2 Objectives of the research .....	6
1.3 Thesis outline.....	7
<b>2 QUANTITATIVE ANALYSIS OF UNDERWATER STEREO VIDEO IMAGES .....</b>	<b>8</b>
2.1 Conceptual model .....	9
2.2 Multi-media photogrammetric model.....	11
2.2.1 Image geometry.....	11
2.2.2 Landbased vs. underwater photogrammetry .....	14
2.2.3 Ray tracing.....	20
2.2.4 Establishment of underwater photogrammetric model .....	24
2.3 Imaging system calibration.....	30
2.3.1 Calibration procedure.....	30
2.3.2 CCD camera calibration.....	32
2.3.2.1 CCD video camera.....	32
2.3.2.2 CCD camera lens distortion.....	34

2.3.2.3	Least squares model for the camera calibration.....	37
2.3.3	Calibration of the underwater imaging system.....	38
2.4	Spatial intersection .....	40
2.5	Some implementation considerations .....	41
<b>3</b>	<b>IMPLEMENTATION OF UNDERWATER VIDEO IMAGE PROCESSING SYSTEM.....</b>	<b>43</b>
3.1	Background.....	43
3.2	Requirement of underwater measuring system .....	44
3.3	Underwater image data collection .....	46
3.3.1	CCD camera configuration.....	46
3.3.2	Frame grabber .....	48
3.3.3	Calibration frame .....	48
3.3.4	Water tank test .....	49
3.4	Underwater image data processing.....	52
3.4.1	Hardware configuration .....	53
3.4.2	Digital image display.....	53
3.4.3	Image processing .....	56
3.4.4	Calibration and measurement module.....	59
3.4.5	Database generation .....	62
3.4.6	GUI development .....	63
3.5	Experiment results.....	66
3.5.1	Results of CCD camera calibration.....	68
3.5.2	Results of underwater imaging system calibration .....	70
3.5.3	Results of space intersection .....	72
3.5.4	Accuracy assessment.....	73
<b>4</b>	<b>CONCLUSIONS AND RECOMMENDATIONS.....</b>	<b>79</b>
4.1	Conclusions.....	79
4.3	Recommendations.....	81

<b>REFERENCES</b> .....	83
-------------------------	----

**APPENDIX**

A	Coplanarity condition in 3D skew ray tracing.....	90
B	Partial derivatives of the underwater photogrammetric observation equations..	92
C	Singular value decomposition (SVD).....	107

## LIST OF TABLES

No.		Page
3.1	Spatial coordinates of control targets.....	50
3.2	Image & spatial coordinates of control points used for CCD camera calibration	68
3.3	Results of DLT .....	69
3.4	Results of CCD camera calibration.....	69
3.5	Pixel coordinates of control points used for imaging system calibration .....	71
3.6	Results of imaging system calibration with the second stereo pair.....	71
3.7	Results of imaging system calibration with the third stereo pair.....	72
3.8	Object measurement accuracy evaluation using control points on the second stereo pair .....	73
3.9	Object measurement accuracy evaluation using control points on the third stereo pair .....	74
3.10	Spatial coordinates of the exposure stations.....	77
3.11	Object measurement accuracy assessment with increased baseline.....	77

# CHAPTER 1

## INTRODUCTION

### 1.1 Underwater photogrammetry

Photogrammetry is the science, art and technology of obtaining reliable measurements and reliable qualitative information through photography (American Society of Photogrammetry, 1980). With its extension to the underwater environment, photogrammetry is adapted from its original applications in topographic mapping to become a well-established non-contact measurement technique which is suitable for underwater inspection and measurements.

During the past century, the photogrammetric processing of recording, reading and measuring photographs has developed into a highly sophisticated, elaborate, and efficient procedure. For reasons involving the evolutionary capabilities and requirements of human beings, the photogrammetric process has been predominately specialized for the acquisition of photographic recording and for photogrammetric processing in an object space in air. Thus, photogrammetric procedures have only played a secondary role in underwater surveys. This is mainly due to the following factors:

First, the physical properties of water pertaining to density and pressure are vastly different from air, which greatly limits human activities in the underwater environment. Even with the assistance of autonomous underwater vehicles, the efficiency of underwater image data acquisition is still far behind that of the aerial and terrestrial image data collection.

Second, various difficulties will be encountered in underwater photography. A camera used in water requires different construction from one used in the air. Aside from the mechanical considerations such as waterproofing, there are a lot of additional optical problems, such as absorption, scattering, and transparency of water. Therefore, the quality of underwater photographs will be severely deteriorated, so that the image based measurement accuracy will be degraded. This may only be solved, to some extent, by bringing the camera closer to the underwater subject or by employing a high performance illuminating device.

Third, underwater photography involves multi-media photogrammetry, which is a more critical factor that influences the development of underwater photogrammetry. In multi-media photogrammetry, the camera functions in the object space of water and the image space of air. This makes the imaging system deviate from a central perspective projection, which is a fundamental concept of photogrammetry. Therefore, a much more complicated photogrammetric model is required for precise photogrammetric measurement of underwater objects.

At a time where world-wide attention is turning to the exploration of ocean resources, and even though it is facing difficulties in its development, underwater photogrammetry has still become a valuable tool for visualizing and mapping details of the ocean floor, supporting and promoting research in marine environments.

Since the early 1970's there has been an increasing demand in applying photogrammetric measurement techniques to objects in the underwater environment. Initial work focused on underwater mapping of the sea bottom, location and mapping of shipwrecks and measurement of marine biological specimens (Pollio, 1971; Rosencratz, 1971; Torlegard and Lundalv, 1974). Years later, the growth of the offshore oil and gas industry has created new applications for underwater photogrammetry. A regular

inspection and maintenance program must be executed to ensure the safety of underwater oil or gas industrial operations. Some systems have evolved to meet this demand for underwater inspection based on the use of divers, underwater video, photographs and direct visual inspection. Therefore, the results produced are largely of a qualitative instead of quantitative nature. Welsh et al. (1980) demonstrated that photogrammetric technique could generate accurate measurements of the size and shape of a underwater object. This in turn has led to photogrammetry gaining acceptance as a means of producing reliable dimensional information in the underwater environment (Badwin and Newton, 1982; Fryer, 1982; Turner and Letherdale, 1982; Kristof et al., 1988; Letherdale and Turner 1983, 1993).

Any underwater inspection mission requires the use of work system to take the necessary equipment to the site and operate it there. Several systems are available and the selection of the system is dependent on cost factors, the nature of the task and the depth of water in which it is to be performed. Normally, the systems operate from a support ship and obtain underwater images for photogrammetric purposes.

Traditionally divers have taken on the role of underwater inspection and maintenance. Obviously, the operational site is restricted to a small, shallow underwater area. The alternative system replaces the diver with some form of underwater manned vehicle equipped with manipulator arms, sensors and positioning systems. They are especially suited for use in the deep and hostile environment. Since the 1980's, there has been an increasing emphasis on the development of autonomous unmanned vehicle (AUV). AUV's are highly maneuverable, able to enter restricted spaces and can operate for long periods without risk to human life. Gradually, AUV's are becoming a major tool in allowing cameras to access the sea bottom area for efficient imaging data gathering.

For underwater image acquisition, all the cameras are housed in a water tight and

pressure resistant housing. Most are fitted with wide angle lenses to cover a large field of view (Wakimoto, 1967).

Basically all underwater cameras are non-metric and it is necessary to calibrate them if they are to be used for photogrammetric purposes. The usual method of calibration is to photograph a three dimensional test object of known dimensions from the stand-off distance at which the camera will be used. This is performed either in a shallow water tank (Fryer, 1982) or on site in an underwater environment (Torlegard and Lundlav, 1974; Adams, 1982; Badwin, 1984). The latter method is favored, because it has the advantage of including local variables so that the differences from one site to another can be taken into account for during the photogrammetric analysis. For any underwater camera calibration, usually a control frame is used for a local coordinate system control and is often determined by the calibration schemes (Pollio, 1971, Fryer and Fraser, 1986).

Any method of photogrammetric analysis should produce results of an acceptable and consistent level of accuracy and retain simplicity of operation and versatility in application. The choice of any particular method is controlled by the environmental and operational considerations. Generally, there are two types of photography encountered in underwater photogrammetry.

One is to use airborne cameras to record underwater objects for photogrammetric processing. In this case, the quantitative use of photography is limited to downward-looking cameras in which a known altitude and angular field of view provides information on the area of coverage (Shmutter and Bonfiglioli, 1967; Rinner, 1969). This technique is still in use today (Rosman and Borland, 1986; MacDonald et al., 1992). Similarly, if the height-above-bottom, inclination angle, and field of view for a forward-looking camera are known, a perspective grid can be generated and superimposed on the image (Wakefield and Genin, 1987). In this case, the establishment of the photogrammetric model will encounter

orientation problems of multi-media photographs with curved boundaries (Okamoto, 1984). Furthermore, this method can only be performed in shallow water areas and no large scale information about the underwater environment will be obtained.

The other approach is to take photographs with both camera and object submerged. Extensive research has been carried out in this area on how to establish underwater photogrammetric models accurately and efficiently. McNeil (1968, 1969) did a lot of fundamental research on underwater imaging, which established a basis for underwater photogrammetric studies. Rosecrantz (1971) investigated various problems existing in the accuracy of sea bottom mapping with underwater photogrammetric procedures.

The underwater environment is one of uncertain and variable properties which are radically different from those of the terrestrial environment. Refractive index changes in water, resulting from variations in density, salinity, pressure and temperature, cannot be controlled. These variations and the non-metric character of underwater cameras suggest the use of an analytical procedure with on-site camera calibration instead of the use of analog procedures. Analytical methods of analysis are free from many of the limitations of analog methods. They are more flexible and have been widely accepted as an efficient way of underwater photogrammetric procedures (Badwin and Newton, 1982; 1984; Dorrer, 1986). Specifically, Höhle and Okamoto (1971, 1972) proposed a three-dimensional optical ray tracing based space-resection method to establish the analytical underwater photogrammetric model, which constitutes a starting point of this thesis research work.

Assuming all the planes of boundaries of two-media are strictly parallel, Höhle (1971) established a simple model to reconstruct the numerous disturbances caused by multi-media imaging. Later, Okamoto and Höhle (1972) extended this thinking to a more complicated situation, i.e., where one of the refractive surfaces is spherical. With this restriction, the mathematical model became much more complex. They formulated the

conceptual model but did not implement the whole design due to the difficulties in solving the large number of unknowns involved in the photogrammetric model. Therefore, the implementation of this type of multi-media photogrammetric model constitutes the main part of this research.

It is well known that the emergence of digital imaging techniques make photogrammetric systems evolve from hardcopy to softcopy (Gruen, 1989). Different from their applications in the aerial photogrammetry, CCD video cameras are primarily used for the guidance of underwater vehicles, such as providing an awareness of depth underwater (Przybilla, 1986). Most of the underwater photogrammetric tasks were carried out through photogrammetric processing of film-based images by means of highly precise, costly optical equipment without thinking about the accuracy required (Pollio, 1971; Badwin 1986). So far, only a limited number of softcopy photogrammetric systems have been developed for underwater applications (Turner and Yule, 1993). In general, the photogrammetric processing model of any system is highly dependent on the imaging system configuration. To implement the model presented in this research, a softcopy photogrammetric system is developed to improve the efficiency of quantitative processing of underwater video images.

## **1.2 Objectives of the research**

In this study, underwater stereo video images will be used as the data source for the quantitative analysis of objects in underwater environment. A geometrical optical technique - 3D skew ray tracing will be adopted to establish the photogrammetric model for the stereo image processing. The primary objectives are:

- to investigate the imaging properties in an underwater environment;
- to establish a photogrammetric model for calibrating an underwater CCD camera system

based on its configuration;

- to construct a measuring model for underwater object measurement;
- to build a processing system to enhance the quality of underwater video images for further photogrammetric processing;
- to generate a database for storing all the underwater measurement results;
- to develop a Graphical User Interface to integrate the underwater digital photogrammetric system.

### **1.3 Thesis outline**

There are four chapters in this thesis. The main contents of each chapter are briefly described as follows:

In Chapter 1, the necessity of this research is briefly introduced and the objectives of the research are then described.

Chapter 2 gives all the rigorous formulas used in establishing the underwater photogrammetric model. This chapter also gives the derivations of the calibration procedures and the space intersection. The methods used in the system evaluation will be introduced.

Chapter 3 introduces the experiment designed for the research. For data collection, the characteristics of CCD cameras will be described. For data processing, a concrete software design will be introduced. Based on field data and measurement results, the accuracy and efficiency of the system will be evaluated.

Chapter 4 makes conclusions for this research and indicates some recommendations for further studies on this topic.

## CHAPTER 2

# QUANTITATIVE ANALYSIS OF UNDERWATER STEREO VIDEO IMAGES

This chapter presents the establishment of the mathematical model for photogrammetric processing of underwater stereo video images. The emphasis will be put on the problems of multi-media and multi-lens in the reconstruction of photogrammetric model and imaging system calibration.

One of the major tasks in applying photogrammetric principles is the construction of a mathematical model to represent the relation of the image coordinates with the corresponding spatial coordinates, so that the three-dimensional information of an object can be determined through the measurement of its image points. The accuracy and precision of object measurements depend on the quality of the hardware and software used in both data collection and data processing. Accordingly, the main problem lies in how to derive the mathematical model and obtain all essential elements related to measuring requirements through detailed analysis of the specific imaging system.

Usually, in computational photogrammetry, the path of each light ray may be described by a mathematical expression which is a function of the position of the point in the object space, position of the image point in the image plane, position of the exposure center in the ground reference system, and direction of the optical axis of the camera. Traditionally, for aerial or terrestrial photogrammetry, the imaging procedure follows the central perspective geometry. In this case, if the perspective geometry of the camera has

been determined by camera calibration, the position of the camera and its attitude with respect to the ground control reference system can be determined. Once the orientation of both of the images of a stereo pair is known, the position of any object point, which can be located in the overlap area of the image pair, may be computed as the point of intersection of two imaging rays. In an underwater situation, refraction of imaging ray exists and the central perspective geometry of the imaging procedure will not hold. Therefore, the establishment of the mathematical model and calibration procedure will be much more complicated compared to conventional photogrammetric methods.

To apply the photogrammetric techniques in an underwater environment in order to obtain quantitative information about the underwater objects, based on particular imaging system configurations, a rigorous photogrammetric model is proposed. The practical considerations of calibration design are also included. In the remainder of this chapter, some implementation considerations will be discussed.

## **2.1 Conceptual model**

It is known that stereo images can be used to produce a three-dimensional visual model with characteristics analogous to those of actual features viewed using true binocular vision. One of the primary applications of stereo images in photogrammetry is to be an interpretation aid in recognizing the three-dimensional form of an object through photogrammetric techniques. Throughout this chapter it is assumed that the image pair used for the photogrammetric processing is taken by a pair of underwater stereo video cameras. Therefore, the imaging geometry needs to be analyzed based on a practical imaging system configuration and the special condition in the underwater environment.

Figure 2.1 shows the conceptual model of the underwater imaging system to be used for underwater image data collection. For stereo vision, the imaging system consists

of a pair of CCD cameras joined together so that the relative position of the two CCD cameras can be fixed. The exposure stations are represented as  $O$  and  $O'$  respectively.  $I$  and  $I'$  are the image planes, and  $f$  and  $f'$  correspond to the focal lengths.

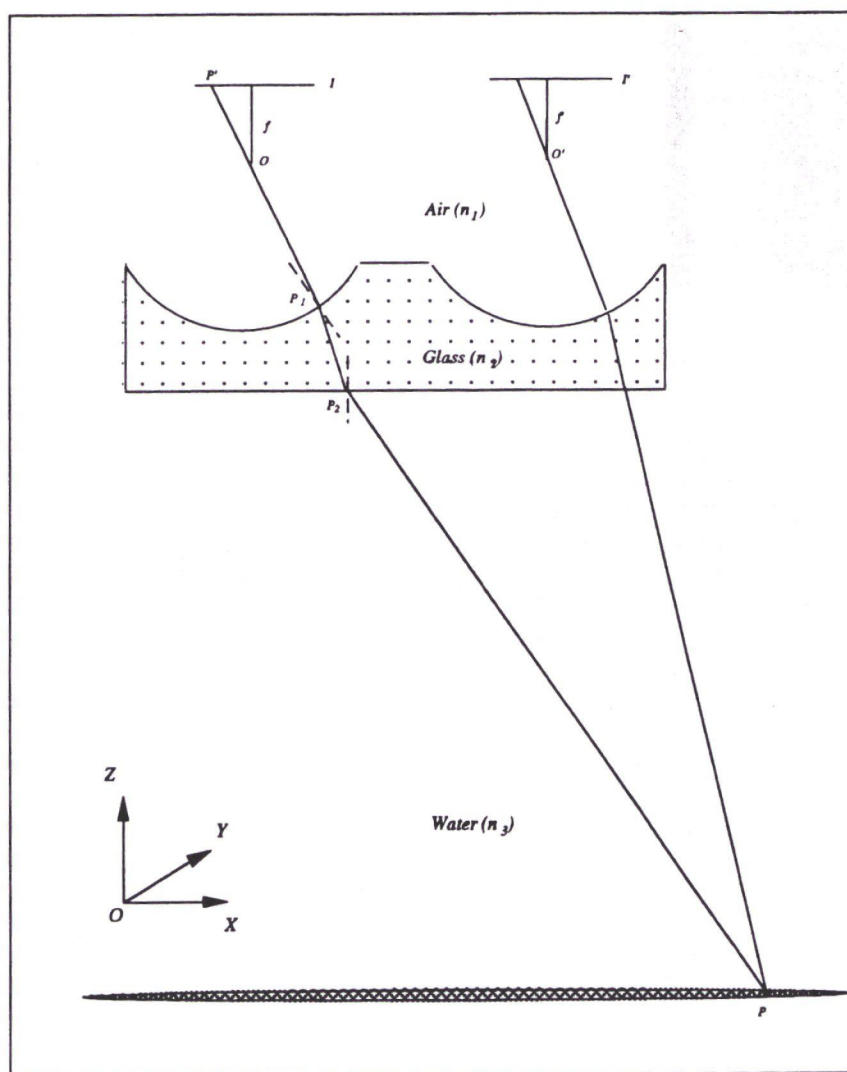


**Figure 2.1** An overview of the underwater imaging

In general, the underwater imaging system is assembled in a water-proof container with a piece of cover glass in the front window. Then the refraction of light takes place at the boundary surface between different media, thus giving rise to various multi-media problems for photogrammetric processing of the images. Therefore in selecting an imaging

system the difference of refractive index between the object and image area should be considered. In the situation shown in Figure 2.1, there is an integrated cover lens in front of each CCD camera on the cover window to provide a large view field for the imaging system.

The situation in taking images with the aforementioned camera configuration may be quite different from conventional photogrammetry. The camera functions in the object space of water and the image space of air, between which is the cover lens. The object point  $P$  is imaged at the point  $P'$ . The imaging ray passes through three media: water, glass and air, which are signified by their indices of refraction  $n_1$ ,  $n_2$ , and  $n_3$  respectively. It is apparent that, at the boundary surface between two media, ray refraction is involved. This makes the system deviate from a central perspective projection, which is a fundamental concept of photogrammetry. In this case, the establishment of an underwater photogrammetric model is quite different from the traditional one.

## **2.2 Multi-media photogrammetric model**

Mathematical model is an elementary preparation for the quantitative analysis of stereo images in an analytical photogrammetric application. Conventional methods, such as using collinearity equations, will not be practical in the underwater multi-media situation. Therefore, a universal analytical strategy, three-dimensional optical ray tracing is proposed to establish rigorous equations to model the underwater imaging procedure.

### **2.2.1 Image geometry**

In geometric optics, light ray is considered to travel through homogeneous media in straight lines. When light rays pass from one homogenous transparent medium to a second such medium having a different refractive index, the path of the light ray is bent or refracted unless it intersects the second medium normal to the interface. If the intersection occurs

obliquely, as shown in Figure 2.2, then the angle of incidence,  $\theta$  is related to the angle of refraction,  $\theta'$  by the law of refraction, or called Snell's law of refraction. This law is stated as follows:

$$n \sin \theta = n' \sin \theta' \quad (2.1)$$

where  $n$  is the refractive index of the first medium and  $n'$  is the refractive index of the second medium.

In Figure 2.2,  $IA$  is the incident light ray,  $AR$  is the refracted ray, and  $NN'$  is the normal to the interface between the two media. The angles  $\theta$  and  $\theta'$  are measured from  $NN'$  to the incident ray and refracted rays, respectively. A light ray is refracted such that the incident and refracted rays lie in the same plane.

The refractive index for any transparent substance is determined through experimental measurement. Typical values for indices of refraction of common media are vacuum, 1.000; air, 1.0003; water, 1.33; and glass, 1.5 to 1.7.

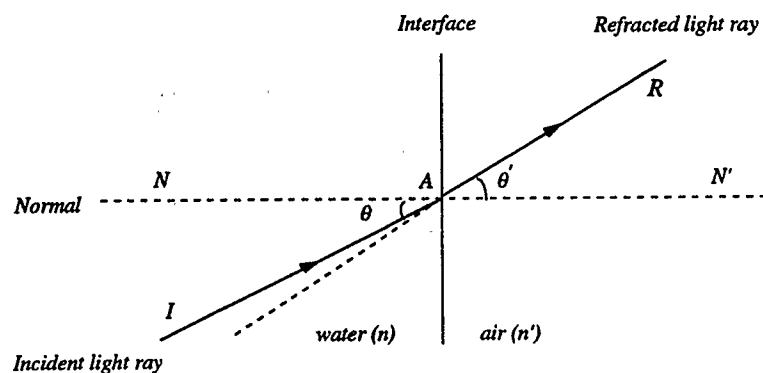


**Figure 2.2** Refraction of light rays

Usually, the lens, for underwater use, has a plane-parallel glass cover in front (Wakimoto, 1968). In this case, the field angle covered is reduced to about 3/4, compared

with that covered in the air. To prevent the angular field from decreasing, there is a method in which a plane-concave lens can be properly placed in front of the camera to increase the divergence of the refractive ray, as shown in Figure 2.1. In this case, the plane-concave lens is designed with its spherical surface center nearly coincident with the front principal point of the CCD camera lens. Therefore, the light rays passing through the center of the sphere will undergo no refraction, keeping the incidence angle normal. Thus the underwater imaging field angle will be increased compared to that with the plane glass cover (Figure 2.3). If the imaging system shown in Figure 2.1 is to be designed in this ideal case, with sufficient knowledge of the cameras and cover lenses, a compound lens system could be considered for the whole imaging system modeling. In this case, the photogrammetric model could be constructed much more simply and easily

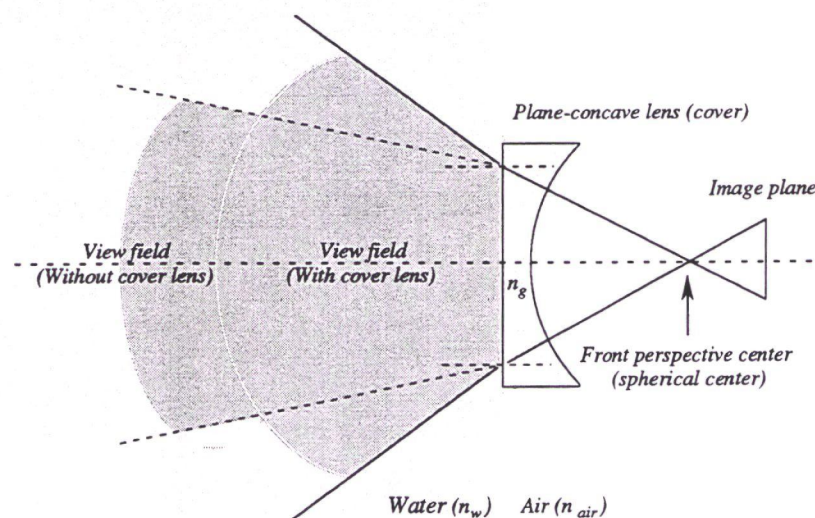


**Figure 2.3** A lens element may be added to enlarge the angular field

However, the practical designing and manufacturing of the imaging system shown in Figure 2.1 might not meet the requirements for precise underwater image taking. This is mainly due to the following factors:

- The size of the cover lens is very big which is hard to make as an ideal imaging component.
- Since the cover lens is integrated into the watertight window which is moveable, it is difficult to make the cover lens well aligned with the camera lens.

Apparently there are a number of uncertainties existing in the front cover lens. If a compound lens scheme is used to construct the underwater imaging model, it is quite difficult to form a rigorous photogrammetric model which can precisely reflect the geometric relation between an object and its corresponding image point.

### 2.2.2 Landbased vs. underwater photogrammetry

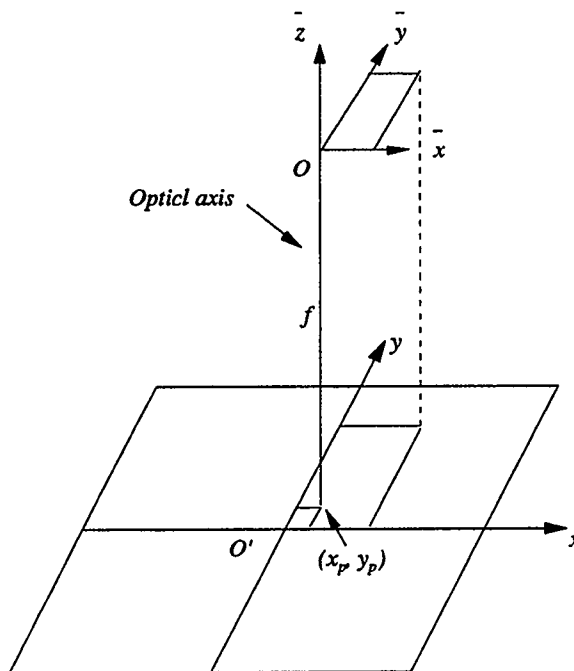
One of the main approaches to the study of photogrammetric application requires the establishment of a mathematical model for transformation from a 2-D image coordinate system to the three-dimensional object space coordinate system (Brown, 1957).

Figure 2.4 illustrates a three-dimensional image coordinate system commonly used to define the location of image points with respect to the exposure station. It is defined by the axes  $\bar{x}$ ,  $\bar{y}$  and  $\bar{z}$  with the origin of the system located at the exposure station ( $O$ ). The  $\bar{z}$  axis coincides with the optical axis of the camera and is positive along the direction towards the image plane of the camera. The  $\bar{x}$  axis is parallel to the  $x$  axis on the image plane. The  $\bar{y}$  axis is parallel to the  $y$  axis on the image plane. Therefore, the  $\bar{x}$ - $\bar{y}$  plane is parallel to the image plane. The position of the principal point can be defined by its coordinates  $x_p$  and  $y_p$ . The position of an image point can be defined by its coordinates  $x$  and  $y$ . The position of the same image point with respect to the exposure station ( $O$ ) is then defined by its image coordinates  $\bar{x}$ ,  $\bar{y}$  and  $\bar{z}$  as follows:

$$\bar{x} = x - x_p \quad (2.2a)$$

$$\bar{y} = y - y_p \quad (2.2b)$$

$$\bar{z} = -f \quad (2.2c)$$



**Figure 2.4** An image coordinate system

In general photogrammetric problems, the relationship between image coordinate system and object-space system is expressed by the collinearity condition equations which are the most useful equations in photogrammetry (Wolf, 1974). The collinearity condition equations express the fact that the image point, the center of projection, and the object point are all on one straight line. Collinearity equations are used in analytical photogrammetry as a dominant approach to the relationship between correct image coordinates and the object-space coordinates. This relationship is expressed as follows (Wolf, 1974):

$$\begin{pmatrix} x_i - x_p \\ y_i - y_p \\ -f \end{pmatrix} = \lambda_i \begin{pmatrix} m_{11} & m_{12} & m_{13} \\ m_{21} & m_{22} & m_{23} \\ m_{31} & m_{32} & m_{33} \end{pmatrix} \begin{pmatrix} X_i - X_0 \\ Y_i - Y_0 \\ Z_i - Z_0 \end{pmatrix} \quad (2.3)$$

where:

$x_i, y_i$  are image coordinates of point  $i$ ;

$x_p, y_p$  are the coordinates of the principal point relative to image coordinate system;

$X_i, Y_i, Z_i$  are object-space coordinates of point  $i$ ;

$f$  is the focal length of the camera;

$\lambda_i$  is a scale factor which has different values for different points;

$X_0, Y_0, Z_0$  are the object-space coordinates of the exposure station;

$m_{ij}$  are the coefficients of the rotation matrix for transformation.

Equation (2.3) can be expressed in the following form:

$$x_i - x_p = -f \frac{m_{11}(X_i - X_0) + m_{12}(Y_i - Y_0) + m_{13}(Z_i - Z_0)}{m_{31}(X_i - X_0) + m_{32}(Y_i - Y_0) + m_{33}(Z_i - Z_0)} \quad (2.4a)$$

$$y_i - y_p = -f \frac{m_{21}(X_i - X_0) + m_{22}(Y_i - Y_0) + m_{23}(Z_i - Z_0)}{m_{31}(X_i - X_0) + m_{32}(Y_i - Y_0) + m_{33}(Z_i - Z_0)} \quad (2.4b)$$

The relationship between  $(x_i, y_i)$  and  $(X_i, Y_i, Z_i)$  can be determined if the coefficients in the above two Equations (2.4a) and (2.4b) are known. These coefficients are the interior orientation parameters  $(x_p, y_p, f)$ , the exposure station coordinates  $(X_0, Y_0, Z_0)$  and the three orientation angles  $(\omega, \phi, \text{and } \kappa)$  which define the elements of rotation matrix  $m_{ij}$ .

Collinearity condition equations are considered as the basic concept in photogrammetric theory, therefore, they are applied to the analytical solution of almost every aerial or terrestrial photogrammetry problem by means of space resection (Wolf, 1974). Also, its application can be seen in Section 2.3 for the camera system calibration. However, it should be specified that collinearity equations take effect specifically under restrictive conditions, i.e. the imaging procedure should precisely follow the central

projection rule, which shows its limitations in the underwater photogrammetry.

With the imaging system proposed in Figure 2.1, which introduces the case of multi-media photogrammetry, from object point  $P$  to its corresponding point  $P'$ , the ray passes through three media, and each time the ray refracts at the boundary of two different media following the law of refraction. Consequently, the object point, perspective center and the corresponding image point are obviously not in a straight line. Therefore, collinearity equations are not satisfied in this application and cannot be chosen as a means for the construction of the rigorous underwater photogrammetric model.

In order to model the imaging system analytically, basically there are two methods that could be used: experimental method and rigorous formulation method.

With experimental adjustment, a polynomial approximation for lens distortion correction is often implemented for image distortion when mapping the object space to the image space (Karara and Abdel-Aziz, 1974). Usually it is assumed that collinearity equations are still satisfied, and some complicated situations disturbing the imaging procedure, such as multi-media and multi-lens interference, can be ascribed to the image distortion. In this case, as constructing the observation equations, the image distortion could be represented by two polynomials:

$$\delta x = f(x, y) \quad (2.5a)$$

$$\delta y = g(x, y) \quad (2.5b)$$

where:

$x, y$  are image coordinates of a point;

$\delta x, \delta y$  are image distortions at point  $(x, y)$ .

Considering the application of a complicated imaging system for photogrammetric

purposes, experimental method possesses the following advantages:

- It is easy and simple to construct the mathematical model without the consideration of the numerous deviations involved;
- It requires small amounts of calculation to determine those coefficients of the polynomials.

Therefore, experimental method combined with collinearity equations has been widely adopted as a tool for the construction of underwater photogrammetric models (Leatherdale and Turner, 1983; Welham, 1984; Tolegard and Lundalv, 1984; Fryer and Fraser, 1986).

However, there are too many options for the formation of approximation polynomial, especially in the underwater photogrammetric field which has a much more complicated imaging system and imaging environment. The polynomial equation used could be linear or non-linear, dependent or independent along x and y directions, and low order or high order. Also, according to the imaging system itself, the correlation between the multi-media and multi-lens effects should be taken into consideration. Thus, it is quite subjective and requires a lot of experimental experience to obtain appropriate polynomial models. Due to missing information on the exact refraction index of water at the operation time, it is hard to acquire a rigorous and universal model to describe a complicated imaging system using the experimental approximation method.

As long as we have a certain prior knowledge about the imaging system, an analytical rigorous formulation could be derived. In general terms, analytical photogrammetry can be considered as the mathematical transformation between an image point in one rectangular coordinate system (image space) and an object point in another rectangular coordinate system (object space) (American Society of Photogrammetry, 1980).

The most important property of the analytical technique is that the basic concept of analytical photogrammetry is valid for all applications of photogrammetry (e.g., terrestrial, aerial, non-topographic) using any sensing device (frame camera, panoramic camera, raster scan, etc.) to record directional information to objects in any media (air, water, etc.). Karara and Marks (1968) have proved that the analytical method is a very versatile, accurate and flexible approach in photogrammetric applications

However, for analytical photogrammetry, there is no such complex theory which can handle all situations. Usually, analytical photogrammetric theory can be broken into a number of separated theories each adapted to particular situations. For example, while the equations for central projection are suitable, with only slight modification, in aerial photogrammetry, they often require great modification to be applicable in some other photogrammetric fields, such as in a close-range photogrammetry. This is particularly true when images are taken with a special lens system, such as the imaging system shown in Figure 2.1.

From an operational point of view, there are generally two basic phases of an analytical operation:

- defining the image geometry;
- reconstructing the detailed photogrammetric model.

Due to the complexity of the proposed imaging system in an underwater environment, the existing traditional model will not be applicable in defining the imaging geometry. Therefore, based on the theory of geometrical optics, a three-dimensional skew ray tracing technique could be considered as a universal method to define the image geometry (Born and Wolf, 1975). Obviously, the image geometry essentially affects the reconstruction of the photogrammetric model, which results in a good description of

relations between the images and the object by means of interior, exterior orientation parameters and some other related parameters of the imaging system.

For underwater photogrammetry, the establishment of multi-media photogrammetric model has been investigated (Höhle, 1971; Okamoto and Höhle, 1972). But mathematical procedures for the general measuring application have hardly been discussed (Okamoto, 1982, 1984). In this research, the basic idea is to find an appropriate model applying a three-dimensional optical ray tracing procedure into a photogrammetric model for the object measurement.

### **2.2.3 Ray tracing**

Ray tracing comes from geometric optics and is used as a method to determine the path of light rays through an optical system with fundamental laws of geometrical optics.

With an imaging system, a light ray originating from an arbitrary selected point in object space with a given starting propagation direction can be traced through the optical system by the successive use of the law of refraction. Originating from the same object point, this procedure can be repeated. Based on the characteristics of light rays propagation, algebraic and trigonometric expressions governing the precise path of a chosen initial ray through an optical system, can be derived as ray tracing equations. After application of these equations one can determine the exact intercept ray on the image plane or indeed on any chosen image surface. Usually, ray tracing technique is used in lens design to detect image distortion and aberration with reference to an ideal optical system (Herzberger, 1958). Using a perfect imaging system, all rays in the image space should intersect at a common image point. Also, the application of the above mentioned procedure to all points on a straight line in object space should result in a straight line in image space with a perfect imaging system. A deviation from this situation is called lens distortion and

may also be detected by ray tracing (Herzberger, 1958; Cox, 1964).

According to the principle of Fermat (Born and Wolf, 1975), each component of an optical system has to be selected in a way that all rays propagating from a point in object space to the corresponding image point have equal optical path length. Starting from the basic principle of geometrical optics, the ray tracing can be applied in a modified manner to develop an algorithm for the purpose of multi-media photogrammetry.

In Figure 2.5, a light ray originating at a point  $P_0 (X_0, Y_0, Z_0)$  propagates to  $P_{p+1} (X_{p+1}, Y_{p+1}, Z_{p+1})$  through  $p$  refractive surfaces, which are separated homogenous media with refractive indices  $n_i (n_i \neq n_{i+1})$ .  $\overline{P_{i-1}P_i}$  is represented as an auxiliary quantity  $\rho_i$ , where

$$\rho_i = \sqrt{(X_i - X_{i-1})^2 + (Y_i - Y_{i-1})^2 + (Z_i - Z_{i-1})^2}. \quad (2.6)$$

Generally, a light ray between  $P_0$  to  $P_{p+1}$  will be refracted at every refractive surface. In this case, it is assumed that the coordinates of  $P_0$  and  $P_{p+1}$  are given, as well as the refractive surfaces by their implicit functions  $F_i = F_i(X_i, Y_i, Z_i)$ ,  $i = 1, 2, \dots, p$ . All the parameters are defined in the three-dimensional rectangular coordinate system. Assuming that the intersection points at each refractive surface are  $P_1, P_2, \dots, P_p$ , a group of derivations can be obtained.

Each intersection point  $P_i$  is situated on the corresponding refractive surface  $F_i$ :

$$F_i(X_i, Y_i, Z_i) = 0. \quad (2.7)$$

At each refractive point the law of refraction is applied:

$$n_i \sin \theta_i = n_{i+1} \sin \theta_i' \quad (2.8)$$

In order to trace the ray, it is necessary to find  $\theta_i$  and  $\theta_i'$  in terms of the incident ray, the normal to the surface and refracted ray. For  $\theta_i$ , it can be obtained from:

$$\cos \theta_i = \alpha_i \lambda_i + \beta_i \mu_i + \gamma_i \nu_i$$

(2.9)

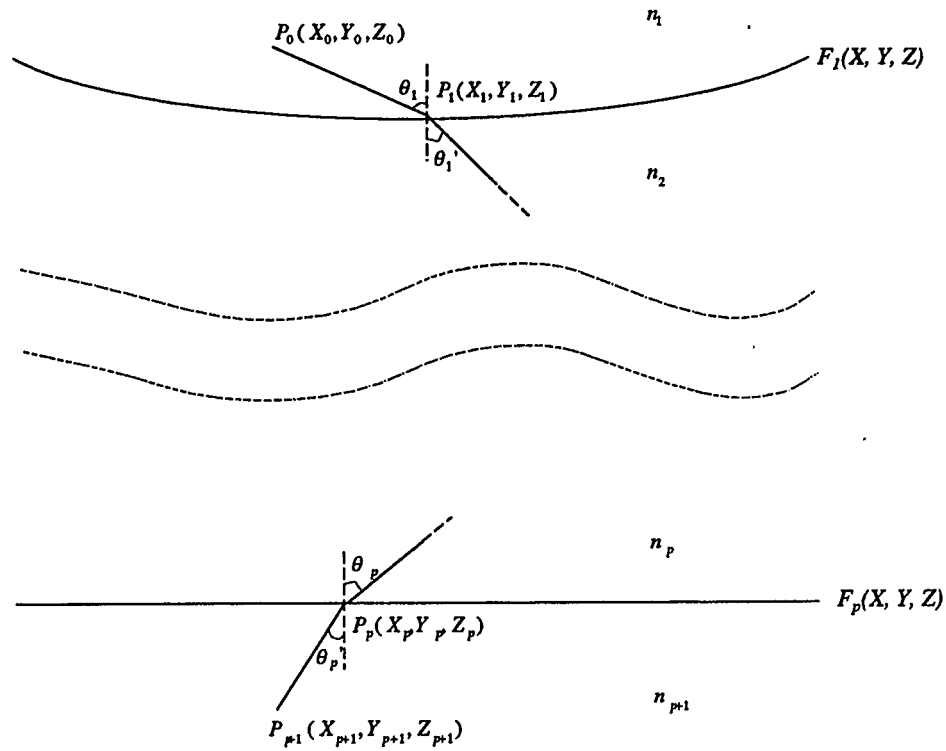


**Figure 2.5** Overview of ray tracing through  $p$  refractive surfaces

where  $\alpha_i, \beta_i, \gamma_i$  are the direction cosines of the ray from  $P_{i-1}$  to  $P_i$  and  $\lambda_i, \mu_i, \nu_i$  are the elements of the normal vector of refractive surface  $F_i$  at point  $P_i$ .  $\alpha_i, \beta_i, \gamma_i$  can be derived from:

$$\begin{pmatrix} \alpha_i \\ \beta_i \\ \gamma_i \end{pmatrix} = \frac{1}{\rho_i} \begin{pmatrix} X_i - X_{i-1} \\ Y_i - Y_{i-1} \\ Z_i - Z_{i-1} \end{pmatrix} \quad (2.10)$$

and  $\lambda_i, \mu_i, \nu_i$  can be expressed by:

$$\begin{pmatrix} \lambda_i \\ \mu_i \\ \nu_i \end{pmatrix} = \left[ \left( \frac{\partial F_i}{\partial X_i} \right)^2_{P_i} + \left( \frac{\partial F_i}{\partial Y_i} \right)^2_{P_i} + \left( \frac{\partial F_i}{\partial Z_i} \right)^2_{P_i} \right]^{-\frac{1}{2}} \begin{pmatrix} \left( \frac{\partial F_i}{\partial X_i} \right)_{P_i} \\ \left( \frac{\partial F_i}{\partial Y_i} \right)_{P_i} \\ \left( \frac{\partial F_i}{\partial Z_i} \right)_{P_i} \end{pmatrix} \quad (2.11)$$

Similarly, as in Equation (2.9),  $\theta_i'$  can be obtained so that

$$\cos \theta_i' = \alpha_{i+1} \lambda_i + \beta_{i+1} \mu_i + \gamma_{i+1} \nu_i \quad (2.12)$$

where  $\alpha_{i+1}, \beta_{i+1}, \gamma_{i+1}$  are the direction cosines of the refracted ray or the incident ray referring to the next refractive surface.

Using Equations (2.8) (2.9) and (2.12) plus the property that the incident ray, the normal and the refracted ray lie in the same plane it can be derived that (Appendix A)

$$n_{i+1} \begin{pmatrix} \alpha_{i+1} \\ \beta_{i+1} \\ \gamma_{i+1} \end{pmatrix} = n_i \begin{pmatrix} \alpha_i \\ \beta_i \\ \gamma_i \end{pmatrix} - (n_i \cos \theta_i - n_{i+1} \cos \theta_i') \begin{pmatrix} \lambda_i \\ \mu_i \\ \nu_i \end{pmatrix} \quad (2.13)$$

Thus the refracted ray can be calculated if we know the direction cosines of the incident ray, the point of interception of the incident ray with the surface and the direction cosines of the normal to the surface at that point.

In Figure 2.5, an image point and its corresponding space object point can be considered as the starting point  $P_o$  and the ending point  $P_{p+l}$ , respectively. The fundamental characteristic of an image taken by a camera is that each point on the image corresponds to a unique point in the object scene. A definite geometric relationship exists between the relative spatial positions of the image points and their corresponding positions in the three-dimensional space. From the above analysis, their geometrical relationship can

be represented through the full ray tracing procedure in a multi-media environment. In multi-media imaging environment, the basic formulas (Equations 2.6-2.13) for ray tracing can be treated as a kind of framework for multi-media photogrammetric application.

The refractive surfaces are given in a general function (Equation 2.7) without concerning shape and spatial position. If the specific physical information of the refractive surface can be acquired, suitable functions could be used to form a rigorous mathematical model for the photogrammetric purpose.

#### **2.2.4 Establishment of underwater photogrammetric model**

As discussed in the last sub-section, optical ray tracing can be implemented in the analysis of the imaging procedure using the optical system shown in Figure 2.1. One of the major advantages of ray tracing is that as long as the initial conditions and parameters of an optical system can be obtained, one can obtain analytic expressions for the coordinates of the intercept of a ray on the image surface as a function of those parameters of the optical system and the object points. Nevertheless, for any given optical system with known constants and features, one can trace a pattern of rays sufficient to provide a knowledge of the performance of the system in terms of a photogrammetric method.

Comparing the special imaging configuration described in Figure 2.1 with the general case multi-media imaging shown in Figure 2.5, only three media are involved in the imaging procedure. A light ray between image point  $P'$  and its corresponding object point  $P$  is bent twice. The first refraction is on the boundary of air and inner spherical surface of the cover lens at point  $P_1$  and the second is on the boundary of water and outer planar surface of the cover lens at point  $P_2$ .

To perform 3D image ray tracing, a spatial coordinate system and an image coordinate system may be set up to mathematically represent the ray propagation. In

computational photogrammetry, the locations of points in the object space may be defined by a three-dimensional rectangular coordinate system. The origin and orientation of the coordinate system may be arbitrarily defined. In this case, the position of the exposure station  $O$  can be defined by its coordinates  $X_0$ ,  $Y_0$ , and  $Z_0$ . Similarly, locations of the first and second intersection points  $P_1$  and  $P_2$ , and the object can be defined as  $(X_1, Y_1, Z_1)$ ,  $(X_2, Y_2, Z_2)$  and  $(X_p, Y_p, Z_p)$  respectively. The image coordinate system is chosen as described in Figure 2.4.

Through the analysis of ray tracing in Section 2.2.3, in order to perform a full three dimensional ray tracing, the basic procedures should be set up as follows:

- Set up an incident ray;
- Define refractive surfaces;
- Calculate intersection point with each refractive surface;
- Determine normal at intersection surface;
- Calculate incident angle and, thus, refractive angle;
- Calculate the refracted ray ready for the next surface;
- Repeat the steps for following surfaces;
- Use information of all rays to calculate the object space positions from corresponding image coordinates.

In order to develop a detailed functional model which is able to define the relationship of one image point and its object point, three steps can be followed by integrating the ray tracing algorithm (Figure 2.6):

1) Determination of the first intersection point  $P_1(X_1, Y_1, Z_1)$

With the definition of the coordinate systems, the incident ray from image point  $P'$

$(x, y)$  passing through the exposure station  $O$ , its direction cosines can be obtained from:

$$\begin{pmatrix} \alpha_1 \\ \beta_1 \\ \gamma_1 \end{pmatrix} = \frac{1}{\rho_0} R \begin{pmatrix} x \\ y \\ -f \end{pmatrix} \tag{2.14}$$

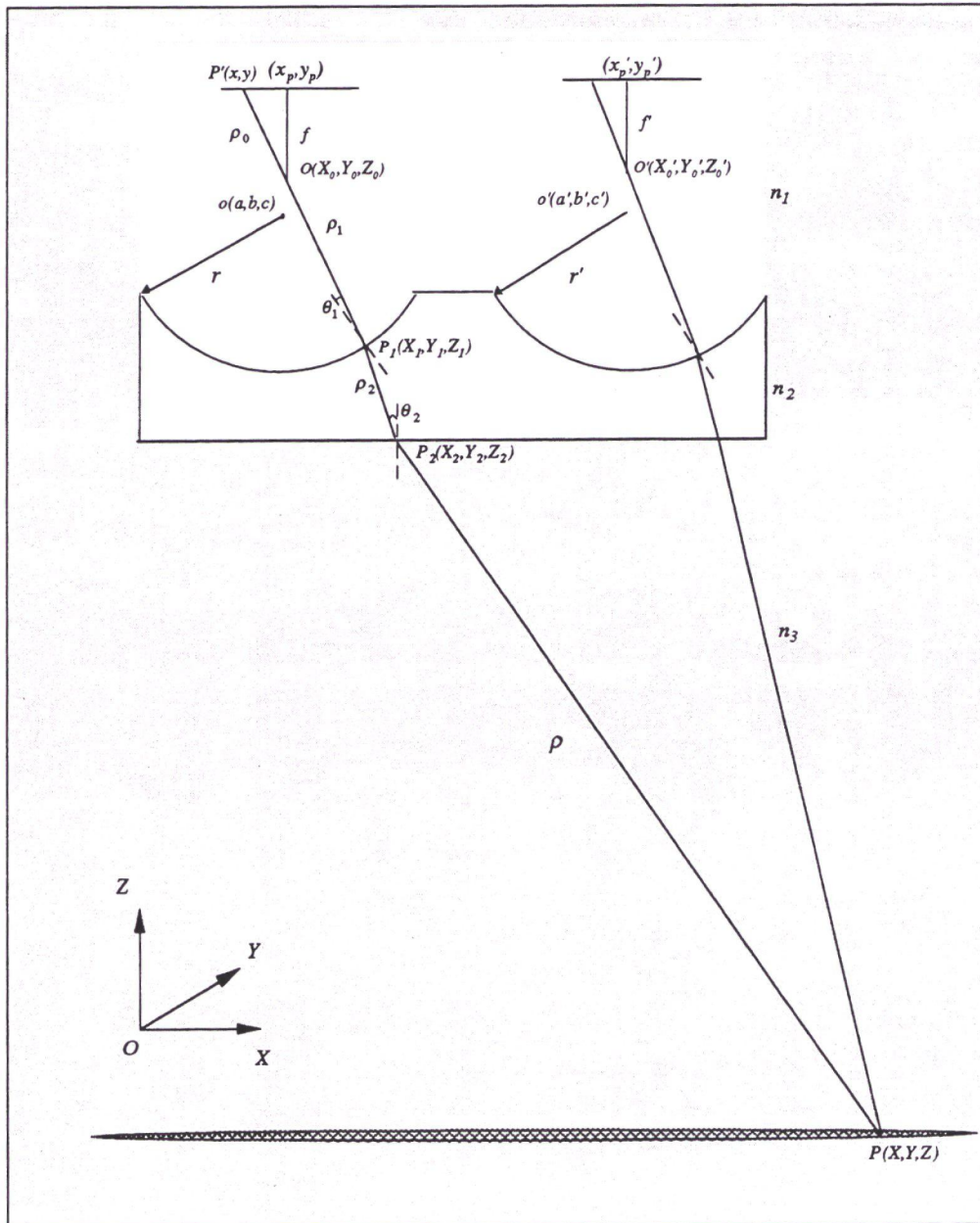


**Figure 2.6** 3D ray tracing for the underwater imaging system

where:

$\rho_0$  is equal to  $\overline{P'O}$  which is  $\rho_0 = (x^2 + y^2 + f^2)^{1/2}$ ;

$R$  is the rotation matrix from the image coordinate system to the object space coordinate system;

$f$  is the focal length of the camera.

The first refractive surface is considered as a sphere, which can be defined as

$$(X - a)^2 + (Y - b)^2 + (Z - c)^2 = r^2 \quad (2.15)$$

where

$a, b, c$  are the coordinates of the center of the sphere;

$r$  is the radius of the sphere.

Let  $\rho_1$  represent  $\overline{OP_1}$  and it assumes the following value:

$$\rho_1 = -[\alpha_1(X_0 - a) + \beta_1(Y_0 - b) + \gamma_1(Z_0 - c)] + \sqrt{[\alpha_1(X_0 - a) + \beta_1(Y_0 - b) + \gamma_1(Z_0 - c)]^2 - [(X_0 - a)^2 + (Y_0 - b)^2 + (Z_0 - c)^2 - r^2]} \quad (2.16)$$

Therefore, coordinates of  $P_1$  can be provided as functions of  $\rho_1$  which depend on the boundary surface:

$$\begin{pmatrix} X_1 \\ Y_1 \\ Z_1 \end{pmatrix} = \rho_1 \begin{pmatrix} \alpha_1 \\ \beta_1 \\ \gamma_1 \end{pmatrix} + \begin{pmatrix} X_0 \\ Y_0 \\ Z_0 \end{pmatrix}. \quad (2.17)$$

2) Determination of the second intersection point  $P_2(X_2, Y_2, Z_2)$

Cosines  $(\lambda_1, \mu_1, \nu_1)$  of the normal to the spherical surface at point  $P_1$  are obtained

using Equation 2.11:

$$(\lambda_1, \mu_1, \nu_1) = \left( \frac{X_1 - a}{r}, \frac{Y_1 - b}{r}, \frac{Z_1 - c}{r} \right) \quad (2.18)$$

From Equation (2.13), the change in direction due to refraction by the cover lens on the spherical surface is expressed as:

$$\begin{pmatrix} \alpha_2 \\ \beta_2 \\ \gamma_2 \end{pmatrix} = \frac{n_1}{n_2} \begin{pmatrix} \alpha_1 \\ \beta_1 \\ \gamma_1 \end{pmatrix} - \left( \frac{n_1}{n_2} \cos \theta_1 - \sqrt{1 - \left( \frac{n_1}{n_2} \right)^2 + \left( \frac{n_1}{n_2} \cos \theta_1 \right)^2} \right) \begin{pmatrix} \lambda_1 \\ \mu_1 \\ \nu_1 \end{pmatrix} \quad (2.19)$$

where:

$n_1$  and  $n_2$  are the refractive indices of air and glass, respectively

$$\cos \theta_1 = \alpha_1 \lambda_1 + \beta_1 \mu_1 + \gamma_1 \nu_1. \quad (2.20)$$

The second refractive surface is considered as a plane, which can be defined as

$$dX + eY + Z + g = 0. \quad (2.21)$$

Let  $\rho_2$  represent  $\overline{P_1 P_2}$  and it assumes the following value:

$$\rho_2 = \frac{dX_1 + eY_1 + Z_1 + g}{d\alpha_2 + e\beta_2 + \gamma_2}. \quad (2.22)$$

Similarly, coordinates of  $P_2$  can be obtained as

$$\begin{pmatrix} X_2 \\ Y_2 \\ Z_2 \end{pmatrix} = \rho_2 \begin{pmatrix} \alpha_2 \\ \beta_2 \\ \gamma_2 \end{pmatrix} + \begin{pmatrix} X_1 \\ Y_1 \\ Z_1 \end{pmatrix}. \quad (2.23)$$

3) Determination of the object point  $P(X_p, Y_p, Z_p)$

Cosines  $(\lambda_2, \mu_2, \nu_2)$  of the normal to the planar surface at point  $P_2$  are obtained using Equation (2.11):

$$(\lambda_2, \mu_2, \nu_2) = \frac{1}{(d^2 + e^2 + 1)^{1/2}} (d, e, 1) \quad (2.24)$$

From Equation (2.13), the change in direction due to refraction by the cover lens on the planar surface is expressed as:

$$\begin{pmatrix} \alpha_3 \\ \beta_3 \\ \gamma_3 \end{pmatrix} = \frac{n_2}{n_3} \begin{pmatrix} \alpha_2 \\ \beta_2 \\ \gamma_2 \end{pmatrix} - \left( \frac{n_2}{n_3} \cos \theta_2 - \sqrt{1 - \left(\frac{n_2}{n_3}\right)^2 + \left(\frac{n_2}{n_3} \cos \theta_2\right)^2} \right) \begin{pmatrix} \lambda_2 \\ \mu_2 \\ \nu_2 \end{pmatrix} \quad (2.25)$$

where:

$n_3$  is the refractive index of water

$$\cos \theta_2 = \alpha_2 \lambda_2 + \beta_2 \mu_2 + \gamma_2 \nu_2. \quad (2.26)$$

Assuming  $\rho$  denotes  $\overline{P_2P}$ , coordinates of the object point  $P$  can be obtained as

$$\begin{pmatrix} X \\ Y \\ Z \end{pmatrix} = \rho \begin{pmatrix} \alpha_3 \\ \beta_3 \\ \gamma_3 \end{pmatrix} + \begin{pmatrix} X_2 \\ Y_2 \\ Z_2 \end{pmatrix}. \quad (2.27)$$

Alternatively, an extended mathematical model for intersection can be formed:

$$G_1 = \gamma_3 X - (Z - Z_2) \alpha_3 - \gamma_3 X_2 = 0. \quad (2.28a)$$

$$G_2 = \gamma_3 Y - (Z - Z_2) \beta_3 - \gamma_3 Y_2 = 0 \quad (2.28b)$$

Equation (2.28) describes the functional model for the relationship of the image space and the object space in the specified multi-media photogrammetry. Through the imaging system calibration, the model can be used to determine the position and shape of light refracting surfaces, and refraction indices, as well as interior and exterior orientations of the imaging system. Also, the model can be used to set up a stereo photogrammetric model for space intersection based on the calibration results.

## **2.3 Imaging system calibration**

In the previous section, a mathematical photogrammetric model for the whole imaging system has been established. In order to make the system suitable for the underwater object measurement based on stereography, imaging system calibration needs to be performed. The calibration should be emphasized since a pair of CCD cameras with no high-grade optics were used and a pair of cover lenses were included in the imaging system. With the investigations of the properties of the CCD camera, several aspects are considered for the imaging system calibration, including a separate step calibration procedure, lens principal point location, lens distortion of CCD camera, ray bending parameters, as well as multi-lens function.

### **2.3.1 Calibration procedure**

A photogrammetric model has been built up through optical ray tracing in the Section 2.2 for the imaging system shown in Figure 2.1. In order to calculate three dimensional coordinates in object space through photogrammetric operations based on the observation Equations (2.28), a number of unknown parameters of the whole imaging system in the equations need to be determined. Basically, the purpose of the imaging system calibration is to obtain those unknowns and to reconstruct the precise geometry of the imaging rays that entered the cameras. These imaging rays form the two-dimensional measurement of points on the resulting images (Wolf, 1974).

In order to establish a reference system for all photogrammetric data, a local frame with control targets is set up for the calibration. The calculation of all parameters by using a collection of control points on the frame in the object space can be performed.

The unknown parameters of the photogrammetric model for the stereo imaging system include (Figure 2.6):

- 8 interior parameters for CCD cameras, including locations of the principal points  $(x_p, y_p, x'_p, y'_p)$ , the focal lengths  $(f, f')$  and the y-scale factors  $(s_y, s'_y)$ ;
- 12 exterior parameters for the locations and rotation parameters of the camera exposure stations  $(X_0, Y_0, Z_0, \omega, \phi, \kappa, X'_0, Y'_0, Z'_0, \omega', \phi', \kappa')$ ;
- 8 polynomial coefficients for radial and decentering lens distortion correction  $(K_1, K_2, P_1, P_2, K'_1, K'_2, P'_1, P'_2)$ ;
- 11 multi-lens parameters for the spatial definition of the cover lens surfaces  $(a, b, c, r, a', b', c', r', d, e, g)$ ;
- 2 multi-media parameters of refraction indices of cover lens and water  $(n_2, n_3)$ .

Considering the underwater photogrammetric model, in total 41 unknowns exist and need to be determined through the calibration procedure. Based on the analytical model derived, by using least squares adjustment, the linearization algorithm to be used will make the design matrix of the observation equations very complicated. Furthermore, the possibility of strong correlation among unknowns can generate a singular matrix which is a disadvantage in obtaining the solution.

To avoid the above problems and simplify the computations, we can take advantage of a step by step calibration procedure. First, perform the CCD cameras calibration with the aid of a pair of control frame images photographed in air. Traditional space resection can be employed to solve the interior and exterior parameters as well as the camera lens distortion correction parameters and y-scale factors. In this case, the consideration of ray bending and multi-lens effects could not be included and also the calibration analysis can be processed with clear and sharp images compared to those taken underwater. Therefore high accurate calibration results can be achieved. Second, perform the calibration of the

whole imaging system. In this step, keeping the relative position of the imaging system and control frame the same as that when taking pictures for CCD camera calibration, photograph the underwater frame. Based on the underwater image pair, we can calibrate the imaging system in an underwater environment to obtain the rest of the unknown parameters using the results of CCD camera calibration. In the second step, the number of unknowns is reduced to 13. They are (Figure 2.6):

- $a, b, c, r$  and  $a', b', c', r'$ , parameters for defining the spherical surfaces of the left and right cover lenses respectively;
- $d, g,$  and  $e,$  parameters for defining the planar surface of the left and right cover lenses (in the same plane);
- $n_w$  and  $n_g,$  refraction indices of water and the glass of cover lenses respectively.

### 2.3.2 CCD camera calibration

The cameras are calibrated, either in air or underwater, to allow for the determination of the interior and exterior orientation parameters and the correction of camera lens distortions. The procedure, which is almost the same for CCD video cameras, has been developed from that used to calibrate film-based cameras, except that a scale factor caused by the physical characteristics of CCD cameras has to be included. Before establishing the procedure for the CCD camera calibration, it is necessary to introduce some of the features of CCD video imaging.

#### 2.3.2.1 CCD video camera

CCD camera is the product of the development of semiconductor and microelectronic techniques. It is one type of solid state camera, which uses a Charged Coupled Device (CCD) as a focal plane. The focal plane consists of regularly arranged

sensor elements. The geometric fidelity of the focal plane is limited only by the accuracy with which the sensor elements can be set in the array during the manufacturing process. When an object is focused by lens system on the linear sensor array, each element cell detects the intensity of the light incident on it and transfers the intensity to an electrical signal. With the help of a frame grabber, the analog signal can be digitized. Thus, the electrical record of each sensor element can be transferred to a single digital value resulting in an image element (pixel), and the linear array of individual pixel constitutes the image.

For non-topographical photogrammetric applications, digital images are becoming a replacement of conventional photographs. In comparison with film-based cameras, CCD video sensors have many advantages, including:

- no film distortion;
- no emulsion problems;
- geometric stability of the image element array;
- the need for fiducial marks to define the interior geometry of the cameras is eliminated. (Curry et al., 1986)

Also one of the major advantages of the CCD video images is the high computer compatibility. Therefore, with the ever-increasing power and availability of computer, digital images can be acquired at low cost with high volume, and they are easy to install and manage as they use commonly available transmission systems. Moreover, there are special significances for underwater digital images because enhanced images can be achieved through digital image processing from the original ones taken in poor underwater lighting conditions.

However, CCD video images have one major disadvantage, i.e., they have a poor spatial resolution. Therefore, video cameras are not the choice when highly precise

measurements are required. Fortunately, the resolution of the CCD camera can be improved with the advance of manufacturing techniques. Furthermore, the accuracy of object detection based on digital images can be achieved at 0.01 pixel with certain algorithms (Stanton et al., 1987), which can compensate the shortcoming of the low resolution of the video images.

### **2.3.2.2 CCD camera lens distortion**

As it has been mentioned, the first step for underwater imaging system calibration is to do the CCD camera calibration.

Although by using CCD cameras, some of the errors associated with traditional methods can be avoided, such as those introduced by deformation of the film, it is noticed that the CCD video cameras usually are not highly and precisely designed and manufactured for accurate photogrammetric applications.

It is noted that the quality of lenses used on most commercially available video cameras is not as good as that of single-lens reflex cameras and the CCD camera lens is most likely to exhibit relatively large radial and decentering lens distortions (Fryer, 1987). Usually, because it is very popular to have zoom lenses with video cameras, the variations in radial and decentering distortions when the focusing is altered are much larger than those of most simple non-metric film-based cameras. Therefore the calibration of the CCD lens is essential and should be efficient at whatever the focus setting it is operating.

Usually CCD cameras are non-metric cameras, therefore, the determination of the principal point is very important. Sometimes, it may be up to 40 pixels off the center of the imaging array (Lentz, 1987). This can occur due to misalignment of optical axis or the array focal plane not being aligned perpendicular to the optical axis.

Conventionally, there are various methods used for film-based camera calibration, which are applicable to the CCD cameras. The significant increases in accuracy which have been obtained with non-metric cameras over decades can be attributed largely to a greater understanding of the nature of the radial and decentering distortions and the consequent improved modeling of the photogrammetric solution to incorporate their effects. Many researchers, notably Karara and Abdel-Aziz (1974), have discussed various techniques for incorporating the lens distortion into photogrammetric solutions and have obtained good results for non-metric cameras.

Another of the most popular methods is the plumbline lens calibration procedure proposed by Brown (1971). It is based on the principle that a straight line in object space should perspectively project through a lens to become a straight line in image space. Any deviations from linearity are attributed to radial and decentering distortions in the lens. Usually a self-calibration bundle adjustment is performed to derive the calibration parameters (Fryer and Fraser, 1986).

Due to the complexity of the configuration of the underwater imaging system and unsuitability for the design of a stable plumbline control in an operational underwater environment, we will not consider using the plumbline calibration procedure. It is assumed when calculating the calibration parameters and the accuracy statistics, that the coordinates of the control points are error free. In practice, we only assume that the residual errors in the control coordinates are so small that they do not affect the accuracy of the calibration techniques. Starting from the above assumption, collinearity equations based model will be constructed for the space-resection to obtain the calibration parameters. Meanwhile, lens distortion correction and scale factor determination will be incorporated into the above model.

The pixel coordinates of all targets can be measured semi-automatically with the

area-based matching. The pixel coordinates are subsequently transformed to image coordinates with the pixel-to-image coordinate transformation (Figure 2.7):

$$\bar{x} = (x' - x'_p) \times P_{sx} \quad (2.29a)$$

$$\bar{y} = (y'_p - y') \times P_{sy} \quad (2.29b)$$

with:

$\bar{x}$  and  $\bar{y}$  are image coordinates;

$x'$  and  $y'$  are pixel coordinates;

$x'_p$  and  $y'_p$  are pixel coordinates of the principal point;

$P_{sx}$  and  $P_{sy}$  are pixel spacing in  $x$ - and  $y$ - directions respectively.

Thus the  $y$ -scale factor can be obtained from:

$$s_y = \frac{P_{sy}}{P_{sx}} \quad (2.30)$$

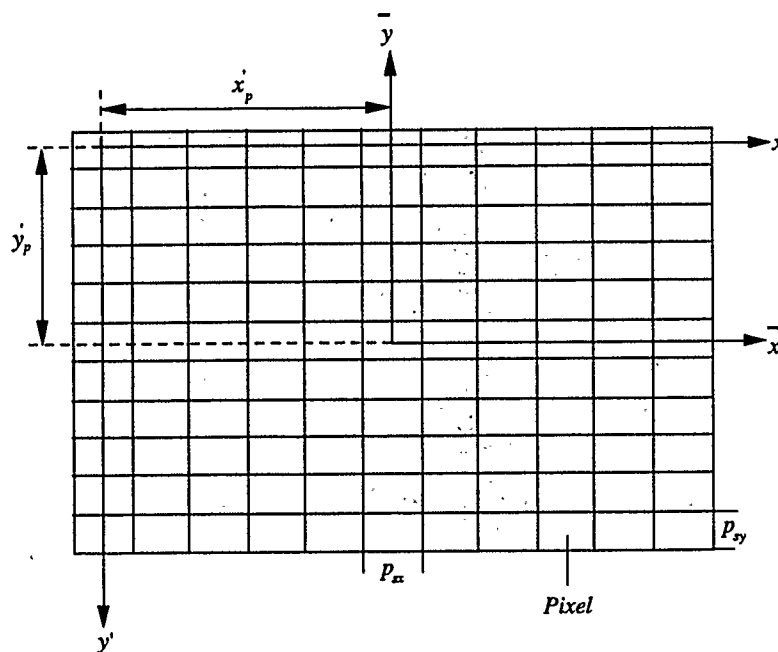


Figure 2.7 Pixel and image coordinate system

Additional parameters modeling the interior orientation, radial lens distortion and decentering distortion can be formulated as (Equation 2.5):

$$\delta x = K_1 \bar{x} r^2 + K_2 \bar{x} r^4 + P_1 (r^2 + 2\bar{x}^2) + 2P_2 \bar{x} \bar{y} \quad (2.31a)$$

$$\delta y = K_1 \bar{y} r^2 + K_2 \bar{y} r^4 + P_2 (r^2 + 2\bar{y}^2) + 2P_1 \bar{x} \bar{y} \quad (2.31b)$$

with:

$$r = \sqrt{\bar{x}^2 + \bar{y}^2} ;$$

$K_1$  and  $K_2$ , the first two parameters for radial lens distortion correction;

$P_1$  and  $P_2$ , the first two parameters for decentering lens distortion correction.

The model for lens distortion correction is a quite popular and effective form which was proposed by Brown (1968). Usually the location of the principal point is not specified for most CCD cameras and varies from camera to camera. The y-scale factor is necessary to model the sensor element spacing and additional imprecision introduced by line-synchronization (Gulch, 1987).

### 2.3.2.3 Least squares model for the camera calibration

Incorporating lens distortion correction equations (Equation 2.31) with collinearity equations (Equation 2.4), respectively and using a linearization version for a pair of stereo cameras, observation equations can be constructed for each control image point:

$$v = AX + l \quad (2.32)$$

where:

$A$  is the design matrix for observation equations;

$X$  is the vector of number of unknowns, which include unknown parameters for the left CCD camera ( $X_0, Y_0, Z_0, \omega, \phi, \kappa, x_p, y_p, f, k_1, k_2, p_1, p_2, s_y$ ) and for the right one ( $X'_0, Y'_0, Z'_0, \omega', \phi', \kappa', x'_p, y'_p, f', k'_1, k'_2, p'_1, p'_2, s'_y$ );

$l$  is the constant vector;

$v$  is the vector of residuals.

Using enough control points (at least 7 control points required for this case), 28 unknown parameters of the pair of CCD cameras can be obtained with a least squares solution of Equation (2.32) (Mikhail 1976):

$$X = -(A^T A)^{-1} A^T l \quad (2.33)$$

These calculated unknown parameters, except the exterior parameters, will be used as known parameters for the whole underwater imaging system calibration to determine the multi-lens and multi-media parameters.

### 2.3.3 Calibration of the underwater imaging system

With the calibration procedure presented in this research, one of the advantages of this method is that there is freedom in the choice of unknowns. If the calibration procedure strictly follows the steps described in Section 2.3.1 and the CCD camera calibration can obtain accurate results, the parameters derived can be transferred to the photogrammetric model and thus make the number of unknowns existing in the underwater photogrammetric model be reduced to 13. This significance can be shown as dealing with the linearization of the multi-media equation. On the other hand, if the calibration procedure fails to follow the proposed steps, the exterior orientation parameters (in total 12) of the camera exposure stations will be considered as unknowns during the imaging system calibration stage, which will result in complexity of the calibration procedure.

After the CCD camera calibration (Section 2.3.2), the reference frame system can be transferred to the left image based photo-coordinate system. The imaging system will take pictures at the same status as it did in the first calibration stage to guarantee there is no more unknowns introduced during the rest of the calibration procedure. The pair of CCD cameras and their corresponding cover lenses can be considered as being relatively fixed in position and orientation. Thus the parameters defining the geometry and refraction index of the cover lens surfaces could be adopted as the inner orientation parameters with respect to the whole imaging system. However, the conventional relative orientation concept (Wolf, 1974) is not suitable to the stereo imaging system because the commonly used coplanarity condition for stereo photography is not satisfied in the multi-media and multi-lens situation.

The 3D ray tracing technique has been used in the underwater stereo video system. A rigorous mathematical model has been established (Equation 2.28), and all the physical elements involved in the imaging taking procedure have been considered. For the purpose of obtaining all the orientation parameters of this system, the calibration method is used to calculate all the unknowns in the photogrammetric model, i.e. some control points are used to perform the space resection.

In ray tracing procedure, a light ray starts from an image point, goes through several different media, and finally reaches the corresponding object point. The image coordinates are still considered as the observations, and the non-linear observation equations are established based on the mathematical model (Equation 2.28). In the implementation, first the mathematical model is linearized, then least squares adjustment is used to calculate all the 25 unknowns (13 multi-lens and multi-media parameters and 12 exterior orientation parameters of the exposure stations of the pair of CCD cameras). Because the original non-linear observation equations are multi-level compound functions,

the linearization and computation are much more complicated than the traditional case (Appendix B).

## 2.4 Spatial intersection

Generally, the main task of the photogrammetric applications is to determine the object space coordinates through the measurement of the corresponding image points. For stereo pair images, if they are well georeferenced, spatial intersection allows the calculation of the object spatial coordinates based on the analytical photogrammetric model as long as the object point can be seen on both images.

Through the analysis of the proposed underwater imaging system, a rigorous mathematical model is constructed which can reflect the geometrical relationship of the underwater object points with their corresponding image points (Equation 2.28). Through the calibration procedure, the determined orientation parameters, lens distortion correction coefficients, multi-lens and multi-media parameters can be used for a rigorous spatial intersection of all object points exposed on the stereo images.

For conjugate points of an object on the pair of underwater stereo images, four equations can be established to determine the object space coordinates  $X$ ,  $Y$ , and  $Z$  (Equation 2.28):

$$G_1 = \gamma_3 X - (Z - Z_2)\alpha_3 - \gamma_3 X_2 = 0 \quad (2.34a)$$

$$G_2 = \gamma_3 Y - (Z - Z_2)\beta_3 - \gamma_3 Y_2 = 0 \quad (2.34b)$$

$$G'_1 = \gamma'_3 X - (Z - Z'_2)\alpha'_3 - \gamma'_3 X'_2 = 0 \quad (2.34c)$$

$$G'_2 = \gamma'_3 Y - (Z - Z'_2)\beta'_3 - \gamma'_3 Y'_2 = 0 \quad (2.34d)$$

Except for  $X$ ,  $Y$ , and  $Z$ , the rest of the parameters in the above equations are known. Therefore, the object coordinates  $(X, Y, Z)$  can be easily obtained by the least squares

adjustment method.

The determination of spatial coordinates of an underwater object based on the underwater video imaging system provides us a tool for three dimensional underwater object surface reconstructing, object physical size measuring, as well as underwater object locating.

## **2.5 Some implementation considerations**

A very important part of this research is the implementation of the underwater imaging system calibration. The accurate calibration results will provide reliable spatial object measurement based on image coordinate measurement.

The photogrammetric model developed for the imaging system is very complicated. A large number of unknown parameters are involved in the model and there exists correlation among some of these unknowns. During the underwater imaging system calibration procedure, it is difficult to directly use the least squares adjustment to obtain the solution. In practice, the least squares method can be used in such a way that the unknown parameters are weighted. In this case, the influence of the correlation among some of the unknowns could be reduced or restricted and this could improve the quality of the adjustment results.

For least squares problems, it usually involves the computation of inverse matrix. For instance, the requirement for the inverse of normal matrix  $A^T A$  can be found in the least squares solution for the camera calibration (Equation 2.33). Singular value decomposition (SVD) can be applied to solve this type of problems (Press et al., 1988). Using SVD, the characteristics of the square normal matrix  $A^T A$  can be diagnosed in terms of the condition number (Appendix C).

There are various methods to the accuracy evaluation for photogrammetric applications. Complex criteria, such as least squares accuracy criteria (Mikhail and Ackermann, 1976), could be developed to estimate accuracy, but usually many factors need to be considered.

Root mean square value analysis provides a simple and reliable way to evaluate the measurement accuracy (Hottier, 1976). Consider a number of check points in the object space, i.e., points whose true spatial coordinates are known, but which have not been used in the photogrammetric computation. Then if  $(X_{it}, Y_{it}, Z_{it})$  are the true coordinates of a check point ( $i = 1, 2, \dots, n$ ) and  $(X_{im}, Y_{im}, Z_{im})$  are its measurement coordinates, an estimation of the RMS spatial values along any direction, x-direction say, is:

$$RMS_x = \sqrt{\frac{\sum_{i=1}^n (X_{im} - X_{it})^2}{n}} \quad (2.35)$$

This criteria is simple and good estimations can be obtained provided that:

- the number of check points is sufficient and satisfactory results can be obtained if the number of check points is about 15 (Hottier, 1976);
- the check points in the object space are well distributed;
- the object space is not too deep; otherwise, the measurement accuracy has to be estimated for successive slices.

## CHAPTER 3

# IMPLEMENTATION OF UNDERWATER VIDEO IMAGE PROCESSING SYSTEM

This chapter presents the implementation of the underwater photogrammetric model and a PC based prototype system developed for underwater stereo video image processing.

At the stage of implementation, the emphasis will be put on the processes of calibration and measurement, because they are the two most decisive parts of any photogrammetric system and because of the special solutions in our system. To test the developed underwater photogrammetric model, a water tank and a calibration frame was designed to provide practical data for the camera system calibration and three dimensional measurements. The calibration and measurement results will be presented and analyzed.

In order to make the underwater photogrammetric model suitable for routine work of underwater object measuring and information gathering, a PC based system will be developed based on the fundamental photogrammetric model. With the software development, several modules including the measuring and calibration module, image processing, and database generation module will be integrated together, so that the system could be a cost-efficient tool for underwater applications.

### 3.1 Background

The Institute of Ocean Science (IOS) of Canadian Hydrographic Service (CHS) was investigating technology which could be used by fisheries and underwater

environmental surveys, with emphasis on fish stock assessment.

During the past, at IOS, most of the research on the underwater resource management depended on the analysis of sonar images. Generally, sonar image data, can be acquired only at small scale, such as multi-beam data and side scan sonar images, with a resolution of tens to hundreds of meters. Furthermore, there exist some difficulties in obtaining direct visual interpretations from sonar images. Thus, sonar techniques cannot meet the requirements of acquiring detailed information concerning the underwater environment.

With the emerging of the digital imaging technique, video imaging systems are considered one of the most widely used and versatile tools to obtain high resolution underwater data. But until recently, in the underwater environment, the aforementioned system has been applied primarily to provide viewers with qualitative or descriptive information rather than quantitative information (Tusting and Davis, 1992), such as reconstruction of three dimensional object shapes. This is mainly due to the hostile underwater environment and the requirement of expensive and carefully equipment to collect the underwater image data.

Recent advances in both underwater vehicles and lighting make it practical to consider an underwater survey and measuring system to access the near sea bottom. The research project was initialized to study and implement methods for making quantitative measurements for underwater objects, and consequently this led to the proposal to develop a PC based system by making use of non-contact measurement features of digital underwater photogrammetry.

### **3.2 Requirement of underwater measuring system**

Photogrammetry has been used occasionally to measure underwater objects

(Badwin, 1984). Generally speaking the methods developed were dependent on the use of very expensive and sophisticated equipment and complicated analysis techniques. Therefore they were relatively inaccessible to the underwater researchers (Welham, 1984).

In our case, if the photogrammetric system is to be used as a tool for fishery assessment or other underwater object measuring, then the following approaches need to be considered:

- The system must allow users to make their own observations and conduct computation themselves;
- Only minimal photogrammetric knowledge and skill are required;
- The method must be simple, fast, and accurate (accuracy within 5 cm).

Based on the above considerations, an image acquisition system, as illustrated in Figure 2.1, has been developed by IOS. Unlike commonly used underwater inspection systems (Turner et al., 1992), the system possesses two specific aspects: a) it applies a pair of video cameras for stereo image acquisition instead of film-based cameras; b) it incorporates concave lenses into its glass window to provide larger view field other than a simple plane window. Given the photogrammetric model could be well developed to meet the object measuring accuracy, the specific configuration of the imaging system will bring the following benefits to the underwater survey:

First, the image acquisition can be highly efficient due to view angle enlargement configurations. Also, the underwater images captured using video cameras can be made available to the measurement system instantly.

Second, the images can be analyzed using a microcomputer based system applying digital photogrammetric principles without the aid of the optical equipment operated by

highly trained specialists. The images are allowed to be viewed stereoscopically, so as to be easy for direct visual interpretation. Also, it has the potential for viewing real stereoscopic videos to assist the underwater inspection.

Third, by making optimal use of microcomputer hardware, a system can solve the underwater photogrammetric problem in a user-friendly and efficient way.

### **3.3 Underwater image data collection**

Underwater data collection provides practical images and corresponding photogrammetric data for testing the underwater photogrammetric model. The underwater data collection involves several components, which include a pair of housed CCD cameras, a frame grabber, a calibration frame and a water tank for simulating underwater environment.

#### **3.3.1 CCD camera configuration**

Two Cosmicar brand CCD cameras with standard NTSC video signal output were the major components of the underwater imaging system. The resolution for this particular pair of cameras was 739 columns and 488 rows. It was fitted with a standard Auto-Iris 6 mm, f1.2 lens which provided view angles of 58°00' and 45°00' along the horizontal and vertical directions, respectively. The focus distance of this system was from 0.2 m to infinity.

This lens arrangement was not suited to the very close-range inspection, and for underwater application the stand-off distance for this lens was around 2-3 m. Due to the physical configuration of the CCD camera, any misalignment of the lens elements was considered as a possible source of lens distortion.

To provide stereo vision, the two CCD cameras were combined together to maintain

a fixed base of about 7.0 cm (Figure 3.1a). Approximately, the optical axis of the two cameras were parallel and this ensured that each pair of images produced a usable stereo model (more than 90% overlap for the stereo image pair). For underwater operation, the pair of CCD cameras were housed in a cylinder-shaped container (Figure 3.1b). Besides being waterproof, the movable front cover had the function of increasing the viewing angle by integrating two concave lenses in front of each CCD camera. Because there was little information about the cover lens, it was difficult to perform accurate analysis of the features of the whole imaging system, such as view field, by only applying geometrical optical principles. But through the analysis of the conceptual imaging model and the exhibition of experimental images, it could be confirmed that the view angle had been increased with the combined imaging system compared to that without the cover lenses combination. Because the establishment of the photogrammetric model was based on three dimensional optical ray tracing, the cover lenses were considered as refractive media instead of optical components. Thus, misalignment of the CCD camera and its corresponding cover lens could be neglected.

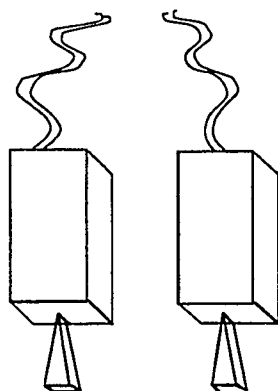


**Figure 3.1a** Internal configuration

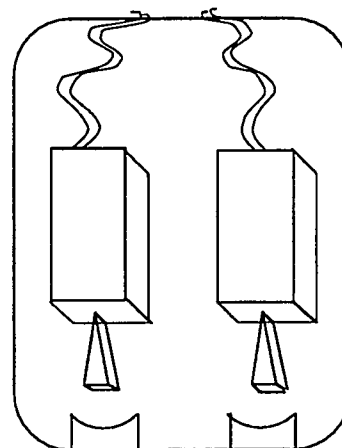


**Figure 3.1b** External configuration

**Figure 3.1** Internal and external configurations of the pair of CCD cameras

### 3.3.2 Frame grabber

The PC based frame grabber used for testing was a prototype real time stereo vision system that digitized two images and interlaced them for display. The digitized images were stored in an on-board frame memory card within the computer. The characteristics of this particular frame grabber included:

- simultaneous record of 30 image frames per second;
- digitizing of video signal to 8 bits (256 gray levels);
- capacity to store two 568 by 468 images in frame memory.

### 3.3.3 Calibration frame

Due to the operational environment, it was very difficult to obtain accurate control in object space for underwater photogrammetry. The problem was resolved by introducing a portable and stable frame with well defined targets. The framework could be positioned over the area of interest introducing an arbitrary reference system for imaging system calibration.

The reference system consisted of a  $1.4 \times 1.4 \times 0.7$  m rectangular aluminum frame with 24 control targets (Figure 3.2). These targets were marked with well reflective circular disc, each of about 8 cm diameter with a black and white cross and marked numbers printed. This type of design ensured systematic targets and the best possible conformal representation of all the targets in the image. Also, the size, shape, and contrast of the targets formed the basis of successful target center determination.

The spatial coordinates of the control targets had been determined prior to underwater work. They were surveyed with metal tape and adjusted by a program GHOST (Curran, 1993). The accuracy of these control targets was within 0.5 mm, 0.2 mm and 2.0

mm along x-, y- and z- directions, respectively. The coordinates of the control targets in the spatial reference system are shown in Table 3.1.

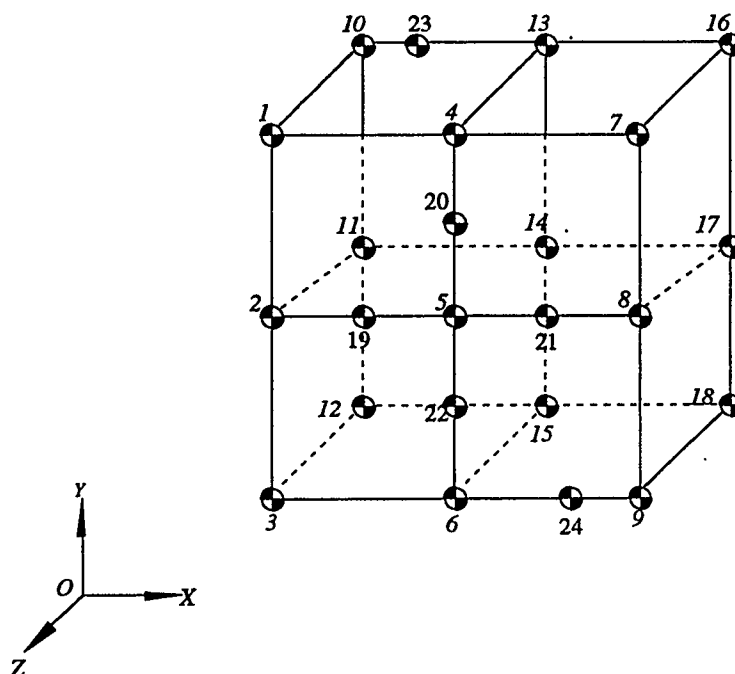


**Figure 3.2** Calibration frame and control targets

### 3.3.4 Water tank test

With the selected camera system and a well defined calibration frame, and if a remote operated underwater vehicle could be available, the operation of the system would be relatively straightforward. Following the calibration procedure mentioned in Section 2.3, initially, the pair of cameras must have been well calibrated in air. Then the underwater vehicle and the calibration frame are deployed to the work-site and the calibration frame is photographed in such a way that it fills the camera format (i.e. required measurement distance). The vehicle then moves off to perform its imaging tasks and photographs any objects of interest it encounters. The calibration frame can be rephotographed at the end of the data collection period. The image data can be recorded and processed either onshore or offshore.

**Table 3.1** Spatial coordinates of control targets

Target No.	X (m)	Y (m)	Z (m)
1	100.0053	101.4396	-100.0010
2	100.0016	100.7216	-100.0001
3	100.0000	100.0000	100.0000
4	100.7276	101.4402	-100.0048
5	100.7232	100.7216	-100.0001
6	100.7226	99.9994	-100.0029
7	101.4492	101.4415	-100.0062
8	101.4467	100.7219	-100.0043
9	101.4440	99.9996	-100.0001
10	100.0027	101.4423	-100.4579
11	99.9999	100.7197	-100.4563
12	99.9970	100.0003	-100.4549
13	100.7236	101.4407	-100.4595
14	100.7216	100.7323	-100.4549
15	100.7193	99.9973	-100.4563
16	101.4450	101.4389	-100.4620
17	101.4434	100.7174	-100.4597
18	101.4389	100.0071	-100.4552
19	100.4472	100.7224	-100.4540
20	100.7189	101.0046	-100.4572
21	101.0163	100.7198	-100.4575
22	100.7222	100.4735	-100.4529
23	100.3645	101.4414	-100.0038
24	101.1094	100.0011	-100.0021

As a matter of fact, the underwater operation is quite expensive, and the implementation procedure can only be accomplished after solving some problems, such as camera system mounting on the underwater platform, efficient artificial lighting system installation, and connection of frame grabber to the CCD cameras, etc. Obviously, the testing of a prototype system is neither practical nor economical. Therefore, it was planned

to move the system test into the laboratory using a water tank to simulate the underwater operation.

The water tank was built as a cylinder-shape with both height and bottom diameter of about 2.5 m, and was well compatible with the calibration frame. Two bars across the edge of the water tank were built to facilitate the motion of the camera system. Thus, the camera system was movable along the bars and allowed cameras to take pictures from different view angle. At the same time, devices were provided to fix the camera system on bars and maintain the system stability during the photographing.

As we have discussed, the quality of underwater image can deteriorate due to the effects of attenuation and scattering of light rays by water. In our data acquisition procedure, there was no artificial underwater lighting provided. Therefore, to improve the imaging quality, two methods were adopted: a) improve the lighting condition in the testing laboratory by increasing the lighting source power; b) process the water in the tank with chemicals and filtering to improve the clearance of the water used.

To facilitate the camera system calibration, we set up the following procedures:

- (1) Place the calibration frame on the bottom of the dry tank and mount the camera system on the bars facing the bottom of the water tank vertically.
- (2) Take photographs without the housing cover.
- (3) Keep the position of the camera system and mount the housing cover, then load the water until the housing cover is submerged in the water, then photograph.
- (4) Move the camera system and repeat steps (1)-(3) to acquire several pair of images for photogrammetric processing.

With the photogrammetric model developed and calibration procedure, calibration and measurement could be implemented for the system evaluations. Due to the fact that the image acquisition procedure differed to the form originally planned in that the position of the camera system was not fixed (Step 3 was not followed), the exterior orientation parameters had to be calculated again in the second stage of the calibration where images acquired with cover lenses and water were used.

### **3.4 Underwater image data processing**

The implementation of the underwater photogrammetric model is crucial to this research. Through this stage, the underwater photogrammetric model can be examined and the effectiveness of the technique can be evaluated. Another aim at this stage is to develop a digital photogrammetric system - Underwater Stereo Video Image Processing System (USVIPS).

Due to the fact that the advances in computer technology offers increasing performance at decreasing hardware cost, digital image handling has now become easy and cheap enough to be used on low cost systems for photogrammetric applications (Gruen, 1989). Different from traditional photogrammetric systems which need optical instruments and perform measurements on film-based photographs, digital photogrammetric systems use computers to handle digital images. As mentioned before, although digital imagery cannot compare the resolution of traditional photographs, they can be obtained in large quantities at low cost. With the strong computational ability of computers, sophisticated photogrammetric model and algorithms can be developed to compensate for the low resolutions effects. Furthermore, the high efficiency of the data storage and management using computers gives the digital photogrammetric systems the potential to replace conventional ones.

An important part of USVIPS implementation was the design of the graphical user interface (GUI). The GUI played an important role in handling the different applications and affected the efficiency of the whole system. The system was designed in a modular fashion, so as to provide the system with the possibility of supplying new modules later. Generally, the system has functions for digital image displaying, image processing, underwater imaging system calibration, and three dimensional object point computation. Also the system has the function to manage the extracted information for later retrieval. The image data processing procedure is illustrated in Figure 3.3.

#### **3.4.1 Hardware configuration**

The hardware components of USVIPS have been kept simple and standard. They consist of:

- an IBM PC with 8 MByte RAM, an 80486 processor at a frequency of 33 MHz, and a 600 MByte hard disk;
- a high resolution graphic board which supports image displaying at a resolution of 1024x768 with 256 color or gray level values;
- an Ethernet board for a large amount of image data transformation through network communication.

#### **3.4.2 Digital image display**

Before being used for photogrammetric processing, digital images obtained from CCD cameras were preprocessed into the format recognized by the system. Some information concerning these digital images, such as image size and three dimensional information of control targets were stored as the head of image data along with the corresponding image pairs.

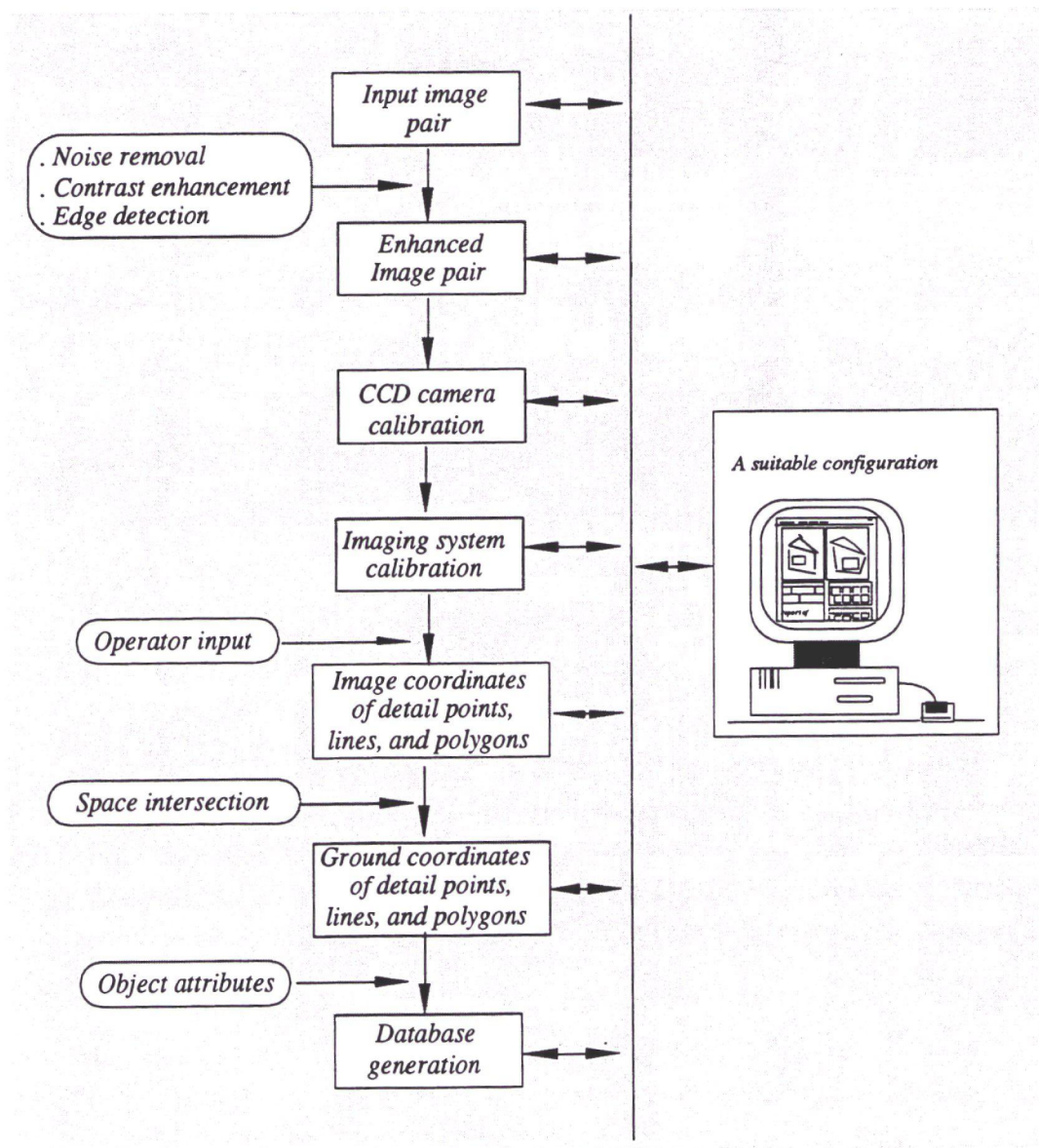


**Figure 3.3** Image data processing procedure

A very important component for digital image handling was the image display which formed the basis for photogrammetric measurement procedures. Most digital photogrammetric systems display stereo images using certain type of view devices connected to computers, therefore, viewing of the three dimensional model of the object can be conducted (Mori et al., 1992). In our system, there is no aid of additional stereo

viewing apparatus, and the establishment of stereo model is simply performed by bringing to the screen a pair of rectangular figures in split independent windows. The position of image point can be quickly located with cursor function, so that the image coordinates can be determined for further photogrammetric processing.

The graphic board of the PC used in this research can offer 8-bit image display, i.e. it supports 256 colors or gray scales. The digital image prepared for processing is 8-bit gray-scale image and the full scale display will occupy all the color indices of the system. However, the window system requires a default color map for its own application. Moreover, some GUI elements also need color indices for the graphic design, such as menus, buttons, etc. Therefore, there is a tradeoff between the image display and system presentation. In order to make full use of the graphic resources of the system and improve the quality of the image display environment, the following color mapping between RGB values and color indices from 0 - 255 was applied (Qian et al., 1994):

0 - 63:	System default settings
64 - 127:	(255 0 0)
128 - 191:	(0 255 0)
192:	(0 0 0)
193:	(4 4 4)
194:	(8 8 8)
...	...
255:	(252 252 252)

Images with 256 gray scales were compressed to those with 64 gray scales and mapped to the end of the color map (192 - 255). Two colors, green (0, 255, 0) and red (255, 0, 0) were used to present cursor and temporary marks during photogrammetric measuring. The first 64 colors were applied for permanent marks.

Through the experimental results, it has been proved that it is hard for the human eye to distinguish images with 256 gray scales and 64 gray scales on the monitor. The way that the number of gray scales of images are reduced achieves a consistent and user friendly graphic environment.

Although the monitor provides a limited area for displaying images, the GUI provides an efficient and convenient way to solve the problem through the implementation of a multi-window structure. Images are initially displayed in independent windows of reasonable size on a single screen. Image portions outside the windows can also be displayed by using the scroll bar in two directions or resizing the image windows. The multi-window structure makes the GUI flexible to handle large images independently.

### **3.4.3 Image processing**

In comparison to aerial or terrestrial photographs, the quality of underwater video images is much poorer. In our testing case under underwater imaging conditions this was caused by the following factors:

- particularly low illumination because of no special underwater lighting source;
- low visibility caused by attenuation underwater;
- noise introduced by video sensors and data transmission.

Thus, the underwater video images were first preprocessed and then used for photogrammetric processing. Through the image processing tools provided by the system, the image quality was improved. The collection of underwater image data could be processed with greater ease and accuracy by removing the undesired features and emphasizing the interesting features.

The user can choose one image in a certain window to perform image processing

tasks. For comparison, the respective histograms of the original and processed counterpart will be displayed in an independent graphic window. Several approaches can be conducted for the processing depending on the characteristics of the underwater video images, which include brightness adjustment, contrast enhancement, edge enhancement, and noise removal.

(1) Brightness adjustment

Due to the insufficient lighting underwater, the underwater video images are usually acquired with low intensity. Moreover, the brightness of the stereo pair is not balanced. The brightness adjustment of an image is implemented simply by modifying the gray scale value range of that image, i.e. adding or subtracting a certain value from each pixel gray value of the image. In this case, normalization is required if the adjustment results in that the gray value of the images is out of the range of 0-256. By interactively operating the scroll bars in two directions, continuous brightness adjustment can be performed until the results are satisfactory to the user.

(2) Contrast enhancement

Images of poor contrast characteristics usually result in poor recognition of object features and thus decrease the targeting accuracy. The purpose of the contrast enhancement option is to modify the structure of the original histogram in such a way that the percentage contribution of each gray value to the cumulative histogram can be changed. Since the original histogram is already stored, the user is given the alternatives of modifying it into a uniform or linear stretch.

The system first provides a default stretch, histogram equalization (Gonzalez and Wintz, 1987), which works reasonably for a variety of underwater images. However, histogram equalization produces contrast which are too harsh, with a large number of

pixels redistributed to the low and high ends of the gray level scale. This technique is also not particularly well suited to images that have skewed histograms with a large number of pixels in a limited gray level range.

Another common contrast enhancement technique is simple linear transformation with saturation and piece wise linear transformation that stretches different parts of the gray level scale differently (Gong, 1993). Thus, histogram asymmetry can be accommodated. To implement this type of contrast stretch, the system allows the user to define his own linear stretch curve interactively with respect to the histogram of the original image.

### (3) Edge enhancement

Sharpening of the edges is a feature that provides for better recognition of the points (pixels) lying on a line. Therefore more accurate measurements can be achieved. The edge enhancement is provided by the system with the option of any of two operators, Sobel and Laplacian (Gonzalez and Wintz, 1987).

### (4) Noise removal

Generally the system handles two types of noise, random and isolated. Random noise is displayed as gray level noise at every pixel, usually originating in the image detectors. Isolated noise is presented as extreme noise at relatively few pixels resulting in zero or maximum gray level values at the affected pixels, usually caused by bit loss in data transmission.

K-nearest neighbor averaging is applied to smooth the isolated noise in a very efficient way (Davis and Rosenfeld, 1978). For random noise removal, the user has the option to use one of the two filters provided by the system, mean and median. Also, the user can design and use his own masks which can be input interactively.

### 3.4.4 Calibration and measurement module

The USVIPS consists of a suite of functions which are designed to capture information from the displayed stereo images, derive the calibration parameters, compute three dimensional coordinates and present the results in a convenient way. These functions are selected and executed from a graphics control. Job managing is by means of parameter files which enable all data processing to be carried out under direct program control. The schematic representation of calibration and measurement module is shown in Figure 3.4.

The task of the imaging system calibration is to determine unknown parameters within the mathematical photogrammetric model. Since the photogrammetric model is so complicated, the procedures are divided into two independent steps (Section 2.3). Consequently, the software has been structured to make the operations follow those two steps (Figure 3.4):

- (1) With one image pair of calibration frame taken in air, conventional collinearity equations with an added polynomial for lens distortion model are used to perform the calibration adjustment. In this case, the interior parameters, such as focal length, principal points and the scale of digital image, exterior parameters, and lens distortion parameters can be obtained. Also the distortion model can be applied to all the images taken during the same period of operations.
- (2) Using the parameters derived from the first step, with another image pair of calibration frame taken underwater, photogrammetric model developed by ray tracing is applied to calibrate the rest of the parameters of the imaging system, such as the surface parameters determining the geometry of the surfaces of cover lenses and the refraction indices of water and the cover glass.

There are no extra devices for stereo viewing added to the system. During the

calibration procedures, the input of image coordinates of control targets are performed by finding corresponding points in stereo images manually. Once a pair of conjugate points are chosen by cursor locating, the user can input the index of the control target and the software allows the system instantly to query and retrieve the corresponding three dimensional coordinates stored in the system. As long as enough well distributed controls are selected, both image and space coordinates of the control points can be sent to the calibration process for space resection computing.

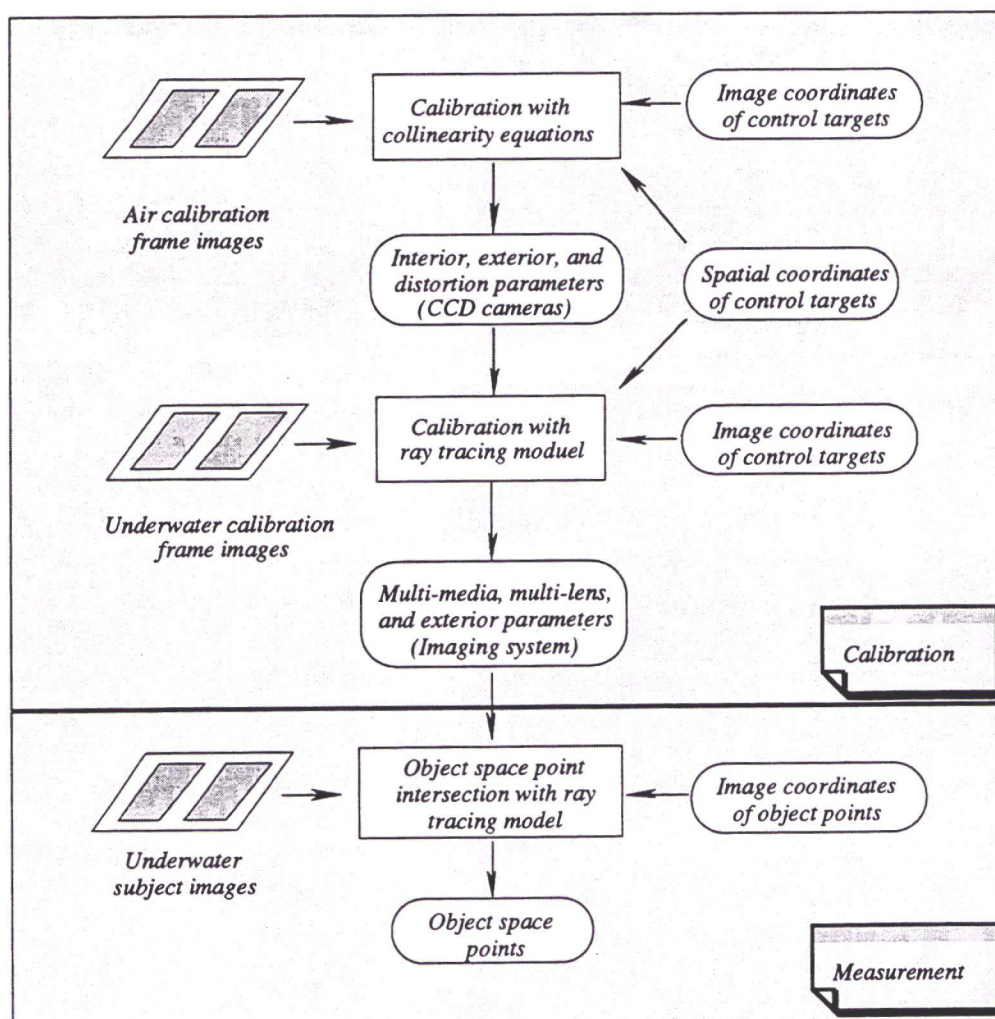


**Figure 3.4** Schematic representation of calibration procedures and object measurement

Due to the fact that the field data collection did not exactly follow the procedure

designed (Section 3.3), i.e. the imaging system did not fix at the same position when photographing the calibration frame with and without water in the test tank, the second step of the calibration model must be modified. Six more unknowns related to the exposure stations of the stereo cameras are added to the adjustment model, which makes the calibration model more complicated.

The calibration program is used to control the image captured for the calibration frame. The observations to the control points on the calibration frame are made in two rounds and editing of entries is fully supported. Execution of the two calibration programs for the calibration frame images creates a parameter file which is subsequently used to control the processing of all other image pairs associated with the same operation. This ensures that all files are instantly identifiable and that the other images are processed with the correct calibration values. After the calibration operation, the derived parameters are instantly used to compute values of control points. Control point differences are abstracted and these are used to assess the accuracy of the solution. Generally the solution producing the smallest standard deviation for the control point differences is accepted.

During the calibration procedure, the system allows input from external software, such as initial approximations for unknowns through direct linear transformation (DLT) to acquire good initial approximations for unknown parameters (Abdel-Aziz and Karara, 1971). The system controls these operations by file management.

Based on photogrammetric model derived in Section 2.3, the object measuring program is used to control image data captured for objects to be measured. The program accepts image coordinates measured by the cursor and applies a ray tracing scheme to compute the object space coordinates by intersection. These spatial coordinates are in an arbitrary reference system, as defined by the initial position of the calibration frame. By treating control targets as object points to be measured, coordinates of these points can be

computed. A comparison of the calculated and known coordinate values for these points provides a realistic estimation of the accuracy of the system. System reliability can be monitored through checks on the variance-covariance matrix, the residual of control points and by independent check whenever needed.

The accuracy of spatial object measurements result greatly relies on the conjugate point selection in the stereo images. In aerial or terrestrial photogrammetry, the conjugate point determination can be assisted by epipolar geometry (Wolf 1971). In this case, for example, once a point is selected in one of the image pair windows using mouse-control cursor, epipolar lines of the point can be calculated and be displayed in both image windows. Since the identical point in the other image window should be on or near the epipolar line depending on the accuracy of orientation parameters (Li et al., 1994), the user can easily search the conjugate point along the epipolar line. For the multi-media photogrammetry, the epipolar geometry will not be followed. Therefore one of basic procedures to improve the accuracy of locating conjugate points is to use zooming function to obtain a detailed and clear view of objects to facilitate accurate targeting.

The system provides the capability to measure three major geometric elements, namely points, arcs and polygons. Also the system provides a geo-calculator which looks like a math-calculator (Li et al., 1994). It will have handy functions such as calculations of distance/size, elevation difference, azimuth etc. based on photogrammetric processing of image information.

#### **3.4.5 Database generation**

One of the distinct advantages of the digital approach is the ability of using computers to manage the extracted information from the photogrammetric measurement.

Generally three basic geometric elements can be generated by the system, which are

points, arcs, and polygons. An element consists of several three dimensional coordinates. To generate an element, the type has to be first selected, then the three dimensional coordinates are measured one by one. For all of the three object types, points are the basic elements and their three dimensional coordinates are obtained through intersection. Every three dimensional coordinate triplet constitutes a vertex. Also for every object, there is an attribute associated to it, which describes the type of the subject. After measuring an object, a record is generated in the database to describe the object which can be used for later applications. Basically the data consists of the following items, where (x, y, z) are the coordinates of the vertex:

Time

Object-ID

Type

Attribute

Number of vertices

Vertex index

x y z

Vertex index

x y z

...

### **3.4.6 GUI development**

A friendly graphic user interface (GUI) is an important part of the system. With the GUI design, several modules involved in the system are integrated in a graphic environment, where the user is linked with the computer to perform photogrammetric tasks. The construction of a GUI makes the digital photogrammetric systems significantly different from the conventional ones.

Figure 3.5 shows the interface of the USVIPS system. It has been developed on a IBM PC in a Microsoft window environment. A highly object-oriented window toolkit WNDX (WNDX, 1992) is used for the graphics development. This toolkit provides functions for creating highly reusable and configurable GUI elements which can be integrated in programs written in C or C++ programming languages.

Supported by Microsoft window environment and WNDX toolkit, a pair of images are displayed and viewed for the directly interactive photogrammetric processing. By cursor locating on the image surface, the image coordinates of object can be acquired and constitute a basic and necessary input for the photogrammetric measurement.

Generally a GUI is designed in such a way that all the modular functions are grouped logically according to different tasks by using menu systems and on-line tools. In this case, the user does not need to directly deal with the programs which provide photogrammetric functions. Usually, menu systems are mostly used in GUI design, because: a) commands performing similar or related functions can be grouped into a sub-menu system; b) functions requiring hierarchical processing steps can be implemented using menus with hierarchical levels; and c) intuitive menu item names can be associated with corresponding program commands (OSF, 1992). There are various types of menus, such as pulldown menu, side bar menu, tablet menu, etc. Appropriate applications of these menu styles could create an efficient photogrammetric measuring procedure. Because of screen size limitation and visual simplicity, menus mainly organize those functions which are frequently used by users, for instance, the point measurement and zooming function in the USVIPS. But if a large number of functions and commands are involved, a multi-level hierarchical menu system may be applied. While hierarchical menu systems help the application and the user organize menu elements, each level of a submenu reduces the ease of access to the menu elements and multiple levels of cascading submenus can also quickly

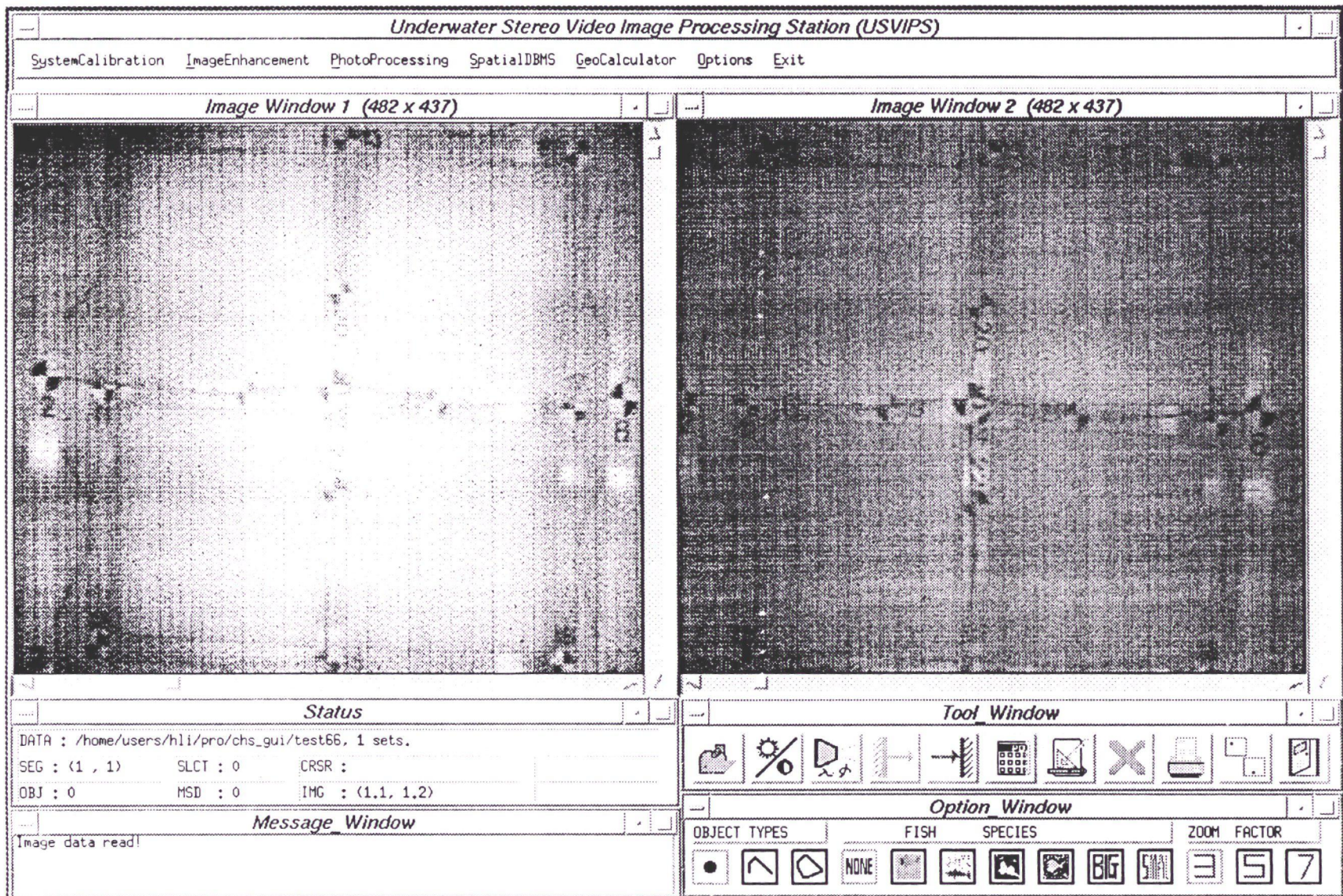


Figure 3.5 The Graphical User Interface (GUI) of the USVIPS

create visual clutter.

Depending on applications, some functions needed frequently during the photogrammetric measuring might be implemented as on-line tools such as icons and mouse button functions. This allows quick access to a certain function instead of searching along the menu elements or typing commands. In the system, some functions may be driven by icons, such as starting and ending of an arc or polygon measurement, and associating attributes to objects. Zooming function could be accessed by pressing mouse button. These functions make the system more flexible because they provide the user with multiple ways to access application functions and accomplish his tasks.

With the GUI system, every direct manipulation of graphic components from the user can obtain feedback of an observable response, such as highlighting a softbutton or an icon after being selected. Usually the user can also get an immediate visible result from each action, which helps the user to inspect the quality of the processing procedure. These responses can be either in text or graphic manners. For imaging calibration, as the user completes the procedure, the calibration results could be instantly presented; meanwhile, the quality of the solution can be examined by displaying the control differences from measuring results. For photogrammetric measurement, as each point is measured, its coordinates ( $X$ ,  $Y$ ,  $Z$ ) are displayed with estimated error in  $X$ ,  $Y$ , and  $Z$  directions, through which the quality of the measuring can be checked. Another way to check the consistency of the measuring results is to display the resulting positions by marking them graphically on the images. This provides the operator with an overview of what has been finished or what is needed to be measured.

### **3.5 Experiment results**

The experiment results of the calibration and measurement algorithms discussed in

the previous chapter are presented in this section.

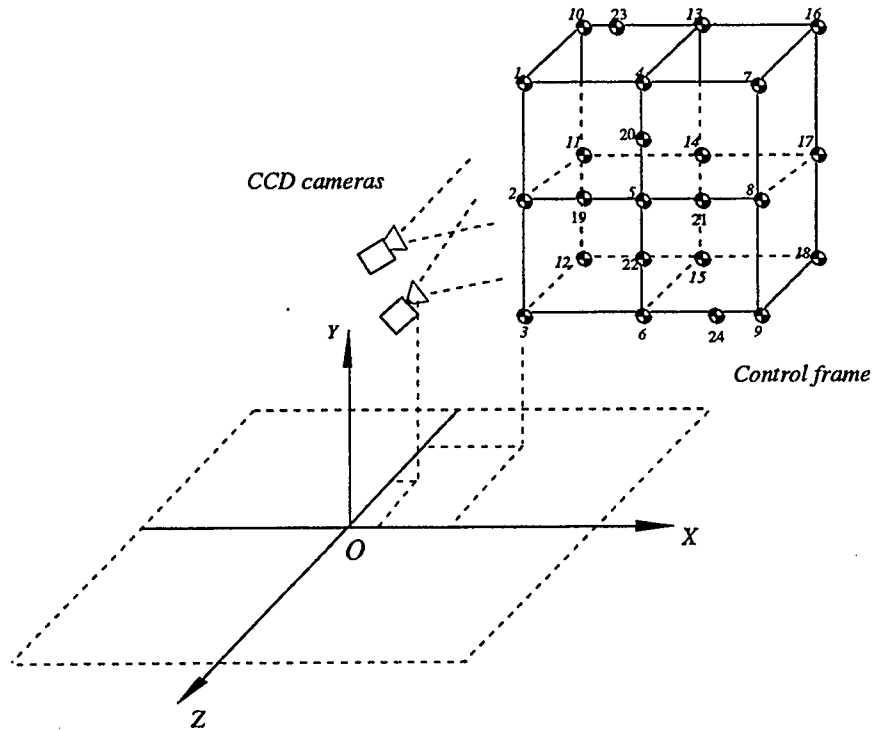


**Figure 3.6** CCD cameras and the control frame in the spatial reference system

From the water tank test (Section 3.3.1), three pairs of stereo digital imagery were used for testing. The size of each image is 568 pixels by 488 pixels. The first pair of images were taken in air, and specifically used for the separate calibration of the pair of CCD cameras. The second and third pairs were taken underwater from different view angles, then used for the whole imaging system calibration and for object measurement accuracy assessment. The image data to be processed were loaded onto the USVIPS. Objects on all of the testing images were the control targets distributed on the calibration frame (Figure 3.6). There were about 19 of the 24 control targets that could be recognized on each of the images (Section 3.3). The spatial coordinate information of those control points was provided by IOS (Table 3.1). The image coordinates of the control targets were obtained from cursor locating manually, and the accurate targeting was aided by the image processing functions provided by the USVIPS. All the data processing procedures were

accomplished using the USVIPS, such as imaging system calibration, object point measurement, etc.

### 3.5.1 Results of CCD camera calibration

The first stereo pair were used for the left and the right CCD camera calibration to determine the interior orientation parameters. In order to impose strong constraint on the solution, 14 control points, which were evenly distributed throughout the image pair, were used for the calibration (Table 3.2).

**Table 3.2** Image and spatial coordinates of control points used for CCD camera calibration

Target No.	Pixel coordinates ( <i>pixel</i> )				Spatial coordinates ( <i>m</i> )		
	<i>x<sub>l</sub></i>	<i>y<sub>l</sub></i>	<i>x<sub>r</sub></i>	<i>y<sub>r</sub></i>	<i>X</i>	<i>Y</i>	<i>Z</i>
1	146	42	118	46	100.0053	101.4396	-100.0010
2	141	249	113	252	100.0016	100.7216	-100.0001
3	143	464	115	466	100.0000	100.0000	-100.0000
6	326	454	299	457	100.7226	99.9994	-100.0029
7	480	66	453	66	101.4492	101.4415	-100.0062
8	485	249	460	251	101.4467	100.7219	-100.0043
9	485	440	460	443	101.4440	99.9996	-100.0001
15	302	425	278	429	100.7193	99.9973	-100.4563
16	436	99	410	97	101.4450	101.4389	-100.4620
18	439	414	416	415	101.4389	100.0071	-100.4552
19	245	254	219	257	100.4472	100.7224	-100.4540
21	360	255	334	257	101.0163	100.7198	-100.4575
22	302	313	278	316	100.7222	100.4735	-100.4529
23	236	45	207	48	100.3645	101.4414	-100.0038

Because of little knowledge about the properties of the pair of CCD cameras, DLT method was employed to obtain approximate values of interior orientation parameters, such as focal lengths (*f*), principal points (*x<sub>p</sub>*, *y<sub>p</sub>*) and y-scale factor (*s<sub>y</sub>*), so that they could be of

benefit for the next calibration procedures (Abdel-Aziz and Karara, 1971). The DLT results are shown in Table 3.3 (Chapman, 1994).

**Table 3.3** Results of DLT

Parameters	Left camera	Right camera
$f(pixel)$	562.9961	568.8597
$x_p(pixel)$	264.0215	245.1877
$y_p(pixel)$	254.7435	251.6867
$s_y$	1.1039	1.1224

**Table 3.4** Results of CCD camera calibration

Parameter	Left camera	Right camera
$f(pixel)$	572.99220	590.29455
$x_p(pixel)$	304.91166	279.57429
$y_p(pixel)$	231.7966	234.51888
$s_y$	1.1449	1.1487
$X_o(m)$	100.6695	100.6010
$Y_o(m)$	100.6110	100.6013
$Z_o(m)$	-97.6994	-97.6875
$\omega(rads)$	0.0417	0.0500
$\phi(rads)$	-0.2064	-0.1884
$\kappa(rads)$	0.0014	-0.0025
$K_1(10^{-2})$	-0.008378	-0.001182
$K_2(10^{-6})$	0.481934	0.337597
$P_1(10^{-4})$	-0.034693	-0.006720
$P_2(10^{-4})$	-0.088645	-0.189452

The results of DLT were introduced as initial approximations for the interior orientation parameters of the CCD cameras in the calibration program based on collinearity equations. By the least squares adjustment (Equation 2.33), the interior and exterior orientation parameters ( $f, x_p, y_p, s_y, X_o, Y_o, Z_o, \omega, \phi, \kappa$ ), the radial lens distortion

parameters ( $K_1, K_2$ ), the decentering correction parameters ( $P_1, P_2$ ) could be obtained (Table 3.4). In total, 28 unknowns were determined after the calibration of the stereo CCD cameras. These unknown parameters obtained except the exterior orientation parameters were considered to be accurate and could be carried over for the whole underwater imaging system calibration.

### 3.5.2 Results of underwater imaging system calibration

In order to accomplish photogrammetric measurement task using the underwater imaging system, the unknowns determining the imaging geometry of the system need to be calculated. For each camera, these parameters include exterior orientation parameters of the exposure station ( $\omega, \phi, \kappa, X_0, Y_0,$  and  $Z_0$ ), multi-lens parameters consisting of those defining the spherical surface of the cover lens ( $a, b, c,$  and  $r$ ) and those defining the plane surface of the cover lens ( $d, e,$  and  $g$ ), and the multi-media parameters ( $n_2, n_3$ ). For the two CCD cameras, they share the same plane surface and multi-media parameters; therefore, in total 25 unknowns need be determined.

The second stereo pair of images, which were taken with the camera system submerged underwater, were used for the testing and 9 control points was selected for the calibration (Table 3.5).

Among those unknown parameters, there are relatively good prior knowledge about refraction indices of water and cover lens, which are considered as constants of about 1.6000 and 1.3300, respectively. Therefore, in doing the least squares adjustment, a value of 2.0 was added as weight to these two parameters so as to restrict their adjustment range. Meanwhile, there were no weight factors added to the rest of the unknown parameters. A solution was obtained for the unknown parameters after accomplishing the calibration of the underwater imaging system. (Table 3.6).

**Table 3.5** Pixel coordinates of control points used for imaging system calibration

Target No.	Pixel coordinates ( <i>pixel</i> )			
	<i>xl</i>	<i>yl</i>	<i>xr</i>	<i>yr</i>
2	91	404	57	213
3	85	456	52	466
5	316	211	280	217
8	535	220	501	228
10	137	11	106	20
13	315	15	284	23
16	490	27	460	33
18	479	430	450	439
24	425	471	393	478

**Table 3.6** Results of imaging system calibration with the second stereo pair

Parameter	Left camera	Right camera
$\omega$ ( <i>rads</i> )	0.0032	0.0040
$\phi$ ( <i>rads</i> )	-0.0340	-0.0250
$\kappa$ ( <i>rads</i> )	-0.0330	-0.0287
$X_o$ ( <i>m</i> )	100.6554	100.7176
$Y_o$ ( <i>m</i> )	100.6132	100.6012
$Z_o$ ( <i>m</i> )	-98.2413	-98.2104
$a$ ( <i>m</i> )	100.6451	100.7122
$b$ ( <i>m</i> )	100.6069	100.5919
$c$ ( <i>m</i> )	-98.2102	-98.1710
$r$ ( <i>m</i> )	0.0885	0.0909
$d$	0.0001	0.0001
$e$	-0.0041	-0.0041
$g$ ( <i>m</i> )	98.0779	98.0779
$n_2$ ( <i>cover-lens</i> )	1.5999	1.5999
$n_3$ ( <i>water</i> )	1.3402	1.3402

From the calibration results, the small values of altitude parameters reflected that the optical axis of the two CCD cameras were approximately vertical to the x-y reference plane. The center of the spherical surface was quite close to its corresponding CCD exposure station, which was consistent with the initial system design. The small values of  $d$  and  $e$  illustrated that the plane surface of the cover lens was nearly parallel to the x-y reference plane. Baseline could be easily obtained and was about 7.0 cm.

This calibration procedure was repeated with the third pair of underwater images with a different view from the second pair. Similar results had been obtained (Table 3.7).

**Table 3.7** Results of imaging system calibration with the third stereo pair

Parameter	Left camera	Right camera
$\omega$ (rads)	-0.0095	0.0010
$\phi$ (rads)	-0.0281	-0.02741
$\kappa$ (rads)	-0.0386	-0.0333
$X_0$ (m)	100.8303	100.9003
$Y_0$ (m)	100.6192	100.6009
$Z_0$ (m)	-98.2490	-98.2202
$a$ (m)	100.8218	100.8968
$b$ (m)	100.6178	100.5934
$c$ (m)	-98.2420	-98.1833
$r$ (m)	0.0879	0.0898
$d$	-0.0011	-0.0011
$e$	-0.0029	-0.0029
$g$ (m)	98.0782	98.0782
$n_2$ (cover-lens)	1.6005	1.6005
$n_3$ (water)	1.3401	1.3401

### 3.5.3 Results of space intersection

The control points of the second and third image pairs, which had not been used for the system calibration, served as measurement objects. The evaluation of measurement accuracy was carried out by deriving RMS error by comparing calculated results with the known control coordinates for each point in object space. Table 3.8 and 3.9 show the results of the photogrammetric evaluation of the underwater imaging system.

**Table 3.8** Object measurement accuracy evaluation using control points on the second stereo pair

Target No.	Pixel coordinates ( <i>pixel</i> )				Difference ( <i>m</i> )		
	$x_l$	$y_l$	$x_r$	$y_r$	$X_c - X_t$	$Y_c - Y_t$	$Z_c - Z_t$
6	306	470	273	478	0.0010	-0.0169	-0.0318
11	127	213	96	224	-0.0285	0.0001	-0.0585
12	122	420	93	428	0.0285	0.0225	0.1035
15	302	431	272	439	-0.0046	0.0007	0.0576
17	489	228	459	236	0.0171	-0.0009	-0.0508
19	238	216	207	224	-0.0250	0.0026	-0.0841
20	312	137	280	144	-0.0047	-0.0072	0.0501
21	384	223	353	230	0.0000	-0.0020	-0.0329
22	308	294	277	300	-0.0062	-0.0070	0.0587
RMS ( <i>m</i> )					0.0171	0.0100	0.0625

From the measurement testing, the attainable accuracy in object space lies at 1.0 cm - 2.0 cm in x- and y- directions respectively. But in the direction of optical axis (z-direction), the accuracy is over 6.0 cm, which is worse than that in x- or y- direction.

#### 3.5.4 Accuracy assessment

Considering the measurement results, the accuracy obtained in x- and y- directions is good, however the RMS error in the z-direction is relatively high. A number of factors might contribute to the object measurement errors. For example, the errors from the

separate calibration procedure could be introduced to the whole imaging system calibration. From the configuration of the imaging system, one of the main factors causing the poor object measurement results in z-direction might be the small size of baseline.

**Table 3.9** Object measurement accuracy evaluation using control points on the third stereo pair

Target No.	Pixel coordinates ( <i>pixel</i> )				Difference ( <i>m</i> )		
	<i>x<sub>l</sub></i>	<i>y<sub>l</sub></i>	<i>x<sub>r</sub></i>	<i>y<sub>r</sub></i>	$X_c - X_t$	$Y_c - Y_t$	$Z_c - Z_t$
6	254	461	223	473	0.0085	0.0188	0.0631
9	474	466	446	475	-0.0140	0.0288	0.0473
11	86	205	60	217	0.0073	-0.0008	0.0453
12	79	409	55	423	0.0109	0.0069	0.0498
15	258	423	232	435	-0.0013	0.0050	0.0661
17	448	221	422	232	0.0163	0.0011	-0.0722
19	196	208	168	220	-0.0036	-0.0025	0.0493
20	269	129	240	141	-0.0005	-0.0132	0.0862
21	343	216	315	227	0.0001	-0.0048	0.0201
22	263	286	235	297	-0.005	-0.0044	0.0905
RMS ( <i>m</i> )					0.0087	0.0122	0.0623

The imaging system calibration results show that the base length of the system is about 7.0 cm. The object to be measured is over 2.5 m. It becomes evident that the main error will be in the direction of the optical axis (z-direction). In addition, due to the application of digital image, a pointing accuracy of about 1/2 pixel is the best that could be achieved without subpixel techniques. For the underwater imaging system, the CCD camera has a horizontal field of view 58° and is quantitized at 774 pixels, one pixel angular value is 1.31E-3 radians. Over 2.5 m, an error of 1/2 pixel generates a cross-track error of 4 cm. However, the 1/2 pixel yields an along-track error of 1.5 m. Figure 3.7 shows the geometry of this situation for the underwater imaging system without considering the cover lenses.

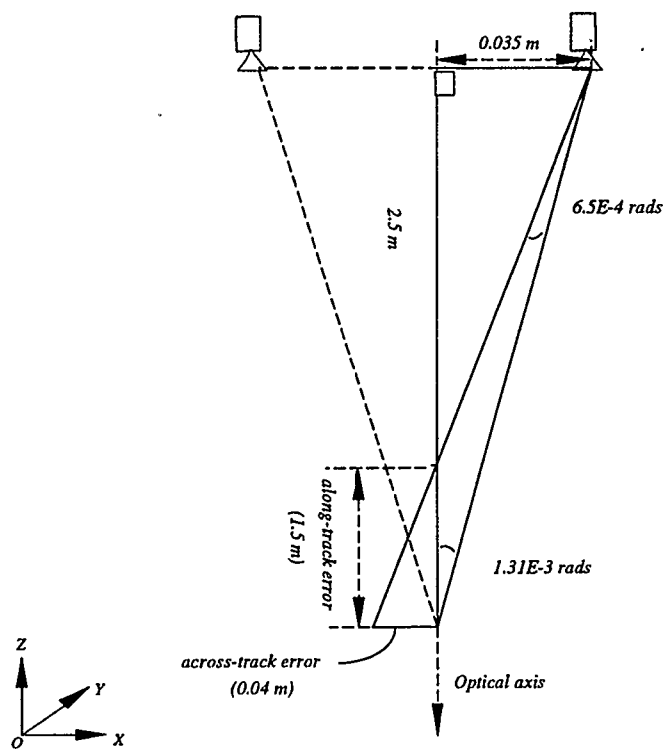


**Figure 3.7:** Geometry of photogrammetric intersection

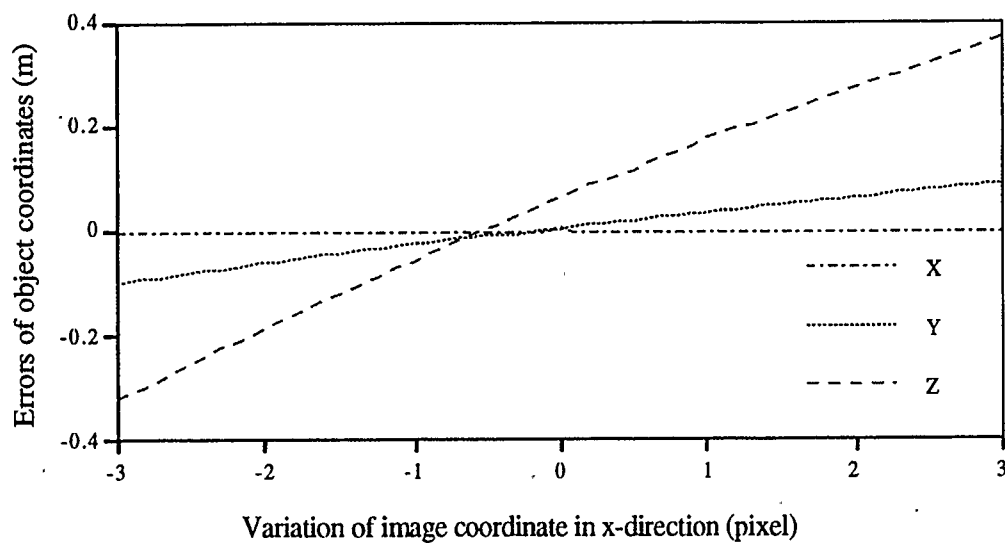


**Figure 3.8** Object measurement error caused by the variation of target pointing in x-direction (Target 15 on left image of the second stereo pair)

To describe the influence of pointing error on the measurement results, the test can be implemented by adding various shifts of image coordinate of a certain control target in image x-direction. Therefore, the variation of the control target in spatial coordinates can be seen in Figure 3.8 - 3.9. Obviously the z-coordinate is very sensitive to image pointing error.

A test was made to show that increasing the size of the baseline could improve the measurement accuracy. A new stereo pair was formed by selecting the left and right images of the second and the third image pairs, respectively. In this case, the size of the baseline increased compared to the original imaging system. The control points used for calibration procedure and for measurement were the same as the testing using the second image pair only. By the imaging system calibration, the spatial positions of the pair of CCD cameras were obtained (Table 3.10). The length of baseline is around 0.24 m, which is two times longer than the designed underwater imaging system. Table 3.11 shows the results of object measurement with RMS evaluation.

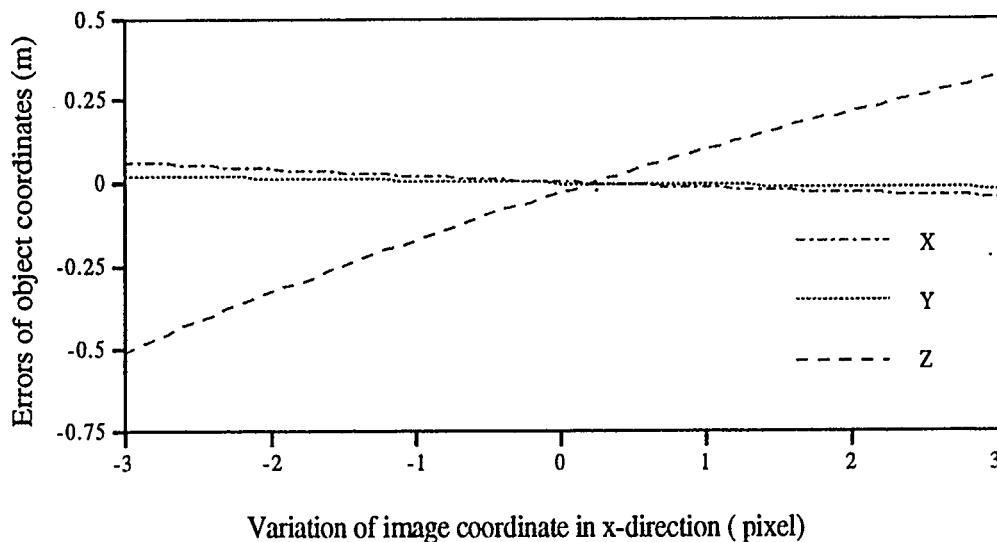


**Figure 3.9** Object measurement error caused by the variation of target pointing in x-direction (Target 20 on left image of the second stereo pair)

**Table 3.10** Spatial coordinates of the exposure stations

Parameter	Left camera	Right camera
$X_o(m)$	100.6533	100.8909
$Y_o(m)$	100.6218	100.6109
$Z_o(m)$	-98.2095	-98.2302

Obviously the measurement accuracy has been improved in every direction. The sensitivity of pointing error on the spatial coordinates decreases and demonstrates that the underwater photogrammetric system would be much more stable if a stereo imaging system could have good photogrammetric geometry.

**Table 3.11** Object measurement accuracy assessment with increased baseline

Target No.	Difference (m)		
	$X_c - X_t$	$Y_c - Y_t$	$Z_c - Z_t$
6	0.00013	-0.00804	-0.01842
11	-0.0158	0.0054	-0.0404
12	0.0013	-0.0009	0.0024
15	-0.0020	-0.0046	0.0084
17	0.0018	-0.0001	-0.0088
19	-0.0145	0.0025	-0.0384
20	-0.0015	-0.0063	0.0357
21	0.0067	0.0011	-0.0708
22	-0.0042	-0.0044	0.0563
RMS(m)	0.0077	0.0045	0.0381

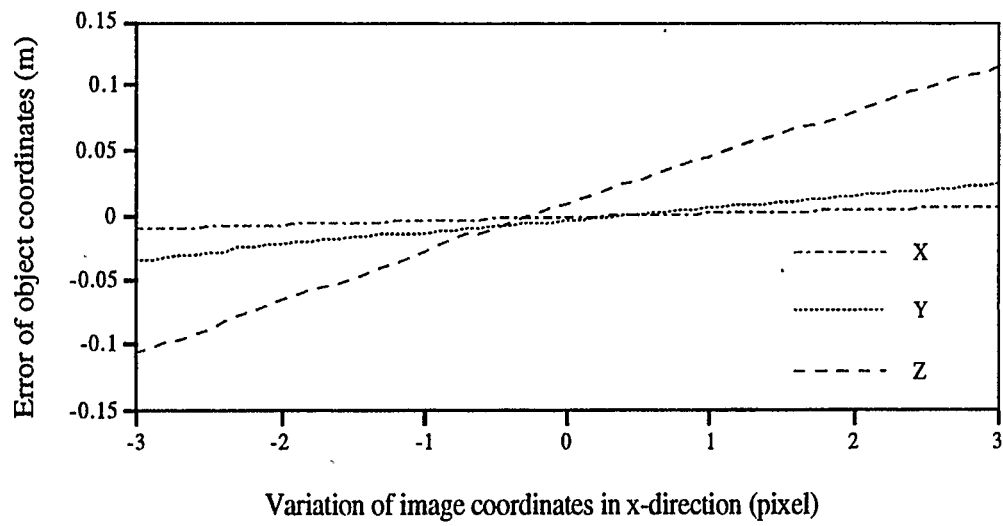


**Figure 3.10** Object measurement error caused by the variation of target pointing in x-direction (Target 15 on left image of the formed image pair)

## CHAPTER 4

### CONCLUSIONS AND RECOMMENDATIONS

#### 4.1 Conclusions

In this research, the development and implementation of photogrammetric techniques to model an underwater imaging system for extracting quantitative spatial information from CCD stereo video images has been successfully carried out. In addition, a PC based digital photogrammetric system has been developed to make the underwater photogrammetric processing in an efficient way and in a user-friendly environment.

From testing results of several pairs of underwater images and implementation of the digital photogrammetric system, the following conclusions can be made:

- 1) It is achievable to use the 3D optical ray tracing technique to describe the imaging procedure and, therefore, to construct a rigorous photogrammetric model with multi-media and multi-lens involvement in the imaging system.
- 2) Separated imaging system calibration has been proved to be efficient in simplifying the computation and improving the calibration accuracy. For the CCD camera calibration, lens distortion corrections and y-scale factor determinations were necessary for the non-metric CCD cameras. The DLT method could be used as an efficient tool to obtain a good initial approximation for the least squares adjustment. In addition, some numerical analysis techniques, such as weighted unknown parameter considerations and SVD implementation, have been proved to be very practical to analyze and adjust

the normal equations so as to reach reasonable imaging system calibration and object measurement results.

- 3) The data collection using CCD video camera was relatively simple and convenient for data management and processing. A reference coordinate system was applied in the field of the underwater imaging and it proved to be sufficient for the camera system calibration and the object accuracy evaluation.
- 4) The method applied allowed an accuracy of 1.0-2.0 cm along x- and y-direction and 6.0 cm along z-direction in object space at the photographic scale from 1:300 to 1:500. The image distance and the scales used are most significant in underwater environment where in average conditions of visibility the very high absorption and scattering by water media, which reduces the light transmission, does not permit an appropriate illumination and resolution for an object distance more than 3-4 m. The accuracy obtained is satisfied. In fact the values are near those declared in terrestrial photogrammetry standard application with non-conventional systems (Li et al., 1994).
- 5) With the implementation of underwater object measurement through photogrammetric techniques, some quantitative information about the underwater object, such as size of the object, can be extracted and the reconstruction of an object in three dimensional space can be achieved.
- 6) The increasing of baseline as tested in Section 3.5.4 demonstrated that the optimization of the imaging system configuration could result in a more accurate object coordinate determination, especially along the camera optical axis direction.
- 7) The development of the PC based underwater processing system demonstrated that the digital photogrammetric system could make the photogrammetric application in an efficient and user friendly environment.

## 4.2 Recommendations

Several recommendations could be made concerning the improvement of the underwater measurement accuracy and the efficiency of the digital photogrammetric processing system:

- 1) The configuration of the imaging system should be optimized in order to form a suitable imaging geometry. In the existing imaging system, the baseline between the two CCD cameras is too short (about 7.0 cm) compared to the object distance to be measured (over 2.0 m), thus the intersection angle is very small. Consequently, the z-direction measurement is very sensitive to the measurement of corresponding image coordinates. With one pixel measurement error in the image plane, spatial coordinates will change dramatically, especially in z-direction (Figures 3.8 and 3.9). If the baseline is two or three times longer than the one used, the base-depth-ratio will be greater than 1:10 (a basic principle in photogrammetry), the object space measuring accuracy of the system could be greatly improved.
- 2) Adequate information of the imaging system and its operational environment should be acquired, which can be helpful in obtaining good initial approximation for the least squares adjustment. In this study, some components of the imaging system are not readily available on the commercial market, such as the big lenses integrated on the housing cover, therefore there will be no specifications of them which are critical for the estimations. This requires sufficient preparation to obtain the prior knowledge of those unknowns ahead of the data processing. Some of the parameters, such as refraction indices of water and cover lenses, the radius of the spherical surface of the cover lenses, are very important to the 3D ray tracing based mathematical model because they dominate the imaging ray path.

- 3) For the camera system calibration, multi-image (more than two) taken from different exposure stations might be used simultaneously to reduce the degree of correlation among the unknown parameters.
- 4) The design of the calibration frame could be modified from a rectangular-shaped frame to a trapezoid one, which could make all the control targets exhibit on the images without blocking each other. Meanwhile, increasing the number of control points could be considered for the system calibration and error evaluation, especially densifying those along camera optical axis direction to strengthen the control in this direction. Circular shaped control targets might be employed to take advantage of sub-pixel techniques currently achievable (Cosandier and Chapman, 1992).
- 5) The lighting condition should be considered in the field data collection. Good underwater lighting condition will improve the quality of the underwater image, and it also can enhance the accuracy in measuring image coordinates of control points.
- 6) The current test undertook only static measurement of underwater object. In the future, the dynamic underwater measuring will be implemented, a number of concerns on the question of whether bubbles, excessive turbidity or even fish would give rise to unacceptable imaging condition. Furthermore, the asynchronization of CCD cameras and such influence on imaging moving objects should be modeled.
- 7) Image pattern recognition technique might be used to identify the measured objects so as to improve the efficiency of the practical application.
- 8) Image clustering technique and classification can be implemented to extract underwater object information, such as numbers and species of fish.

## REFERENCES

- Abdel-Aziz, Y.I. and H.M. Karara, 1971. Direct Linear Transformation from Comparator Coordinates into Object-Space Coordinates in Close Range Photogrammetry. Proceedings of ASP Symposium on Close-Range Photogrammetry, Urbana, Illinois.
- Adams, L.P., 1982. Underwater Analytical Photogrammetry Using Non-Metric Cameras. International Archives of Photogrammetry, 24(5): 12-22.
- American Society of Photogrammetry, 1980. Manual of Photogrammetry (Fourth Edition). Published by the American Society of Photogrammetry, Virginia.
- Badwin, R.A., 1984. An Underwater Photogrammetric Measurement System for Structural Inspection. International Archives of Photogrammetry, 25(A5): 49-58.
- Badwin, R.A., and I. Newton, 1982. A Proposed System for Underwater Photogrammetry from a Manned Submersible Camera Platform. International Archives of Photogrammetry, 24(5): 39-52.
- Born, M and E. Wolf, 1975. Principles of optics. Pergamon Press, Oxford.
- Brown, D. C., 1957. A Treatment of Analytical Photogrammetry with Emphasis on Ballistic Camera Application, RCA Data Reduction Technical Report No. 39.
- Brown, D. C., 1971. Close-Range Camera Calibration. Photogrammetric Engineering, 37(8): 855-866.
- Chapman, M.A., 1994. Software for DLT.

- Cosandier, D. and M.A. Chapman, 1992. High Precision Target Location for Industrial Metrology. Videometrics, SPIE OE/Technology, Boston.
- Cox, A., 1964. A System of Optical Design. The Focal Press, London.
- Curran, T.A., 1993. 3D Coordinates Measurement of the Test Metal Frame. Institute of Ocean Science of Canadian Hydrographic Service Report.
- Curry, S., S. Baumrind, and J.M. Anderson, 1986. Calibration of an Array Camera. Photogrammetric Engineering and Remote Sensing, 52(5): 627-636.
- Davis, L. S. and A. Rosenfeld, 1978. Noise Cleaning by Iterated Local Averaging. IEEE Trans. Syst. Man Cybern., SMC-8, 705-710.
- Dorrer, E., 1986. Precision Analytical Underwater Photogrammetry. International Archives of Photogrammetry, 26(5):176-184.
- Fryer, J.G., 1982, Underwater 35 mm Photogrammetric Applications in Australia. International Archives of Photogrammetry, 24(5): 167-174.
- Fryer, J.G., 1987. Lens Distortion - The Forgotten Component of Digital Photogrammetry. Proceeding of Symposium on "Application of Close-Range Photogrammetry, " University of Melbourne, Australia, pp. 65-77.
- Fryer, J.G., and C.S. Fraser, 1986. On the Calibration of Underwater Cameras. Photogrammetric Record, 12(67): 73-85.
- Gong, P., 1993. Remote Sensing and Image Processing. Lecture Notes, Department of Geomatics Engineering, The University of Calgary.
- Gonzalez, R.C. and P. Wintz, 1987. Digital Image Processing, Addison-Wesley

Publishing Company.

- Gruen, A.W., 1989. Digital Photogrammetric Processing Systems: Current Status and Prospects. *Photogrammetric Engineering and Remote Sensing*, 55(5): 581-586.
- Gulch, E., 1986. Calibration of CCD video Cameras, *Proceedings of ISPRS Symposium on Progress in Imaging Sensors*, Stuttgart, pp. 391-403.
- Herzberger, M., 1958. *Modern Geometrical Optics*. Interscience Publishers, New York.
- Höhle, J., 1971, Reconstruction of the Underwater Object. *Photogrammetric Engineering*, 37(9): 949-954.
- Karara, H.M. and Y. Abdel-Aziz, 1974. Accuracy Aspects of Non-Metric Images. *Photogrammetric Engineering*, 40(11): 1107-1117.
- Karara, H.M. and G.M. Marks, 1968. Mono versus Stereo Analytical Photogrammetry. *Civil Engineering Studies, Photogrammetry Series No. 14*, UI.
- Kristof, E., A. Chandler, and W. Hamner, 1988. 3-D as an Underwater Tool. In: *Ocean '88 Conference Proceedings*. New York: Institute of Electrical and Electronics Engineers, pp. 713-718.
- Leatherdale, J.D. and D.J. Turner, 1983. Underwater Photogrammetry in the North Sea. *Photogrammetric Record*, 11(62): 151-167.
- , 1993. Operational Experience in Underwater Photogrammetry. *ISPRS Journal of Photogrammetry and Remote Sensing*, 46: 104-112.
- Lentz, R., 1987. Lens Distortion Corrected CCD-Camera Calibration with Co-planar Calibration Points for Real-Time 3D Measurements. *Proceedings of ISPRS Inter-*

Commission Conference on "Fast Processing of Photogrammetric Data", Interlaken, pp. 60-67.

Li, R., M.A. Chapman, L. Qian, Y. Xin, and K.-P. Schwarz, 1994. Rapid GIS Database Generation Using GPS/INS Controlled CCD Images. Proceeding of GIS94, Ottawa, pp.465-477.

MacDonald, I.R., S.E. Best, and C.S. Lee, 1992. Biogeochemical Processes at Natural Oil Seeps in the Gulf of Mexico: Field Trials of a Small-Area Benthic Imaging System (SABIS). In: First Thematic Conference on Remote Sensing for Marine and Coastal Environments Ann Arbor: Environmental Research Institute of Michigan.

McNeil, G.T., 1968. Optical Fundamentals of Underwater Photography, Photogrammetry, Inc.

McNeil, G.T., 1969. Underwater Photography. Photogrammetric Engineering, 35(11): 1135-1152.

Mikhail, E.M. and F. Ackermann, 1976. Observations and Least Squares. Thomas Y. Crowell Company, Inc., New York.

Mori, N., S. Masuda, and S. Marai, 1992. Development of a PC-Based Digital Photogrammetric System. International Archives of Photogrammetry, 28(2): 319-322.

Okamoto, A., 1984. "Orientation Problem of Two-Media Photographs with Curved Boundary Surfaces". Photogrammetric Engineering and Remote Sensing", 50(3): 303-316.

- Okamoto, A., Höhle, J., 1972. Allgemeines analytisches Orientierungsverfahren in der Zwei und Mehrmedien-Photogrammetrie und seine Erprobung. *Bul, Feb. & May*.
- OSF, 1992. Published by PTR Prentice-Hall, Inc., New Jersey.
- Pollio, J., 1971. Underwater Mapping with Photography and Sonar. *Photogrammetric Engineering*, 37(9): 955-968.
- Press, W.H., B.P. Flannery, S.A. Teukolsky, and W.T. Vetterling, 1988. *Numerical Recipes in C*. Cambridge University Press, Cambridge.
- Przybilla, H.J., R. Kotowski, A. Meid, and B. Weber, 1988. Geometrical Quality Control in Nuclear Power Stations: A Procedure for High Precision Underwater Photogrammetry. *International Archives of Photogrammetry*, 27(5): 513-526.
- Qian, L., Y. Xin, R. Li, and M.A. Chapman, 1994. Reconstruction of Geometric Elements in GIS Databases Using GPS/INS controlled CCD Images. *Proceedings of GIS94, Vancouver*, pp.395-398.
- Rinner, K., 1969. Problems of Two-Medium Photogrammetry. *Photogrammetric Engineering*, 35(3): 275-282.
- Rosencratz, D.M., 1971. Underwater Photography System. *Photogrammetric Engineering*, 37(9): 969-972.
- Rosman, I. and G.S. Boland, 1986. Quantitative Photography on the Gulf of Mexico Continental Slope. In: *Ocean'86*. New York: Institute of Electrical and Electronics Engineers, pp. 14-18.
- Schmitter, B., and L. Bonfiglioli, 1967. Orientation Problem in Two-Medium Photogrammetry. *Photogrammetric Engineering*. 33(12): 1421-1428.

- Stanton, R.H., J.W. Alexandar, E.W. Dennison, T.A. Glavich, and L.F. Hovland, 1987. Optical Tracking using Charge-Coupled Devices. *Optical Engineering*, 26(9): 930-938.
- Torlegard, A.K.I. and T.L. Lundalv, 1974. Underwater Analytical Systems. *Photogrammetric Engineering*, 40(3): 287-293.
- Turner, D.J. and J.D. Letherdale, 1982. Underwater Photogrammetry for Inspection and Maintenance of North Sea Oil Platforms. *International Archives of Photogrammetry*, 24(5): 507-515.
- Turner, D.J., and D.J. Yule, 1993. A Digital Non-Contact Measurement System. *Photogrammetric Record*, 14(82): 583-594.
- Turner, D.J., D. Yule, and J. Zanre, 1992. A Real Time Photogrammetry System for Underwater and Industrial Applications. *International Archives of Photogrammetry*, 28(5): 507-513.
- Tusting, R.F. and D.L. Davis, 1992. Laser Systems and Structured Illuminations for Quantitative Undersea Imaging. *Marine Technology Society Journal*, 26(4): 5-12.
- WNDX, 1992. Published by WNDX Corporation, Calgary.
- Wakefield, W.W. and A. Genin, 1987. The Use of a Canadian (Perspective) Grid in Deep-Sea Photography. *Deep Sea Research*. 34: 469-478.
- Wakimoto, Z., 1967. On Designing Underwater Camera Lenses. *Photogrammetric Engineering*, 33(8): 925-935.
- Welham, L.G., 1984. The Development of an Underwater Measuring Capability Using Photogrammetric Technique. *International Archives of Photogrammetry*, 25(5):

757-766.

Welsh, N., I.K. Leadbetter, O.W. Cheffins, and H.M. Hall, 1980. Photogrammetric Procedures for a North Sea Oil Rig Leg Repair. *International Archives of Photogrammetry*, 23(B5): 474-483.

## APPENDIX A

### COPLANARITY CONDITION IN 3D SKEW RAY TRACING

Using 3D ray tracing, a ray can be specified by its direction cosines and by the coordinates of the point at which it meets a particular refractive surface. Let  $\alpha_i, \beta_i, \gamma_i, \lambda_i, \mu_i, \nu_i$ , and  $\alpha_{i+1}, \beta_{i+1}, \gamma_{i+1}$  be the direction cosines of the incident ray at the point  $P_i$ , the direction cosines of the normal at  $P_i$ , and the direction cosines of the refracted ray (Figure A.1).

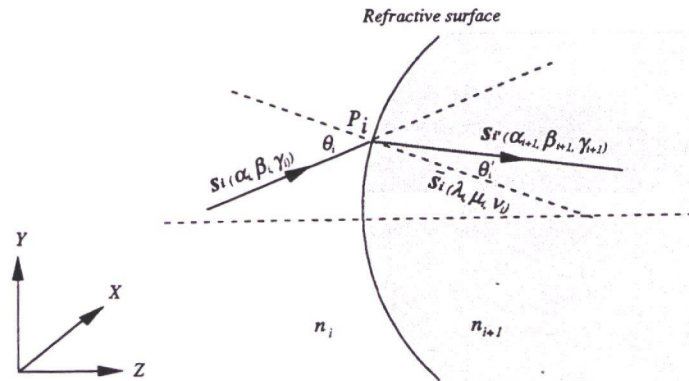


Figure A.1 Tracing of a skew ray

The cosine of the refraction angle be calculated in the form:

$$n_{i+1} \cos \theta'_i = \sqrt{n_{i+1}^2 - n_i^2 + n_i^2 \cos^2 \theta_i} \quad (\text{A.1})$$

Then the fact that the refracted ray lies in the plane specified by the incident ray and the surface normal can be used. Denoting by  $s_i$ ,  $s'_i$  and  $\bar{s}_i$  the unit vectors along the incident

ray, the refracted ray, and the normal, i.e. the vectors with components  $(\alpha_i, \beta_i, \gamma_i)$ ,  $(\alpha_{i+1}, \beta_{i+1}, \gamma_{i+1})$  and  $(\lambda_i, \mu_i, \nu_i)$ , the coplanarity condition gives:

$$s'_i = as_i + b\bar{s}_i \quad (\text{A.2})$$

where  $a$  and  $b$  are certain scalar functions. In order to determine  $a$  and  $b$  Equation (A.2) is first multiplied scalarly by  $s_i$ , and the fact that  $s_i \cdot s'_i = \cos(\theta_i - \theta'_i)$ ,  $s_i \cdot \bar{s}_i = \cos \theta_i$  can be used. (Figure A.1). This gives:

$$\cos(\theta_i - \theta'_i) = a + b \cos \theta_i \quad (\text{A.3})$$

Next Equation (A.2) is multiplied scalarly by  $\bar{s}_i$ , and relations  $\bar{s}_i \cdot s'_i = \cos \theta'_i$  and  $\bar{s}_i \cdot s_i = \cos \theta_i$  can be used. Then this gives:

$$\cos \theta'_i = a \cos \theta_i + b \quad (\text{A.4})$$

From the last two relations it can be derived that:

$$a = \frac{\sin \theta'_i}{\sin \theta_i} = \frac{n_i}{n_{i+1}} \quad (\text{A.5})$$

and

$$b = \frac{1}{n_{i+1}}(n_{i+1} \cos \theta'_i - n_i \cos \theta_i) \quad (\text{A.6})$$

By using Equations (A.2), (A.5) and (A.6), the direction cosines of the refracted ray could be derived as:

$$n_{i+1} \begin{pmatrix} \alpha_{i+1} \\ \beta_{i+1} \\ \gamma_{i+1} \end{pmatrix} = n_i \begin{pmatrix} \alpha_i \\ \beta_i \\ \gamma_i \end{pmatrix} - (n_i \cos \theta_i - n_{i+1} \cos \theta'_i) \begin{pmatrix} \lambda_i \\ \mu_i \\ \nu_i \end{pmatrix} \quad (\text{A.7})$$

## APPENDIX B

### PARTIAL DERIVATIVES OF THE UNDERWATER PHOTOGRAMMETRIC OBSERVATION EQUATIONS

The transformation of image point  $P'(x, y)$  (Figure 2.6) to the object space  $(\bar{X}, \bar{Y}, \bar{Z})$  can be obtained from:

$$\begin{pmatrix} \bar{X} \\ \bar{Y} \\ \bar{Z} \end{pmatrix} = \begin{pmatrix} m_{00} & m_{01} & m_{02} \\ m_{10} & m_{11} & m_{12} \\ m_{20} & m_{21} & m_{22} \end{pmatrix} \begin{pmatrix} x \\ y \\ -f \end{pmatrix} \quad (\text{B.1})$$

where

$$\begin{aligned} m_{00} &= \cos \phi \cos \kappa; \\ m_{01} &= \cos \omega \sin \kappa + \sin \omega \sin \phi \cos \kappa; \\ m_{02} &= \sin \omega \sin \kappa - \cos \omega \sin \phi \cos \kappa; \\ m_{10} &= -\cos \phi \sin \kappa; \\ m_{11} &= \cos \omega \cos \kappa - \sin \omega \sin \phi \sin \kappa; \\ m_{12} &= \sin \omega \cos \kappa + \cos \omega \sin \phi \sin \kappa; \\ m_{20} &= \sin \phi; \\ m_{21} &= -\sin \omega \cos \phi; \\ m_{22} &= \cos \omega \cos \phi. \end{aligned}$$

Let  $\rho_0$  represent the auxiliary quantity from image point  $P'(x, y)$  to the exposure station,

there is:

$$\rho_0 = \sqrt{x^2 + y^2 + f^2} \quad (\text{B.2})$$

Then the direction cosines of  $P'O$  are

$$\begin{pmatrix} \alpha_1 \\ \beta_1 \\ \gamma_1 \end{pmatrix} = \frac{1}{\rho_0} \begin{pmatrix} \bar{X} \\ \bar{Y} \\ \bar{Z} \end{pmatrix} \quad (\text{B.3})$$

Let  $\rho_1$  represent  $\overline{OP_1}$ , there is

$$\rho_1 = -U + \sqrt{W} \quad (\text{B.4})$$

where

$$U = \alpha_1(X_0 - a) + \beta_1(Y_0 - b) + \gamma_1(Z_0 - c);$$

$$V = (X_0 - a)^2 + (Y_0 - b)^2 + (Z_0 - c)^2 - r^2;$$

$$W = U^2 - V.$$

Therefore the coordinates of point  $P_1 (X_1, Y_1, Z_1)$  are

$$\begin{pmatrix} X_1 \\ Y_1 \\ Z_1 \end{pmatrix} = \rho_1 \begin{pmatrix} \alpha_1 \\ \beta_1 \\ \gamma_1 \end{pmatrix} + \begin{pmatrix} X_0 \\ Y_0 \\ Z_0 \end{pmatrix} \quad (\text{B.5})$$

Direction cosines  $(\lambda_1, \mu_1, \nu_1)$  of the normal to the spherical surface at point  $P_1$  are:

$$\begin{pmatrix} \lambda_1 \\ \mu_1 \\ \nu_1 \end{pmatrix} = \frac{1}{r} \begin{pmatrix} X_1 - a \\ Y_1 - b \\ Z_1 - c \end{pmatrix} \quad (\text{B.6})$$

Then the direction cosines  $(\alpha_2, \beta_2, \gamma_2)$  of  $P_1P_2$  can be calculated as

$$\begin{pmatrix} \alpha_2 \\ \beta_2 \\ \gamma_2 \end{pmatrix} = \frac{1}{n_2} \begin{pmatrix} \alpha_1 \\ \beta_1 \\ \gamma_1 \end{pmatrix} - \left( \frac{\cos i_1}{n_2} - \sqrt{T} \right) \begin{pmatrix} \lambda_1 \\ \mu_1 \\ \nu_1 \end{pmatrix} \quad (\text{B.7})$$

where:

$$\cos i_1 = \alpha_1 \lambda_1 + \beta_1 \mu_1 + \gamma_1 \nu_1;$$

$$T = 1 - \frac{1}{n_2^2} + \frac{\cos^2 i_1}{n_2^2}.$$

Let  $\rho_2$  represent  $\overline{P_1P_2}$ , it can be represented as

$$\rho_2 = \frac{T_1}{T_2} \quad (\text{B.8})$$

where

$$T_1 = dX_1 + eY_1 + Z_1 + g;$$

$$T_2 = d\alpha_2 + e\beta_2 + \gamma_2.$$

Therefore the coordinates of point  $P_2 (X_2, Y_2, Z_2)$  can be obtained by:

$$\begin{pmatrix} X_2 \\ Y_2 \\ Z_2 \end{pmatrix} = \rho_2 \begin{pmatrix} \alpha_2 \\ \beta_2 \\ \gamma_2 \end{pmatrix} + \begin{pmatrix} X_1 \\ Y_1 \\ Z_1 \end{pmatrix} \quad (\text{B.9})$$

Direction cosines  $(\lambda_2, \mu_2, \nu_2)$  of the normal to the plane surface of point  $P_2$  are:

$$\begin{pmatrix} \lambda_2 \\ \mu_2 \\ \nu_2 \end{pmatrix} = \frac{1}{\sqrt{T_3}} \begin{pmatrix} d \\ e \\ 1 \end{pmatrix} \quad (\text{B.10})$$

where

$$T_3 = d^2 + e^2 + 1.$$

The direction cosines  $(\alpha_3, \beta_3, \gamma_3)$  of  $P_2P$  become

$$\begin{pmatrix} \alpha_3 \\ \beta_3 \\ \gamma_3 \end{pmatrix} = \frac{n_2}{n_3} \begin{pmatrix} \alpha_2 \\ \beta_2 \\ \gamma_2 \end{pmatrix} - \left( \frac{n_2 \cos i_2}{n_3} - \sqrt{T_4} \right) \begin{pmatrix} \lambda_2 \\ \mu_2 \\ \nu_2 \end{pmatrix} \quad (\text{B.11})$$

where

$$\cos i_2 = \alpha_2 \lambda_2 + \beta_2 \mu_2 + \gamma_2 \nu_2;$$

$$T_4 = 1 - \left( \frac{n_2}{n_3} \right)^2 + \left( \frac{n_2 \cos i_2}{n_3} \right)^2.$$

The two resulting observation equations can then be written as:

$$G_1 = \gamma_3 X - (Z - Z_2)\alpha_3 - \gamma_3 X_2 = 0 \quad (\text{B.12a})$$

$$G_2 = \gamma_3 Y - (Z - Z_2)\beta_3 - \gamma_3 Y_2 = 0 \quad (\text{B.12b})$$

$G_1$  and  $G_2$  are compound functions, in which the unknown parameters are (in total 15 for one camera):

- exterior orientation parameters ( $X_0, Y_0, Z_0, \omega, \phi, \kappa$ );
- multi-lens parameters (spherical surface a, b, c, and r; plane surface d, e, and g);
- multi-media parameters (refractive indices of cover lens  $n_2$  and water  $n_3$ ).

The partial derivatives of the 15 unknown parameters can be acquired by obtaining the intermediate derivatives and they are calculated as follows:

$$\frac{\partial \bar{X}}{\partial \omega} = y(\cos \omega \sin \phi \cos \kappa - \sin \omega \sin \kappa) - f(\sin \omega \sin \phi \cos \kappa + \cos \omega \sin \kappa);$$

$$\frac{\partial \bar{X}}{\partial \phi} = x(-\sin \phi \cos \kappa) + y(\sin \omega \cos \phi \cos \kappa) - f(-\cos \omega \cos \phi \cos \kappa);$$

$$\frac{\partial \bar{X}}{\partial \kappa} = x(-\cos \phi \sin \kappa) + y(-\sin \omega \sin \phi \sin \kappa + \cos \omega \cos \kappa) - f(\cos \omega \sin \phi \sin \kappa + \sin \omega \cos \kappa);$$

$$\frac{\partial \bar{Y}}{\partial \omega} = y(-\cos \omega \sin \phi \sin \kappa - \sin \omega \cos \kappa) - f(-\sin \omega \sin \phi \sin \kappa + \cos \omega \cos \kappa);$$

$$\frac{\partial \bar{Y}}{\partial \phi} = x(\sin \phi \sin \kappa) + y(-\sin \omega \cos \phi \sin \kappa) - f(\cos \omega \cos \phi \sin \kappa);$$

$$\frac{\partial \bar{Y}}{\partial \kappa} = x(-\cos \phi \cos \kappa) + y(-\sin \omega \sin \phi \cos \kappa - \cos \omega \sin \kappa) - f(\cos \omega \sin \phi \cos \kappa - \sin \omega \sin \kappa);$$

$$\frac{\partial \bar{Z}}{\partial \omega} = y(-\cos \omega \cos \phi) - f(-\sin \omega \cos \phi);$$

$$\frac{\partial \bar{Z}}{\partial \phi} = x(\cos \phi) + y(\sin \omega \sin \phi) - f(-\cos \omega \sin \phi);$$

$$\frac{\partial \bar{Z}}{\partial \kappa} = 0;$$

$$\frac{\partial \alpha_1}{\partial \omega} = \frac{\partial \bar{X}}{\partial \omega} / \rho_0, \quad \frac{\partial \beta_1}{\partial \omega} = \frac{\partial \bar{Y}}{\partial \omega} / \rho_0, \quad \frac{\partial \gamma_1}{\partial \omega} = \frac{\partial \bar{Z}}{\partial \omega} / \rho_0;$$

$$\frac{\partial \alpha_1}{\partial \phi} = \frac{\partial \bar{X}}{\partial \phi} / \rho_0, \quad \frac{\partial \beta_1}{\partial \phi} = \frac{\partial \bar{Y}}{\partial \phi} / \rho_0, \quad \frac{\partial \gamma_1}{\partial \phi} = \frac{\partial \bar{Z}}{\partial \phi} / \rho_0;$$

$$\frac{\partial \alpha_1}{\partial \kappa} = \frac{\partial \bar{X}}{\partial \kappa} / \rho_0, \quad \frac{\partial \beta_1}{\partial \kappa} = \frac{\partial \bar{Y}}{\partial \kappa} / \rho_0, \quad \frac{\partial \gamma_1}{\partial \kappa} = \frac{\partial \bar{Z}}{\partial \kappa} / \rho_0;$$

$$\frac{\partial U}{\partial \omega} = (X_0 - a) \frac{\partial \alpha_1}{\partial \omega} + (Y_0 - b) \frac{\partial \beta_1}{\partial \omega} + (Z_0 - c) \frac{\partial \gamma_1}{\partial \omega}, \quad \frac{\partial U}{\partial X_0} = \alpha_1, \quad \frac{\partial U}{\partial a} = -\alpha_1, \quad \frac{\partial U}{\partial r} = 0;$$

$$\frac{\partial U}{\partial \phi} = (X_0 - a) \frac{\partial \alpha_1}{\partial \phi} + (Y_0 - b) \frac{\partial \beta_1}{\partial \phi} + (Z_0 - c) \frac{\partial \gamma_1}{\partial \phi}, \quad \frac{\partial U}{\partial Y_0} = \beta_1, \quad \frac{\partial U}{\partial b} = -\beta_1;$$

$$\frac{\partial U}{\partial \kappa} = (X_0 - a) \frac{\partial \alpha_1}{\partial \kappa} + (Y_0 - b) \frac{\partial \beta_1}{\partial \kappa} + (Z_0 - c) \frac{\partial \gamma_1}{\partial \kappa}, \quad \frac{\partial U}{\partial Z_0} = \gamma_1, \quad \frac{\partial U}{\partial c} = -\gamma_1;$$

$$\frac{\partial V}{\partial \omega} = 0, \quad \frac{\partial V}{\partial X_0} = 2(X_0 - a), \quad \frac{\partial V}{\partial a} = -2(X_0 - a), \quad \frac{\partial V}{\partial r} = -2r;$$

$$\frac{\partial V}{\partial \phi} = 0, \quad \frac{\partial V}{\partial Y_0} = 2(Y_0 - b), \quad \frac{\partial V}{\partial b} = -2(Y_0 - b);$$

$$\frac{\partial V}{\partial \kappa} = 0, \quad \frac{\partial V}{\partial Z_0} = 2(Z_0 - c), \quad \frac{\partial V}{\partial c} = -2(Z_0 - c);$$

$$\frac{\partial W}{\partial \omega} = 2U \frac{\partial U}{\partial \omega} - \frac{\partial V}{\partial \omega}, \quad \frac{\partial W}{\partial X_0} = 2U \frac{\partial U}{\partial X_0} - \frac{\partial V}{\partial X_0}, \quad \frac{\partial W}{\partial a} = 2U \frac{\partial U}{\partial a} - \frac{\partial V}{\partial a}, \quad \frac{\partial W}{\partial r} = 2U \frac{\partial U}{\partial r} - \frac{\partial V}{\partial r};$$

$$\frac{\partial W}{\partial \phi} = 2U \frac{\partial U}{\partial \phi} - \frac{\partial V}{\partial \phi}, \quad \frac{\partial W}{\partial Y_0} = 2U \frac{\partial U}{\partial Y_0} - \frac{\partial V}{\partial Y_0}, \quad \frac{\partial W}{\partial b} = 2U \frac{\partial U}{\partial b} - \frac{\partial V}{\partial b};$$

$$\frac{\partial W}{\partial \kappa} = 2U \frac{\partial U}{\partial \kappa} - \frac{\partial V}{\partial \kappa}, \quad \frac{\partial W}{\partial Z_0} = 2U \frac{\partial U}{\partial Z_0} - \frac{\partial V}{\partial Z_0}, \quad \frac{\partial W}{\partial c} = 2U \frac{\partial U}{\partial c} - \frac{\partial V}{\partial c};$$

$$\frac{\partial \rho_1}{\partial \omega} = -\frac{\partial U}{\partial \omega} + \frac{\partial W}{\partial \omega} \frac{1}{2\sqrt{W}}, \quad \frac{\partial \rho_1}{\partial X_0} = -\frac{\partial U}{\partial X_0} + \frac{\partial W}{\partial X_0} \frac{1}{2\sqrt{W}}, \quad \frac{\partial \rho_1}{\partial a} = -\frac{\partial U}{\partial a} + \frac{\partial W}{\partial a} \frac{1}{2\sqrt{W}};$$

$$\frac{\partial \rho_1}{\partial \phi} = -\frac{\partial U}{\partial \phi} + \frac{\partial W}{\partial \phi} \frac{1}{2\sqrt{W}}, \quad \frac{\partial \rho_1}{\partial Y_0} = -\frac{\partial U}{\partial Y_0} + \frac{\partial W}{\partial Y_0} \frac{1}{2\sqrt{W}}, \quad \frac{\partial \rho_1}{\partial b} = -\frac{\partial U}{\partial b} + \frac{\partial W}{\partial b} \frac{1}{2\sqrt{W}};$$

$$\frac{\partial \rho_1}{\partial \kappa} = -\frac{\partial U}{\partial \kappa} + \frac{\partial W}{\partial \kappa} \frac{1}{2\sqrt{W}}, \quad \frac{\partial \rho_1}{\partial Z_0} = -\frac{\partial U}{\partial Z_0} + \frac{\partial W}{\partial Z_0} \frac{1}{2\sqrt{W}}, \quad \frac{\partial \rho_1}{\partial c} = -\frac{\partial U}{\partial c} + \frac{\partial W}{\partial c} \frac{1}{2\sqrt{W}};$$

$$\frac{\partial \rho_1}{\partial r} = -\frac{\partial U}{\partial r} + \frac{\partial W}{\partial r} \frac{1}{2\sqrt{W}};$$

$$\frac{\partial X_1}{\partial \omega} = \alpha_1 \frac{\partial \rho_1}{\partial \omega} + \rho_1 \frac{\partial \alpha_1}{\partial \omega}, \quad \frac{\partial X_1}{\partial X_0} = \alpha_1 \frac{\partial \rho_1}{\partial X_0} + 1, \quad \frac{\partial X_1}{\partial a} = \alpha_1 \frac{\partial \rho_1}{\partial a}, \quad \frac{\partial X_1}{\partial r} = \alpha_1 \frac{\partial \rho_1}{\partial r};$$

$$\frac{\partial X_1}{\partial \phi} = \alpha_1 \frac{\partial \rho_1}{\partial \phi} + \rho_1 \frac{\partial \alpha_1}{\partial \phi}, \quad \frac{\partial X_1}{\partial Y_0} = \alpha_1 \frac{\partial \rho_1}{\partial Y_0}, \quad \frac{\partial X_1}{\partial b} = \alpha_1 \frac{\partial \rho_1}{\partial b};$$

$$\frac{\partial X_1}{\partial \kappa} = \alpha_1 \frac{\partial \rho_1}{\partial \kappa} + \rho_1 \frac{\partial \alpha_1}{\partial \kappa}, \quad \frac{\partial X_1}{\partial Z_0} = \alpha_1 \frac{\partial \rho_1}{\partial Z_0}, \quad \frac{\partial X_1}{\partial c} = \alpha_1 \frac{\partial \rho_1}{\partial c};$$

$$\frac{\partial Y_1}{\partial \omega} = \beta_1 \frac{\partial \rho_1}{\partial \omega} + \rho_1 \frac{\partial \beta_1}{\partial \omega}, \quad \frac{\partial Y_1}{\partial X_0} = \beta_1 \frac{\partial \rho_1}{\partial X_0}, \quad \frac{\partial Y_1}{\partial a} = \beta_1 \frac{\partial \rho_1}{\partial a}, \quad \frac{\partial Y_1}{\partial r} = \beta_1 \frac{\partial \rho_1}{\partial r};$$

$$\frac{\partial Y_1}{\partial \phi} = \beta_1 \frac{\partial \rho_1}{\partial \phi} + \rho_1 \frac{\partial \beta_1}{\partial \phi}, \quad \frac{\partial Y_1}{\partial Y_0} = \beta_1 \frac{\partial \rho_1}{\partial Y_0} + 1, \quad \frac{\partial Y_1}{\partial b} = \beta_1 \frac{\partial \rho_1}{\partial b};$$

$$\frac{\partial Y_1}{\partial \kappa} = \beta_1 \frac{\partial \rho_1}{\partial \kappa} + \rho_1 \frac{\partial \beta_1}{\partial \kappa}, \quad \frac{\partial Y_1}{\partial Z_0} = \beta_1 \frac{\partial \rho_1}{\partial Z_0}, \quad \frac{\partial Y_1}{\partial c} = \beta_1 \frac{\partial \rho_1}{\partial c};$$

$$\frac{\partial Z_1}{\partial \omega} = \gamma_1 \frac{\partial \rho_1}{\partial \omega} + \rho_1 \frac{\partial \gamma_1}{\partial \omega}, \quad \frac{\partial Z_1}{\partial X_0} = \gamma_1 \frac{\partial \rho_1}{\partial X_0}, \quad \frac{\partial Z_1}{\partial a} = \gamma_1 \frac{\partial \rho_1}{\partial a}, \quad \frac{\partial Z_1}{\partial r} = \gamma_1 \frac{\partial \rho_1}{\partial r};$$

$$\frac{\partial Z_1}{\partial \phi} = \gamma_1 \frac{\partial \rho_1}{\partial \phi} + \rho_1 \frac{\partial \gamma_1}{\partial \phi}, \quad \frac{\partial Z_1}{\partial Y_0} = \gamma_1 \frac{\partial \rho_1}{\partial Y_0}, \quad \frac{\partial Z_1}{\partial b} = \gamma_1 \frac{\partial \rho_1}{\partial b};$$

$$\frac{\partial Z_1}{\partial \kappa} = \gamma_1 \frac{\partial \rho_1}{\partial \kappa} + \rho_1 \frac{\partial \gamma_1}{\partial \kappa}, \quad \frac{\partial Z_1}{\partial Z_0} = \gamma_1 \frac{\partial \rho_1}{\partial Z_0} + 1, \quad \frac{\partial Z_1}{\partial c} = \gamma_1 \frac{\partial \rho_1}{\partial c};$$

$$\frac{\partial \lambda_1}{\partial \omega} = \frac{\partial X_1}{\partial \omega} / r, \quad \frac{\partial \lambda_1}{\partial X_0} = \frac{\partial X_1}{\partial X_0} / r, \quad \frac{\partial \lambda_1}{\partial a} = \left( \frac{\partial X_1}{\partial a} - 1 \right) / r, \quad \frac{\partial \lambda_1}{\partial r} = \left( r \frac{\partial X_1}{\partial r} - X_1 + a \right) / r^2;$$

$$\frac{\partial \lambda_1}{\partial \phi} = \frac{\partial X_1}{\partial \phi} / r, \quad \frac{\partial \lambda_1}{\partial Y_0} = \frac{\partial X_1}{\partial Y_0} / r, \quad \frac{\partial \lambda_1}{\partial b} = \frac{\partial X_1}{\partial b} / r;$$

$$\frac{\partial \lambda_1}{\partial \kappa} = \frac{\partial X_1}{\partial \kappa} / r, \quad \frac{\partial \lambda_1}{\partial Z_0} = \frac{\partial X_1}{\partial Z_0} / r, \quad \frac{\partial \lambda_1}{\partial c} = \frac{\partial X_1}{\partial c} / r;$$

$$\frac{\partial \mu_1}{\partial \omega} = \frac{\partial Y_1}{\partial \omega} / r, \quad \frac{\partial \mu_1}{\partial X_0} = \frac{\partial Y_1}{\partial X_0} / r, \quad \frac{\partial \mu_1}{\partial a} = \frac{\partial Y_1}{\partial a} / r, \quad \frac{\partial \mu_1}{\partial r} = \left( r \frac{\partial Y_1}{\partial r} - Y_1 + b \right) / r^2;$$

$$\frac{\partial \mu_1}{\partial \phi} = \frac{\partial Y_1}{\partial \phi} / r, \quad \frac{\partial \mu_1}{\partial Y_0} = \frac{\partial Y_1}{\partial Y_0} / r, \quad \frac{\partial \mu_1}{\partial b} = \left( \frac{\partial Y_1}{\partial b} - 1 \right) / r;$$

$$\frac{\partial \mu_1}{\partial \kappa} = \frac{\partial Y_1}{\partial \kappa} / r, \quad \frac{\partial \mu_1}{\partial Z_0} = \frac{\partial Y_1}{\partial Z_0} / r, \quad \frac{\partial \mu_1}{\partial c} = \frac{\partial Y_1}{\partial c} / r;$$

$$\frac{\partial v_1}{\partial \omega} = \frac{\partial Z_1}{\partial \omega} / r, \quad \frac{\partial v_1}{\partial X_0} = \frac{\partial Z_1}{\partial X_0} / r, \quad \frac{\partial v_1}{\partial a} = \frac{\partial Z_1}{\partial a} / r, \quad \frac{\partial v_1}{\partial r} = \left( r \frac{\partial Z_1}{\partial r} - Z_1 + c \right) / r^2;$$

$$\frac{\partial v_1}{\partial \phi} = \frac{\partial Z_1}{\partial \phi} / r, \quad \frac{\partial v_1}{\partial Y_0} = \frac{\partial Z_1}{\partial Y_0} / r, \quad \frac{\partial v_1}{\partial b} = \frac{\partial Z_1}{\partial b} / r;$$

$$\frac{\partial v_1}{\partial \kappa} = \frac{\partial Z_1}{\partial \kappa} / r, \quad \frac{\partial v_1}{\partial Z_0} = \frac{\partial Z_1}{\partial Z_0} / r, \quad \frac{\partial v_1}{\partial c} = \left( \frac{\partial Z_1}{\partial c} - 1 \right) / r;$$

$$\frac{\partial \cos i_1}{\partial \omega} = \lambda_1 \frac{\partial \alpha_1}{\partial \omega} + \mu_1 \frac{\partial \beta_1}{\partial \omega} + v_1 \frac{\partial \gamma_1}{\partial \omega} + \alpha_1 \frac{\partial \lambda_1}{\partial \omega} + \beta_1 \frac{\partial \mu_1}{\partial \omega} + \gamma_1 \frac{\partial v_1}{\partial \omega};$$

$$\begin{aligned}
\frac{\partial \cos i_1}{\partial \phi} &= \lambda_1 \frac{\partial \alpha_1}{\partial \phi} + \mu_1 \frac{\partial \beta_1}{\partial \phi} + \nu_1 \frac{\partial \gamma_1}{\partial \phi} + \alpha_1 \frac{\partial \lambda_1}{\partial \phi} + \beta_1 \frac{\partial \mu_1}{\partial \phi} + \gamma_1 \frac{\partial \nu_1}{\partial \phi}; \\
\frac{\partial \cos i_1}{\partial \kappa} &= \lambda_1 \frac{\partial \alpha_1}{\partial \kappa} + \mu_1 \frac{\partial \beta_1}{\partial \kappa} + \nu_1 \frac{\partial \gamma_1}{\partial \kappa} + \alpha_1 \frac{\partial \lambda_1}{\partial \kappa} + \beta_1 \frac{\partial \mu_1}{\partial \kappa} + \gamma_1 \frac{\partial \nu_1}{\partial \kappa}; \\
\frac{\partial \cos i_1}{\partial X_0} &= \alpha_1 \frac{\partial \lambda_1}{\partial X_0} + \beta_1 \frac{\partial \mu_1}{\partial X_0} + \gamma_1 \frac{\partial \nu_1}{\partial X_0}, & \frac{\partial \cos i_1}{\partial a} &= \alpha_1 \frac{\partial \lambda_1}{\partial a} + \beta_1 \frac{\partial \mu_1}{\partial a} + \gamma_1 \frac{\partial \nu_1}{\partial a}; \\
\frac{\partial \cos i_1}{\partial Y_0} &= \alpha_1 \frac{\partial \lambda_1}{\partial Y_0} + \beta_1 \frac{\partial \mu_1}{\partial Y_0} + \gamma_1 \frac{\partial \nu_1}{\partial Y_0}, & \frac{\partial \cos i_1}{\partial b} &= \alpha_1 \frac{\partial \lambda_1}{\partial b} + \beta_1 \frac{\partial \mu_1}{\partial b} + \gamma_1 \frac{\partial \nu_1}{\partial b}; \\
\frac{\partial \cos i_1}{\partial Z_0} &= \alpha_1 \frac{\partial \lambda_1}{\partial Z_0} + \beta_1 \frac{\partial \mu_1}{\partial Z_0} + \gamma_1 \frac{\partial \nu_1}{\partial Z_0}, & \frac{\partial \cos i_1}{\partial c} &= \alpha_1 \frac{\partial \lambda_1}{\partial c} + \beta_1 \frac{\partial \mu_1}{\partial c} + \gamma_1 \frac{\partial \nu_1}{\partial c}; \\
\frac{\partial \cos i_1}{\partial r} &= \alpha_1 \frac{\partial \lambda_1}{\partial r} + \beta_1 \frac{\partial \mu_1}{\partial r} + \gamma_1 \frac{\partial \nu_1}{\partial r};
\end{aligned}$$

$$\begin{aligned}
\frac{\partial \Gamma}{\partial \omega} &= 2 \cos i_1 \frac{\partial \cos i_1}{\partial \omega} / n_2^2, & \frac{\partial \Gamma}{\partial X_0} &= 2 \cos i_1 \frac{\partial \cos i_1}{\partial X_0} / n_2^2, & \frac{\partial \Gamma}{\partial a} &= 2 \cos i_1 \frac{\partial \cos i_1}{\partial a} / n_2^2; \\
\frac{\partial \Gamma}{\partial \phi} &= 2 \cos i_1 \frac{\partial \cos i_1}{\partial \phi} / n_2^2, & \frac{\partial \Gamma}{\partial Y_0} &= 2 \cos i_1 \frac{\partial \cos i_1}{\partial Y_0} / n_2^2, & \frac{\partial \Gamma}{\partial b} &= 2 \cos i_1 \frac{\partial \cos i_1}{\partial b} / n_2^2; \\
\frac{\partial \Gamma}{\partial \kappa} &= 2 \cos i_1 \frac{\partial \cos i_1}{\partial \kappa} / n_2^2, & \frac{\partial \Gamma}{\partial Z_0} &= 2 \cos i_1 \frac{\partial \cos i_1}{\partial Z_0} / n_2^2, & \frac{\partial \Gamma}{\partial c} &= 2 \cos i_1 \frac{\partial \cos i_1}{\partial c} / n_2^2; \\
\frac{\partial \Gamma}{\partial r} &= 2 \cos i_1 \frac{\partial \cos i_1}{\partial r} / n_2^2, & \frac{\partial \Gamma}{\partial n_2} &= (2 - 2 \cos^2 i_1) / n_2^3;
\end{aligned}$$

$$\begin{aligned}
\frac{\partial \alpha_2}{\partial \omega} &= \frac{\partial \alpha_1}{\partial \omega} / n_2 - \lambda_1 \left( \frac{\partial \cos i_1}{\partial \omega} / n_2 - \frac{\partial \Gamma}{\partial \omega} / 2\sqrt{T} \right) - \left( \frac{\cos i_1}{n_2} - \sqrt{T} \right) \frac{\partial \lambda_1}{\partial \omega}; \\
\frac{\partial \alpha_2}{\partial \phi} &= \frac{\partial \alpha_1}{\partial \phi} / n_2 - \lambda_1 \left( \frac{\partial \cos i_1}{\partial \phi} / n_2 - \frac{\partial \Gamma}{\partial \phi} / 2\sqrt{T} \right) - \left( \frac{\cos i_1}{n_2} - \sqrt{T} \right) \frac{\partial \lambda_1}{\partial \phi}; \\
\frac{\partial \alpha_2}{\partial \kappa} &= \frac{\partial \alpha_1}{\partial \kappa} / n_2 - \lambda_1 \left( \frac{\partial \cos i_1}{\partial \kappa} / n_2 - \frac{\partial \Gamma}{\partial \kappa} / 2\sqrt{T} \right) - \left( \frac{\cos i_1}{n_2} - \sqrt{T} \right) \frac{\partial \lambda_1}{\partial \kappa}; \\
\frac{\partial \alpha_2}{\partial X_0} &= -\lambda_1 \left( \frac{\partial \cos i_1}{\partial X_0} / n_2 - \frac{\partial \Gamma}{\partial X_0} / 2\sqrt{T} \right) - \left( \frac{\cos i_1}{n_2} - \sqrt{T} \right) \frac{\partial \lambda_1}{\partial X_0}; \\
\frac{\partial \alpha_2}{\partial Y_0} &= -\lambda_1 \left( \frac{\partial \cos i_1}{\partial Y_0} / n_2 - \frac{\partial \Gamma}{\partial Y_0} / 2\sqrt{T} \right) - \left( \frac{\cos i_1}{n_2} - \sqrt{T} \right) \frac{\partial \lambda_1}{\partial Y_0}; \\
\frac{\partial \alpha_2}{\partial Z_0} &= -\lambda_1 \left( \frac{\partial \cos i_1}{\partial Z_0} / n_2 - \frac{\partial \Gamma}{\partial Z_0} / 2\sqrt{T} \right) - \left( \frac{\cos i_1}{n_2} - \sqrt{T} \right) \frac{\partial \lambda_1}{\partial Z_0}; \\
\frac{\partial \alpha_2}{\partial a} &= -\lambda_1 \left( \frac{\partial \cos i_1}{\partial a} / n_2 - \frac{\partial \Gamma}{\partial a} / 2\sqrt{T} \right) - \left( \frac{\cos i_1}{n_2} - \sqrt{T} \right) \frac{\partial \lambda_1}{\partial a}; \\
\frac{\partial \alpha_2}{\partial b} &= -\lambda_1 \left( \frac{\partial \cos i_1}{\partial b} / n_2 - \frac{\partial \Gamma}{\partial b} / 2\sqrt{T} \right) - \left( \frac{\cos i_1}{n_2} - \sqrt{T} \right) \frac{\partial \lambda_1}{\partial b};
\end{aligned}$$



$$\frac{\partial \gamma_2}{\partial Y_0} = -v_1 \left( \frac{\partial \cos i_1}{\partial \omega} / n_2 - \frac{\partial \Gamma}{\partial Y_0} / 2\sqrt{T} \right) - \left( \frac{\cos i_1}{n_2} - \sqrt{T} \right) \frac{\partial v_1}{\partial Y_0};$$

$$\frac{\partial \gamma_2}{\partial Z_0} = -v_1 \left( \frac{\partial \cos i_1}{\partial Z_0} / n_2 - \frac{\partial \Gamma}{\partial Z_0} / 2\sqrt{T} \right) - \left( \frac{\cos i_1}{n_2} - \sqrt{T} \right) \frac{\partial v_1}{\partial Z_0};$$

$$\frac{\partial \gamma_2}{\partial a} = -v_1 \left( \frac{\partial \cos i_1}{\partial a} / n_2 - \frac{\partial \Gamma}{\partial a} / 2\sqrt{T} \right) - \left( \frac{\cos i_1}{n_2} - \sqrt{T} \right) \frac{\partial v_1}{\partial a};$$

$$\frac{\partial \gamma_2}{\partial b} = -v_1 \left( \frac{\partial \cos i_1}{\partial b} / n_2 - \frac{\partial \Gamma}{\partial b} / 2\sqrt{T} \right) - \left( \frac{\cos i_1}{n_2} - \sqrt{T} \right) \frac{\partial v_1}{\partial b};$$

$$\frac{\partial \gamma_2}{\partial c} = -v_1 \left( \frac{\partial \cos i_1}{\partial c} / n_2 - \frac{\partial \Gamma}{\partial c} / 2\sqrt{T} \right) - \left( \frac{\cos i_1}{n_2} - \sqrt{T} \right) \frac{\partial v_1}{\partial c};$$

$$\frac{\partial \gamma_2}{\partial r} = -v_1 \left( \frac{\partial \cos i_1}{\partial r} / n_2 - \frac{\partial \Gamma}{\partial r} / 2\sqrt{T} \right) - \left( \frac{\cos i_1}{n_2} - \sqrt{T} \right) \frac{\partial v_1}{\partial r};$$

$$\frac{\partial \gamma_2}{\partial n_2} = -\frac{\gamma_1}{n_2^2} + v_1 \left( \frac{\cos i_1}{n_2^2} + \frac{\partial \Gamma}{\partial n_2} / 2\sqrt{T} \right);$$

$$\frac{\partial \Gamma_1}{\partial \omega} = d \frac{\partial X_1}{\partial \omega} + e \frac{\partial Y_1}{\partial \omega} + \frac{\partial Z_1}{\partial \omega},$$

$$\frac{\partial \Gamma_1}{\partial X_0} = d \frac{\partial X_1}{\partial X_0} + e \frac{\partial Y_1}{\partial X_0} + \frac{\partial Z_1}{\partial X_0},$$

$$\frac{\partial \Gamma_1}{\partial d} = X_1;$$

$$\frac{\partial \Gamma_1}{\partial \phi} = d \frac{\partial X_1}{\partial \phi} + e \frac{\partial Y_1}{\partial \phi} + \frac{\partial Z_1}{\partial \phi},$$

$$\frac{\partial \Gamma_1}{\partial Y_0} = d \frac{\partial X_1}{\partial Y_0} + e \frac{\partial Y_1}{\partial Y_0} + \frac{\partial Z_1}{\partial Y_0},$$

$$\frac{\partial \Gamma_1}{\partial e} = Y_1;$$

$$\frac{\partial \Gamma_1}{\partial \kappa} = d \frac{\partial X_1}{\partial \kappa} + e \frac{\partial Y_1}{\partial \kappa} + \frac{\partial Z_1}{\partial \kappa},$$

$$\frac{\partial \Gamma_1}{\partial Z_0} = d \frac{\partial X_1}{\partial Z_0} + e \frac{\partial Y_1}{\partial Z_0} + \frac{\partial Z_1}{\partial Z_0},$$

$$\frac{\partial \Gamma_1}{\partial g} = 1;$$

$$\frac{\partial \Gamma_1}{\partial a} = d \frac{\partial X_1}{\partial a} + e \frac{\partial Y_1}{\partial a} + \frac{\partial Z_1}{\partial a},$$

$$\frac{\partial \Gamma_1}{\partial b} = d \frac{\partial X_1}{\partial b} + e \frac{\partial Y_1}{\partial b} + \frac{\partial Z_1}{\partial b};$$

$$\frac{\partial \Gamma_1}{\partial c} = d \frac{\partial X_1}{\partial c} + e \frac{\partial Y_1}{\partial c} + \frac{\partial Z_1}{\partial c},$$

$$\frac{\partial \Gamma_1}{\partial r} = d \frac{\partial X_1}{\partial r} + e \frac{\partial Y_1}{\partial r} + \frac{\partial Z_1}{\partial r};$$

$$\frac{\partial \Gamma_2}{\partial \omega} = d \frac{\partial \alpha_2}{\partial \omega} + e \frac{\partial \beta_2}{\partial \omega} + \frac{\partial \gamma_2}{\partial \omega}, \quad \frac{\partial \Gamma_2}{\partial X_0} = d \frac{\partial \alpha_2}{\partial X_0} + e \frac{\partial \beta_2}{\partial X_0} + \frac{\partial \gamma_2}{\partial X_0}, \quad \frac{\partial \Gamma_2}{\partial d} = \alpha_2;$$

$$\frac{\partial \Gamma_2}{\partial \phi} = d \frac{\partial \alpha_2}{\partial \phi} + e \frac{\partial \beta_2}{\partial \phi} + \frac{\partial \gamma_2}{\partial \phi}, \quad \frac{\partial \Gamma_2}{\partial Y_0} = d \frac{\partial \alpha_2}{\partial Y_0} + e \frac{\partial \beta_2}{\partial Y_0} + \frac{\partial \gamma_2}{\partial Y_0}, \quad \frac{\partial \Gamma_2}{\partial e} = \beta_2;$$

$$\frac{\partial \Gamma_2}{\partial \kappa} = d \frac{\partial \alpha_2}{\partial \kappa} + e \frac{\partial \beta_2}{\partial \kappa} + \frac{\partial \gamma_2}{\partial \kappa}, \quad \frac{\partial \Gamma_2}{\partial Z_0} = d \frac{\partial \alpha_2}{\partial Z_0} + e \frac{\partial \beta_2}{\partial Z_0} + \frac{\partial \gamma_2}{\partial Z_0};$$

$$\frac{\partial \Gamma_2}{\partial a} = d \frac{\partial \alpha_2}{\partial a} + e \frac{\partial \beta_2}{\partial a} + \frac{\partial \gamma_2}{\partial a}, \quad \frac{\partial \Gamma_2}{\partial b} = d \frac{\partial \alpha_2}{\partial b} + e \frac{\partial \beta_2}{\partial b} + \frac{\partial \gamma_2}{\partial b}, \quad \frac{\partial \Gamma_2}{\partial n_2} = d \frac{\partial \alpha_2}{\partial n_2} + e \frac{\partial \beta_2}{\partial n_2} + \frac{\partial \gamma_2}{\partial n_2};$$

$$\frac{\partial \Gamma_2}{\partial c} = d \frac{\partial \alpha_2}{\partial c} + e \frac{\partial \beta_2}{\partial c} + \frac{\partial \gamma_2}{\partial c}, \quad \frac{\partial \Gamma_2}{\partial r} = d \frac{\partial \alpha_2}{\partial r} + e \frac{\partial \beta_2}{\partial r} + \frac{\partial \gamma_2}{\partial r};$$

$$\frac{\partial \rho_2}{\partial \omega} = (T_2 \frac{\partial \Gamma_1}{\partial \omega} - T_1 \frac{\partial \Gamma_2}{\partial \omega}) / T_2^2, \quad \frac{\partial \rho_2}{\partial X_0} = (T_2 \frac{\partial \Gamma_1}{\partial X_0} - T_1 \frac{\partial \Gamma_2}{\partial X_0}) / T_2^2, \quad \frac{\partial \rho_2}{\partial n_2} = -T_1 \frac{\partial \Gamma_2}{\partial n_2} / T_2^2;$$



$$\begin{aligned}
\frac{\partial Z_2}{\partial \phi} &= \rho_2 \frac{\partial \gamma_2}{\partial \phi} + \gamma_2 \frac{\partial \rho_2}{\partial \phi} + \frac{\partial Z_1}{\partial \phi}, & \frac{\partial Z_2}{\partial Y_0} &= \rho_2 \frac{\partial \gamma_2}{\partial Y_0} + \gamma_2 \frac{\partial \rho_2}{\partial Y_0} + \frac{\partial Z_1}{\partial Y_0}, & \frac{\partial Z_2}{\partial e} &= \gamma_2 \frac{\partial \rho_2}{\partial e}; \\
\frac{\partial Z_2}{\partial \kappa} &= \rho_2 \frac{\partial \gamma_2}{\partial \kappa} + \gamma_2 \frac{\partial \rho_2}{\partial \kappa} + \frac{\partial Z_1}{\partial \kappa}, & \frac{\partial Z_2}{\partial Z_0} &= \rho_2 \frac{\partial \gamma_2}{\partial Z_0} + \gamma_2 \frac{\partial \rho_2}{\partial Z_0} + \frac{\partial Z_1}{\partial Z_0}, & \frac{\partial Z_2}{\partial g} &= \gamma_2 \frac{\partial \rho_2}{\partial g}; \\
\frac{\partial Z_2}{\partial a} &= \rho_2 \frac{\partial \gamma_2}{\partial a} + \gamma_2 \frac{\partial \rho_2}{\partial a} + \frac{\partial Z_1}{\partial a}, & \frac{\partial Z_2}{\partial b} &= \rho_2 \frac{\partial \gamma_2}{\partial b} + \gamma_2 \frac{\partial \rho_2}{\partial b} + \frac{\partial Z_1}{\partial b}; \\
\frac{\partial Z_2}{\partial c} &= \rho_2 \frac{\partial \gamma_2}{\partial c} + \gamma_2 \frac{\partial \rho_2}{\partial c} + \frac{\partial Z_1}{\partial c}, & \frac{\partial Z_2}{\partial r} &= \rho_2 \frac{\partial \gamma_2}{\partial r} + \gamma_2 \frac{\partial \rho_2}{\partial r} + \frac{\partial Z_1}{\partial r}; \\
\frac{\partial Z_2}{\partial n_2} &= \rho_2 \frac{\partial \gamma_2}{\partial n_2} + \gamma_2 \frac{\partial \rho_2}{\partial n_2};
\end{aligned}$$

$$\begin{aligned}
\frac{\partial \lambda_2}{\partial d} &= (\sqrt{T_3} - \frac{d^2}{\sqrt{T_3}}) / T_3, & \frac{\partial \mu_2}{\partial d} &= -\frac{de}{\sqrt{T_3}} / T_3, & \frac{\partial v_2}{\partial d} &= -\frac{d}{\sqrt{T_3}} / T_3; \\
\frac{\partial \lambda_2}{\partial e} &= -\frac{de}{\sqrt{T_3}} / T_3, & \frac{\partial \mu_2}{\partial e} &= (\sqrt{T_3} - \frac{e^2}{\sqrt{T_3}}) / T_3, & \frac{\partial v_2}{\partial e} &= -\frac{e}{\sqrt{T_3}} / T_3;
\end{aligned}$$

$$\begin{aligned}
\frac{\partial \cos i_2}{\partial \omega} &= \lambda_2 \frac{\partial \alpha_2}{\partial \omega} + \mu_2 \frac{\partial \beta_2}{\partial \omega} + v_2 \frac{\partial \gamma_2}{\partial \omega}, & \frac{\partial \cos i_2}{\partial X_0} &= \lambda_2 \frac{\partial \alpha_2}{\partial X_0} + \mu_2 \frac{\partial \beta_2}{\partial X_0} + v_2 \frac{\partial \gamma_2}{\partial X_0}; \\
\frac{\partial \cos i_2}{\partial \phi} &= \lambda_2 \frac{\partial \alpha_2}{\partial \phi} + \mu_2 \frac{\partial \beta_2}{\partial \phi} + v_2 \frac{\partial \gamma_2}{\partial \phi}, & \frac{\partial \cos i_2}{\partial Y_0} &= \lambda_2 \frac{\partial \alpha_2}{\partial Y_0} + \mu_2 \frac{\partial \beta_2}{\partial Y_0} + v_2 \frac{\partial \gamma_2}{\partial Y_0}; \\
\frac{\partial \cos i_2}{\partial \kappa} &= \lambda_2 \frac{\partial \alpha_2}{\partial \kappa} + \mu_2 \frac{\partial \beta_2}{\partial \kappa} + v_2 \frac{\partial \gamma_2}{\partial \kappa}, & \frac{\partial \cos i_2}{\partial Z_0} &= \lambda_2 \frac{\partial \alpha_2}{\partial Z_0} + \mu_2 \frac{\partial \beta_2}{\partial Z_0} + v_2 \frac{\partial \gamma_2}{\partial Z_0}; \\
\frac{\partial \cos i_2}{\partial a} &= \lambda_2 \frac{\partial \alpha_2}{\partial a} + \mu_2 \frac{\partial \beta_2}{\partial a} + v_2 \frac{\partial \gamma_2}{\partial a}, & \frac{\partial \cos i_2}{\partial b} &= \lambda_2 \frac{\partial \alpha_2}{\partial b} + \mu_2 \frac{\partial \beta_2}{\partial b} + v_2 \frac{\partial \gamma_2}{\partial b}; \\
\frac{\partial \cos i_2}{\partial c} &= \lambda_2 \frac{\partial \alpha_2}{\partial c} + \mu_2 \frac{\partial \beta_2}{\partial c} + v_2 \frac{\partial \gamma_2}{\partial c}, & \frac{\partial \cos i_2}{\partial r} &= \lambda_2 \frac{\partial \alpha_2}{\partial r} + \mu_2 \frac{\partial \beta_2}{\partial r} + v_2 \frac{\partial \gamma_2}{\partial r}; \\
\frac{\partial \cos i_2}{\partial d} &= \alpha_2 \frac{\partial \lambda_2}{\partial d} + \beta_2 \frac{\partial \mu_2}{\partial d} + \gamma_2 \frac{\partial v_2}{\partial d}, & \frac{\partial \cos i_2}{\partial n_2} &= \lambda_2 \frac{\partial \alpha_2}{\partial n_2} + \mu_2 \frac{\partial \beta_2}{\partial n_2} + v_2 \frac{\partial \gamma_2}{\partial n_2}; \\
\frac{\partial \cos i_2}{\partial e} &= \alpha_2 \frac{\partial \lambda_2}{\partial e} + \beta_2 \frac{\partial \mu_2}{\partial e} + \gamma_2 \frac{\partial v_2}{\partial e};
\end{aligned}$$

$$\begin{aligned}
\frac{\partial T_4}{\partial \omega} &= 2 n_2^2 \cos i_2 \frac{\partial \cos i_2}{\partial \omega} / n_3^2, & \frac{\partial T_4}{\partial X_0} &= 2 n_2^2 \cos i_2 \frac{\partial \cos i_2}{\partial X_0} / n_3^2; \\
\frac{\partial T_4}{\partial \phi} &= 2 n_2^2 \cos i_2 \frac{\partial \cos i_2}{\partial \phi} / n_3^2, & \frac{\partial T_4}{\partial Y_0} &= 2 n_2^2 \cos i_2 \frac{\partial \cos i_2}{\partial Y_0} / n_3^2; \\
\frac{\partial T_4}{\partial \kappa} &= 2 n_2^2 \cos i_2 \frac{\partial \cos i_2}{\partial \kappa} / n_3^2, & \frac{\partial T_4}{\partial Z_0} &= 2 n_2^2 \cos i_2 \frac{\partial \cos i_2}{\partial Z_0} / n_3^2; \\
\frac{\partial T_4}{\partial a} &= 2 n_2^2 \cos i_2 \frac{\partial \cos i_2}{\partial a} / n_3^2, & \frac{\partial T_4}{\partial b} &= 2 n_2^2 \cos i_2 \frac{\partial \cos i_2}{\partial b} / n_3^2;
\end{aligned}$$

$$\begin{aligned}\frac{\partial \Gamma_4}{\partial c} &= 2n_2^2 \cos i_2 \frac{\partial \cos i_2 / n_3^2}{\partial c}, & \frac{\partial \Gamma_4}{\partial r} &= 2n_2^2 \cos i_2 \frac{\partial \cos i_2 / n_3^2}{\partial r}; \\ \frac{\partial \Gamma_4}{\partial n_2} &= -\frac{2n_2}{n_3^2} + \frac{2n_2 \cos^2 i_2}{n_3^2} + 2n_2^2 \cos i_2 \frac{\partial \cos i_2 / n_3^2}{\partial n_2}, & \frac{\partial \Gamma_4}{\partial n_3} &= \frac{2n_2^2(1 - \cos^2 i_2)}{n_3^3}; \\ \frac{\partial \Gamma_4}{\partial d} &= 2n_2^2 \cos i_2 \frac{\partial \cos i_2 / n_3^2}{\partial d}, & \frac{\partial \Gamma_4}{\partial e} &= 2n_2^2 \cos i_2 \frac{\partial \cos i_2 / n_3^2}{\partial e};\end{aligned}$$

$$\begin{aligned}\frac{\partial \alpha_3}{\partial \omega} &= n_2 \frac{\partial \alpha_2 / n_3 - \lambda_2 (n_2 \frac{\partial \cos i_2 / n_3 - \frac{\partial \Gamma_4}{\partial \omega} / 2 \sqrt{\Gamma_4}}{\partial \omega})}{\partial \omega}; \\ \frac{\partial \alpha_3}{\partial \phi} &= n_2 \frac{\partial \alpha_2 / n_3 - \lambda_2 (n_2 \frac{\partial \cos i_2 / n_3 - \frac{\partial \Gamma_4}{\partial \phi} / 2 \sqrt{\Gamma_4}}{\partial \phi})}{\partial \phi}; \\ \frac{\partial \alpha_3}{\partial \kappa} &= n_2 \frac{\partial \alpha_2 / n_3 - \lambda_2 (n_2 \frac{\partial \cos i_2 / n_3 - \frac{\partial \Gamma_4}{\partial \kappa} / 2 \sqrt{\Gamma_4}}{\partial \kappa})}{\partial \kappa}; \\ \frac{\partial \alpha_3}{\partial X_0} &= n_2 \frac{\partial \alpha_2 / n_3 - \lambda_2 (n_2 \frac{\partial \cos i_2 / n_3 - \frac{\partial \Gamma_4}{\partial X_0} / 2 \sqrt{\Gamma_4}}{\partial X_0})}{\partial X_0}; \\ \frac{\partial \alpha_3}{\partial Y_0} &= n_2 \frac{\partial \alpha_2 / n_3 - \lambda_2 (n_2 \frac{\partial \cos i_2 / n_3 - \frac{\partial \Gamma_4}{\partial Y_0} / 2 \sqrt{\Gamma_4}}{\partial Y_0})}{\partial Y_0}; \\ \frac{\partial \alpha_3}{\partial Z_0} &= n_2 \frac{\partial \alpha_2 / n_3 - \lambda_2 (n_2 \frac{\partial \cos i_2 / n_3 - \frac{\partial \Gamma_4}{\partial Z_0} / 2 \sqrt{\Gamma_4}}{\partial Z_0})}{\partial Z_0}; \\ \frac{\partial \alpha_3}{\partial a} &= n_2 \frac{\partial \alpha_2 / n_3 - \lambda_2 (n_2 \frac{\partial \cos i_2 / n_3 - \frac{\partial \Gamma_4}{\partial a} / 2 \sqrt{\Gamma_4}}{\partial a})}{\partial a}; \\ \frac{\partial \alpha_3}{\partial b} &= n_2 \frac{\partial \alpha_2 / n_3 - \lambda_2 (n_2 \frac{\partial \cos i_2 / n_3 - \frac{\partial \Gamma_4}{\partial b} / 2 \sqrt{\Gamma_4}}{\partial b})}{\partial b}; \\ \frac{\partial \alpha_3}{\partial c} &= n_2 \frac{\partial \alpha_2 / n_3 - \lambda_2 (n_2 \frac{\partial \cos i_2 / n_3 - \frac{\partial \Gamma_4}{\partial c} / 2 \sqrt{\Gamma_4}}{\partial c})}{\partial c}; \\ \frac{\partial \alpha_3}{\partial r} &= n_2 \frac{\partial \alpha_2 / n_3 - \lambda_2 (n_2 \frac{\partial \cos i_2 / n_3 - \frac{\partial \Gamma_4}{\partial r} / 2 \sqrt{\Gamma_4}}{\partial r})}{\partial r}; \\ \frac{\partial \alpha_3}{\partial n_2} &= \frac{\alpha_2}{n_3} + n_2 \frac{\partial \alpha_2 / n_3 - \lambda_2 (\frac{\cos i_2}{n_3} + n_2 \frac{\partial \cos i_2 / n_3 - \frac{\partial \Gamma_4}{\partial n_2} / 2 \sqrt{\Gamma_4}}{\partial n_2})}{\partial n_2}; \\ \frac{\partial \alpha_3}{\partial n_3} &= -\frac{n_2 \alpha_2}{n_3^2} + \frac{n_2 \cos i_2}{n_3^2} + \lambda_2 (\frac{\partial \Gamma_4}{\partial n_3} / 2 \sqrt{\Gamma_4}); \\ \frac{\partial \alpha_3}{\partial d} &= -\lambda_2 (n_2 \frac{\partial \cos i_2 / n_3 - \frac{\partial \Gamma_4}{\partial d} / 2 \sqrt{\Gamma_4}}{\partial d}), & \frac{\partial \alpha_3}{\partial e} &= -\lambda_2 (n_2 \frac{\partial \cos i_2 / n_3 - \frac{\partial \Gamma_4}{\partial e} / 2 \sqrt{\Gamma_4}}{\partial e});\end{aligned}$$

$$\begin{aligned}\frac{\partial \beta_3}{\partial \omega} &= n_2 \frac{\partial \beta_2 / n_3 - \mu_2 (n_2 \frac{\partial \cos i_2 / n_3 - \frac{\partial \Gamma_4}{\partial \omega} / 2 \sqrt{\Gamma_4}}{\partial \omega})}{\partial \omega}; \\ \frac{\partial \beta_3}{\partial \phi} &= n_2 \frac{\partial \beta_2 / n_3 - \mu_2 (n_2 \frac{\partial \cos i_2 / n_3 - \frac{\partial \Gamma_4}{\partial \phi} / 2 \sqrt{\Gamma_4}}{\partial \phi})}{\partial \phi}; \\ \frac{\partial \beta_3}{\partial \kappa} &= n_2 \frac{\partial \beta_2 / n_3 - \mu_2 (n_2 \frac{\partial \cos i_2 / n_3 - \frac{\partial \Gamma_4}{\partial \kappa} / 2 \sqrt{\Gamma_4}}{\partial \kappa})}{\partial \kappa};\end{aligned}$$

$$\begin{aligned}
\frac{\partial \beta_3}{\partial X_0} &= n_2 \frac{\partial \beta_2}{\partial X_0} / n_3 - \mu_2 (n_2 \frac{\partial \cos i_2}{\partial X_0} / n_3 - \frac{\partial \Gamma_4}{\partial X_0} / 2 \sqrt{\Gamma_4}); \\
\frac{\partial \beta_3}{\partial Y_0} &= n_2 \frac{\partial \beta_2}{\partial Y_0} / n_3 - \mu_2 (n_2 \frac{\partial \cos i_2}{\partial Y_0} / n_3 - \frac{\partial \Gamma_4}{\partial Y_0} / 2 \sqrt{\Gamma_4}); \\
\frac{\partial \beta_3}{\partial Z_0} &= n_2 \frac{\partial \beta_2}{\partial Z_0} / n_3 - \mu_2 (n_2 \frac{\partial \cos i_2}{\partial Z_0} / n_3 - \frac{\partial \Gamma_4}{\partial Z_0} / 2 \sqrt{\Gamma_4}); \\
\frac{\partial \beta_3}{\partial a} &= n_2 \frac{\partial \beta_2}{\partial a} / n_3 - \mu_2 (n_2 \frac{\partial \cos i_2}{\partial a} / n_3 - \frac{\partial \Gamma_4}{\partial a} / 2 \sqrt{\Gamma_4}); \\
\frac{\partial \beta_3}{\partial b} &= n_2 \frac{\partial \beta_2}{\partial b} / n_3 - \mu_2 (n_2 \frac{\partial \cos i_2}{\partial b} / n_3 - \frac{\partial \Gamma_4}{\partial b} / 2 \sqrt{\Gamma_4}); \\
\frac{\partial \beta_3}{\partial c} &= n_2 \frac{\partial \beta_2}{\partial c} / n_3 - \mu_2 (n_2 \frac{\partial \cos i_2}{\partial c} / n_3 - \frac{\partial \Gamma_4}{\partial c} / 2 \sqrt{\Gamma_4}); \\
\frac{\partial \beta_3}{\partial r} &= n_2 \frac{\partial \beta_2}{\partial r} / n_3 - \mu_2 (n_2 \frac{\partial \cos i_2}{\partial r} / n_3 - \frac{\partial \Gamma_4}{\partial r} / 2 \sqrt{\Gamma_4}); \\
\frac{\partial \beta_3}{\partial n_2} &= \frac{\beta_2}{n_3} + n_2 \frac{\partial \beta_2}{\partial n_2} / n_3 - \mu_2 (\frac{\cos i_2}{n_3} + n_2 \frac{\partial \cos i_2}{\partial n_2} / n_3 - \frac{\partial \Gamma_4}{\partial n_2} / 2 \sqrt{\Gamma_4}); \\
\frac{\partial \beta_3}{\partial n_3} &= -\frac{n_2 \beta_2}{n_3^2} + \mu_2 \frac{n_2 \cos i_2}{n_3^2} + \mu_2 (\frac{\partial \Gamma_4}{\partial n_3} / 2 \sqrt{\Gamma_4}); \\
\frac{\partial \beta_3}{\partial d} &= -\mu_2 (n_2 \frac{\partial \cos i_2}{\partial d} / n_3 - \frac{\partial \Gamma_4}{\partial d} / 2 \sqrt{\Gamma_4}), \quad \frac{\partial \beta_3}{\partial e} = -\mu_2 (n_2 \frac{\partial \cos i_2}{\partial e} / n_3 - \frac{\partial \Gamma_4}{\partial e} / 2 \sqrt{\Gamma_4});
\end{aligned}$$

$$\begin{aligned}
\frac{\partial \gamma_3}{\partial \omega} &= n_2 \frac{\partial \gamma_2}{\partial \omega} / n_3 - v_2 (n_2 \frac{\partial \cos i_2}{\partial \omega} / n_3 - \frac{\partial \Gamma_4}{\partial \omega} / 2 \sqrt{\Gamma_4}); \\
\frac{\partial \gamma_3}{\partial \phi} &= n_2 \frac{\partial \gamma_2}{\partial \phi} / n_3 - v_2 (n_2 \frac{\partial \cos i_2}{\partial \phi} / n_3 - \frac{\partial \Gamma_4}{\partial \phi} / 2 \sqrt{\Gamma_4}); \\
\frac{\partial \gamma_3}{\partial \kappa} &= n_2 \frac{\partial \gamma_2}{\partial \kappa} / n_3 - v_2 (n_2 \frac{\partial \cos i_2}{\partial \kappa} / n_3 - \frac{\partial \Gamma_4}{\partial \kappa} / 2 \sqrt{\Gamma_4}); \\
\frac{\partial \gamma_3}{\partial X_0} &= n_2 \frac{\partial \gamma_2}{\partial X_0} / n_3 - v_2 (n_2 \frac{\partial \cos i_2}{\partial X_0} / n_3 - \frac{\partial \Gamma_4}{\partial X_0} / 2 \sqrt{\Gamma_4}); \\
\frac{\partial \gamma_3}{\partial Y_0} &= n_2 \frac{\partial \gamma_2}{\partial Y_0} / n_3 - v_2 (n_2 \frac{\partial \cos i_2}{\partial Y_0} / n_3 - \frac{\partial \Gamma_4}{\partial Y_0} / 2 \sqrt{\Gamma_4}); \\
\frac{\partial \gamma_3}{\partial Z_0} &= n_2 \frac{\partial \gamma_2}{\partial Z_0} / n_3 - v_2 (n_2 \frac{\partial \cos i_2}{\partial Z_0} / n_3 - \frac{\partial \Gamma_4}{\partial Z_0} / 2 \sqrt{\Gamma_4}); \\
\frac{\partial \gamma_3}{\partial a} &= n_2 \frac{\partial \gamma_2}{\partial a} / n_3 - v_2 (n_2 \frac{\partial \cos i_2}{\partial a} / n_3 - \frac{\partial \Gamma_4}{\partial a} / 2 \sqrt{\Gamma_4}); \\
\frac{\partial \gamma_3}{\partial b} &= n_2 \frac{\partial \gamma_2}{\partial b} / n_3 - v_2 (n_2 \frac{\partial \cos i_2}{\partial b} / n_3 - \frac{\partial \Gamma_4}{\partial b} / 2 \sqrt{\Gamma_4}); \\
\frac{\partial \gamma_3}{\partial c} &= n_2 \frac{\partial \gamma_2}{\partial c} / n_3 - v_2 (n_2 \frac{\partial \cos i_2}{\partial c} / n_3 - \frac{\partial \Gamma_4}{\partial c} / 2 \sqrt{\Gamma_4});
\end{aligned}$$

$$\begin{aligned} \frac{\partial \gamma_3}{\partial r} &= n_2 \frac{\partial \gamma_2}{\partial r} / n_3 - v_2 \left( n_2 \frac{\partial \cos i_2}{\partial r} / n_3 - \frac{\partial \Gamma_4}{\partial r} / 2\sqrt{\Gamma_4} \right); \\ \frac{\partial \gamma_3}{\partial n_2} &= \frac{\gamma_2}{n_3} + n_2 \frac{\partial \gamma_2}{\partial n_2} / n_3 - v_2 \left( \frac{\cos i_2}{n_3} + n_2 \frac{\partial \cos i_2}{\partial n_2} / n_3 - \frac{\partial \Gamma_4}{\partial n_2} / 2\sqrt{\Gamma_4} \right); \\ \frac{\partial \gamma_3}{\partial n_3} &= -\frac{n_2 \gamma_2}{n_3^2} + v_2 \frac{n_2 \cos i_2}{n_3^2} + v_2 \left( \frac{\partial \Gamma_4}{\partial n_3} / 2\sqrt{\Gamma_4} \right); \\ \frac{\partial \gamma_3}{\partial d} &= -v_2 \left( n_2 \frac{\partial \cos i_2}{\partial d} / n_3 - \frac{\partial \Gamma_4}{\partial d} / 2\sqrt{\Gamma_4} \right), \quad \frac{\partial \gamma_3}{\partial e} = -v_2 \left( n_2 \frac{\partial \cos i_2}{\partial e} / n_3 - \frac{\partial \Gamma_4}{\partial e} / 2\sqrt{\Gamma_4} \right). \end{aligned}$$

The partial derivatives of the functions ( $G_1$  and  $G_2$ ) with respect to the 15 unknown parameters are:

$$\begin{aligned} \frac{\partial G_1}{\partial \omega} &= -\alpha_3 \frac{\partial Z_2}{\partial \omega} + \gamma_3 \frac{\partial X_2}{\partial \omega} + (X_2 - X) \frac{\partial \gamma_3}{\partial \omega} + (Z - Z_2) \frac{\partial \alpha_3}{\partial \omega}; \\ \frac{\partial G_1}{\partial \phi} &= -\alpha_3 \frac{\partial Z_2}{\partial \phi} + \gamma_3 \frac{\partial X_2}{\partial \phi} + (X_2 - X) \frac{\partial \gamma_3}{\partial \phi} + (Z - Z_2) \frac{\partial \alpha_3}{\partial \phi}; \\ \frac{\partial G_1}{\partial \kappa} &= -\alpha_3 \frac{\partial Z_2}{\partial \kappa} + \gamma_3 \frac{\partial X_2}{\partial \kappa} + (X_2 - X) \frac{\partial \gamma_3}{\partial \kappa} + (Z - Z_2) \frac{\partial \alpha_3}{\partial \kappa}; \\ \frac{\partial G_1}{\partial X_0} &= -\alpha_3 \frac{\partial Z_2}{\partial X_0} + \gamma_3 \frac{\partial X_2}{\partial X_0} + (X_2 - X) \frac{\partial \gamma_3}{\partial X_0} + (Z - Z_2) \frac{\partial \alpha_3}{\partial X_0}; \\ \frac{\partial G_1}{\partial Y_0} &= -\alpha_3 \frac{\partial Z_2}{\partial Y_0} + \gamma_3 \frac{\partial X_2}{\partial Y_0} + (X_2 - X) \frac{\partial \gamma_3}{\partial Y_0} + (Z - Z_2) \frac{\partial \alpha_3}{\partial Y_0}; \\ \frac{\partial G_1}{\partial Z_0} &= -\alpha_3 \frac{\partial Z_2}{\partial Z_0} + \gamma_3 \frac{\partial X_2}{\partial Z_0} + (X_2 - X) \frac{\partial \gamma_3}{\partial Z_0} + (Z - Z_2) \frac{\partial \alpha_3}{\partial Z_0}; \\ \frac{\partial G_1}{\partial a} &= -\alpha_3 \frac{\partial Z_2}{\partial a} + \gamma_3 \frac{\partial X_2}{\partial a} + (X_2 - X) \frac{\partial \gamma_3}{\partial a} + (Z - Z_2) \frac{\partial \alpha_3}{\partial a}; \\ \frac{\partial G_1}{\partial b} &= -\alpha_3 \frac{\partial Z_2}{\partial b} + \gamma_3 \frac{\partial X_2}{\partial b} + (X_2 - X) \frac{\partial \gamma_3}{\partial b} + (Z - Z_2) \frac{\partial \alpha_3}{\partial b}; \\ \frac{\partial G_1}{\partial c} &= -\alpha_3 \frac{\partial Z_2}{\partial c} + \gamma_3 \frac{\partial X_2}{\partial c} + (X_2 - X) \frac{\partial \gamma_3}{\partial c} + (Z - Z_2) \frac{\partial \alpha_3}{\partial c}; \\ \frac{\partial G_1}{\partial r} &= -\alpha_3 \frac{\partial Z_2}{\partial r} + \gamma_3 \frac{\partial X_2}{\partial r} + (X_2 - X) \frac{\partial \gamma_3}{\partial r} + (Z - Z_2) \frac{\partial \alpha_3}{\partial r}; \\ \frac{\partial G_1}{\partial n_2} &= -\alpha_3 \frac{\partial Z_2}{\partial n_2} + \gamma_3 \frac{\partial X_2}{\partial n_2} + (X_2 - X) \frac{\partial \gamma_3}{\partial n_2} + (Z - Z_2) \frac{\partial \alpha_3}{\partial n_2}; \\ \frac{\partial G_1}{\partial n_3} &= (X_2 - X) \frac{\partial \gamma_3}{\partial n_3} + (Z - Z_2) \frac{\partial \alpha_3}{\partial n_3}; \\ \frac{\partial G_1}{\partial d} &= -\alpha_3 \frac{\partial Z_2}{\partial d} + \gamma_3 \frac{\partial X_2}{\partial d} + (X_2 - X) \frac{\partial \gamma_3}{\partial d} + (Z - Z_2) \frac{\partial \alpha_3}{\partial d}; \end{aligned}$$

$$\frac{\partial G_1}{\partial e} = -\alpha_3 \frac{\partial Z_2}{\partial e} + \gamma_3 \frac{\partial X_2}{\partial e} + (X_2 - X) \frac{\partial \gamma_3}{\partial e} + (Z - Z_2) \frac{\partial \alpha_3}{\partial e};$$

$$\frac{\partial G_1}{\partial g} = -\alpha_3 \frac{\partial Z_2}{\partial g} + \gamma_3 \frac{\partial X_2}{\partial g};$$

$$\frac{\partial G_2}{\partial \omega} = -\beta_3 \frac{\partial Z_2}{\partial \omega} + \gamma_3 \frac{\partial Y_2}{\partial \omega} + (Y_2 - Y) \frac{\partial \gamma_3}{\partial \omega} + (Z - Z_2) \frac{\partial \beta_3}{\partial \omega};$$

$$\frac{\partial G_2}{\partial \phi} = -\beta_3 \frac{\partial Z_2}{\partial \phi} + \gamma_3 \frac{\partial Y_2}{\partial \phi} + (Y_2 - Y) \frac{\partial \gamma_3}{\partial \phi} + (Z - Z_2) \frac{\partial \beta_3}{\partial \phi};$$

$$\frac{\partial G_2}{\partial \kappa} = -\beta_3 \frac{\partial Z_2}{\partial \kappa} + \gamma_3 \frac{\partial Y_2}{\partial \kappa} + (Y_2 - Y) \frac{\partial \gamma_3}{\partial \kappa} + (Z - Z_2) \frac{\partial \beta_3}{\partial \kappa};$$

$$\frac{\partial G_2}{\partial X_0} = -\beta_3 \frac{\partial Z_2}{\partial X_0} + \gamma_3 \frac{\partial Y_2}{\partial X_0} + (Y_2 - Y) \frac{\partial \gamma_3}{\partial X_0} + (Z - Z_2) \frac{\partial \beta_3}{\partial X_0};$$

$$\frac{\partial G_2}{\partial Y_0} = -\beta_3 \frac{\partial Z_2}{\partial Y_0} + \gamma_3 \frac{\partial Y_2}{\partial Y_0} + (Y_2 - Y) \frac{\partial \gamma_3}{\partial Y_0} + (Z - Z_2) \frac{\partial \beta_3}{\partial Y_0};$$

$$\frac{\partial G_2}{\partial Z_0} = -\beta_3 \frac{\partial Z_2}{\partial Z_0} + \gamma_3 \frac{\partial Y_2}{\partial Z_0} + (Y_2 - Y) \frac{\partial \gamma_3}{\partial Z_0} + (Z - Z_2) \frac{\partial \beta_3}{\partial Z_0};$$

$$\frac{\partial G_2}{\partial a} = -\beta_3 \frac{\partial Z_2}{\partial a} + \gamma_3 \frac{\partial Y_2}{\partial a} + (Y_2 - Y) \frac{\partial \gamma_3}{\partial a} + (Z - Z_2) \frac{\partial \beta_3}{\partial a};$$

$$\frac{\partial G_2}{\partial b} = -\beta_3 \frac{\partial Z_2}{\partial b} + \gamma_3 \frac{\partial Y_2}{\partial b} + (Y_2 - Y) \frac{\partial \gamma_3}{\partial b} + (Z - Z_2) \frac{\partial \beta_3}{\partial b};$$

$$\frac{\partial G_2}{\partial c} = -\beta_3 \frac{\partial Z_2}{\partial c} + \gamma_3 \frac{\partial Y_2}{\partial c} + (Y_2 - Y) \frac{\partial \gamma_3}{\partial c} + (Z - Z_2) \frac{\partial \beta_3}{\partial c};$$

$$\frac{\partial G_2}{\partial r} = -\beta_3 \frac{\partial Z_2}{\partial r} + \gamma_3 \frac{\partial Y_2}{\partial r} + (Y_2 - Y) \frac{\partial \gamma_3}{\partial r} + (Z - Z_2) \frac{\partial \beta_3}{\partial r};$$

$$\frac{\partial G_2}{\partial n_2} = -\beta_3 \frac{\partial Z_2}{\partial n_2} + \gamma_3 \frac{\partial Y_2}{\partial n_2} + (Y_2 - Y) \frac{\partial \gamma_3}{\partial n_2} + (Z - Z_2) \frac{\partial \beta_3}{\partial n_2};$$

$$\frac{\partial G_2}{\partial n_3} = (Y_2 - Y) \frac{\partial \gamma_3}{\partial n_3} + (Z - Z_2) \frac{\partial \beta_3}{\partial n_3};$$

$$\frac{\partial G_2}{\partial d} = -\beta_3 \frac{\partial Z_2}{\partial d} + \gamma_3 \frac{\partial Y_2}{\partial d} + (Y_2 - Y) \frac{\partial \gamma_3}{\partial d} + (Z - Z_2) \frac{\partial \beta_3}{\partial d};$$

$$\frac{\partial G_2}{\partial e} = -\beta_3 \frac{\partial Z_2}{\partial e} + \gamma_3 \frac{\partial Y_2}{\partial e} + (Y_2 - Y) \frac{\partial \gamma_3}{\partial e} + (Z - Z_2) \frac{\partial \beta_3}{\partial e};$$

$$\frac{\partial G_2}{\partial g} = -\beta_3 \frac{\partial Z_2}{\partial g} + \gamma_3 \frac{\partial Y_2}{\partial g}.$$

## APPENDIX C

### SINGULAR VALUE DECOMPOSITION (SVD)

Singular value decomposition (SVD) method is based on the following theorem of linear algebra: any  $m \times n$  matrix  $N$  whose number of rows is greater than or equal to its number of columns  $n$ , can be written as the product of an  $m \times n$  column-orthogonal matrix  $U$ , an  $n \times n$  diagonal matrix  $W$  with positive or zero elements, and the transpose of an  $n \times n$  orthogonal matrix  $V$ . The various shapes of these matrices can be represented as following:

$$\begin{pmatrix} N \end{pmatrix} = \begin{pmatrix} U \end{pmatrix} \begin{pmatrix} w_1 & & \\ & w_2 & \\ & & \ddots \\ & & & w_n \end{pmatrix} \begin{pmatrix} V^T \end{pmatrix} \quad (\text{C.1})$$

The matrix  $U$  and  $V$  are each orthogonal in the sense that their columns are orthonormal.

If the matrix  $N$  is an  $n \times n$  square matrix, then  $U$ ,  $V$ , and  $W$  are all square matrices of the same size.  $U$  and  $V$  are orthogonal so their inverses are equal to their transposes, and  $W$  is diagonal so its inverse elements in the diagonal matrix are the reciprocals of the elements  $w_j$ . From (C.1), the inverse of  $N$  is now allowed to be obtained:

$$N^{-1} = V [\text{diag}(1/w_j)] U^T \quad (\text{C.2})$$

The only thing that might go wrong with this construction is if one of the  $w_j$ 's is zero, or

(numerically) if it is so small that its value is dominated by roundoff error and therefore unknown. If more than one of the  $w_j$ 's have this problem, then the matrix is even more singular. Therefore, the SVD gives a clear diagnosis of the situation.

Usually the condition number of a matrix is defined as the ratio of the largest of the  $w_j$ 's to the smallest of the  $w_j$ 's. A matrix is singular if its condition number is infinite, and it is ill-conditioned if its condition number is too large.